DOI:10.14753/SE.2020.2378

The complex role of N-cadherin and endocannabinoid signaling during cortical development

Ph.D. thesis

Zsófia László

Semmelweis University
János Szentágothai Doctoral School of Neurosciences

Supervisor:	Zsolt Lele, Ph.D.
Official Reviewers of the Ph.D. Dissertation:	Tamás Bíró, M.D., D.Sc. István Adorján, M.D., Ph.D.
Head of the Final Examination Committee:	András Csillag, M.D., D.Sc.
Members of the Final Examination Committee:	Krisztina Herberth-Minkó, Ph.D. Krisztián Tárnok, Ph.D.

Budapest

2019

DOI:10.14753/SE.2020.2378

Table of contents

DOI:10.14753/SE.2020.2378

DOI:10.14753/SE.2020.2378

DOI:10.14753/SE.2020.2378

DOI:10.14753/SE.2020.2378

List of abbreviations

2-AG	2-arachydonoyl-glicerol
Abhd4	Abhydrolase domain containing 4
AEA	Anandamide
AJ	Adherens juncton
aRGPC	Apical radial glia progenitor cell
bRGPC	Basal radial glia progenitor cell
ATGL	Adipose triglyceride lipase
bIP	Basal intermediate progenitor cell
BP	Basal progenitor cell
BrdU	5-bromo-2'-deoxyuridine
Calb2	Calretinin
CBR1	Cannabinoid receptor 1/Cnr1
CC3	Cleaved Caspase-3
CCK	Cholecistokinin
Cdh2	Cadherin-2
CGE	Caudal ganglionic eminence
ChR2	Channelrhodopsin-2
CP	Cortical plate
CR	Cajal-Retzius cell
CytC	Cytochrome C
DAPI	4′,6-diamidino-2-phenylindole
DGL	Diacylglycerol-lipase
Dlx5/6	Distal-less homeobox 5/6
ΔnCdh2	Dominant-negative cadherin-2
ECM	Extracellular matrix
ER	Endoplasmic reticulum

ERK	Extracellular-signal regulated kinase
EtOH	Ethanol
FAAH	Fatty acid amide hydrolase
FWHM	Full width at half maximum
GABA	γ-aminobutyric acid
GAD65	Glutamic acid decarboxylase 65
GE	Ganglionic eminence
GFP	Green fluorescent protein
Glast1	Glutamate Aspartate Transporter 1
HEK-293	Human embryonic kidney 293 cells
IN	Interneuron
IZ	Intermediate zone
KO	Knockout (-/-)
LAMA1	Laminin subunit alpha 1
LGE	Lateral ganglionic eminence
MGE	Medial ganglionic eminence
MGL	Monoacylglycerol lipase
MP	Multipolar cell
mTOR	Mammalian target of rapamycin
MZ	Marginal zone
NAE	N-acylethanolamine
NAPE	N-acyl phosphatidylethanolamine
NAPE-PLD	N-acyl phosphatidylethanolamine phospholipase D
NGN2	Neurogenin 2
NLP	Number of localization point
NSC	Neuronal stem cell
NPY	Neuropeptide Y
PAX6	Paired box protein-6

PBS	Phosphate-buffered saline/ buffer solution
PCR	Polymerase chain reaction
PHH3	Phospho-histone H3
PI3K	Phosphoinositide 3-kinase
PLA2	Phospholipase A2
PLIN1	Perilipin 1
PSB	Pallial-subpallial boundary
PtdSer	Phosphatidylserine
PV	Parvalbumin
Reln	Reelin
RGPC	Radial glia progenitor cell
ROI	Region of interest
SSC	Saline-sodium citrate buffer
SST	Somatostatin
STORM	Stochastic Optical Reconstruction Microscopy
SVZ	Subventricular zone
TAG	Triacylglycerol
TBR1	T-box brain protein 1
TBR2	T-box brain protein 2/Eomes
TBS	Tris-buffered saline/ buffer solution
THC	Δ9-tetrahydrocannabinol
TOM20	Translocase Of Outer Mitochondrial Membrane 20
TRPV1	Transient receptor potential vanilloid receptor 1
TUNEL	Terminal deoxynucleotidyl transferase dUTP nick end labeling
vGlut1	Vesicular glutamate transporter 1
VIP	Vasoactive intestinal peptide
VZ	Ventricular zone
WT	Wild type (+/+)

DOI:10.14753/SE.2020.2378

ZIKV	Zika virus
Z-VAD-FMK	Benzyloxycarbonyl-Val-Ala-Asp(OMe) fluoromethylketoneclose

DOI:10.14753/SE.2020.2378

1. Introduction

The cerebral cortex is the most complex structure in the mammalian brain. During evolution, cortical expansion allowed humans to become a conscious and one of the most versatile species in the world (Van Essen et al., 2018). Naturally, these attributes require the balanced and coordinated activity of excitatory and inhibitory neurons which in turn depend on the proper development of these cells. At the beginning of brain development, the telencephalon is dorso-ventrally divided into two parts, named the pallium and subpallium, respectively (Figure 1). More than 30 years ago scientists were convinced that both excitatory pyramidal neurons and inhibitory interneurons (INs) are originated from the pallium (Rakic, 1988). With the advancement of technology it has been shown, that these two major cell types of the cortex are actually born in distinct germinative niches of the telencephalon (Anderson et al., 1997). Excitatory projection neurons or pyramidal cells of the cortex use glutamate as neurotransmitter and are born in the progenitor pools of the pallium. In contrast, inhibitory interneurons that synthesize GABA (γ-aminobutyric acid) as their main neurotransmitter invade the cortex from the subpallial ganglionic eminences (GE; Marín and Rubenstein, 2003).

The developing embryonic cortex has a multi-layered structure each featuring their own distinct cell types (Figure 1; Buchsbaum and Cappello, 2019). The most apical layer of the pallium is called ventricular zone (VZ) consists of dividing progenitors and newborn daughter cells (Götz and Barde, 2005). Above the VZ, there is another germinative layer called the subventricular zone (SVZ) which is responsible for the generation of both deep (neurons in the layer 5 and 6) and upper layer neurons (layer 2-4; Hevner, 2019). After their birth, newborn neuroblasts start their radial migration by using the elongated fibers of radial glial cells (Hatanaka et al., 2016). They travel through the intermediate zone (IZ), which at later embryonic stages contains a dense neuropil of thalamocortical axons and acts as a barrier between proliferative zones and the forming cortex (Iwashita et al., 2014). The IZ is followed by a transient layer, called subplate (SP), which contains the earliest generated neurons (Hoerder-Suabedissen and Molnár, 2015). Next, pyramidal cells enter the cortical plate (CP), translocate to distinct places and begin their differentiation (Ayala et al., 2007).

Finally, the uppermost layer of the embryonic cortex is the marginal zone (MZ) where Cajal-Retzius cells (CRs) are settled and regulate the final phase of pyramidal cell migration (Gupta et al., 2002). Pyramidal cells are stopped just beneath the MZ and the next generation of excitatory neurons will continuously bypass them in an inside-out manner, hence deep-layer neuron generation is followed by the production of upper-layer neurons (Huang, 2009). In contrast, subpallial interneuron precursors migrate tangentially from the subpallium (Figure 1) and invade the cortex via distinct migratory routes, either through the subventricular or the marginal zone (Marín, 2013). Then, using the radial glia scaffold interneurons migrate radially to their destined places and undergo final differentiation which is strongly influenced by their synaptic interactions with pyramidal cells (Wong et al., 2018).

1.1. Generation of excitatory neurons in the pallium

1.1.1. Neuroepithelial stage (E8-10)

After neural tube closure, the developing neocortex consists of neuronal stem cells (NSCs) forming a single-layer thick neuroepithelium (Johansson et al., 2010). They have apico-basal polarity and are tethered to the pial and the ventricular surface (Arai and Taverna, 2017). At the apical side of the cortex, NSCs are bound to each other via classic cadherin-based adherens junctons (AJs) which together form the adherens junction belt (Chen et al., 2013). NSCs are multipotent and divide symmetrically in order to self-renew and enlarge the stem cell pool of the ventricular zone (Yamaguchi and Miura, 2013). During symmetrical division cells inherit a complete cellular architecture including their apical cadherin-based adherens junctions (Huttner and Kosodo, 2005).

1.1.2. Main neurogenic phase (E11-E16)

1.1.2.1. Apical radial glia progenitor cells

Around embryonic day 10-11 in mice, NSCs start to acquire some astroglial properties (Malatesta et al., 2003) such as the expression of Glast1 (Glutamate Aspartate Transporter 1) and GFAP (Glial fibrillary acidic protein) and become apical radial glia progenitor cells (aRGPCs).

DOI:10.14753/SE.2020.2378

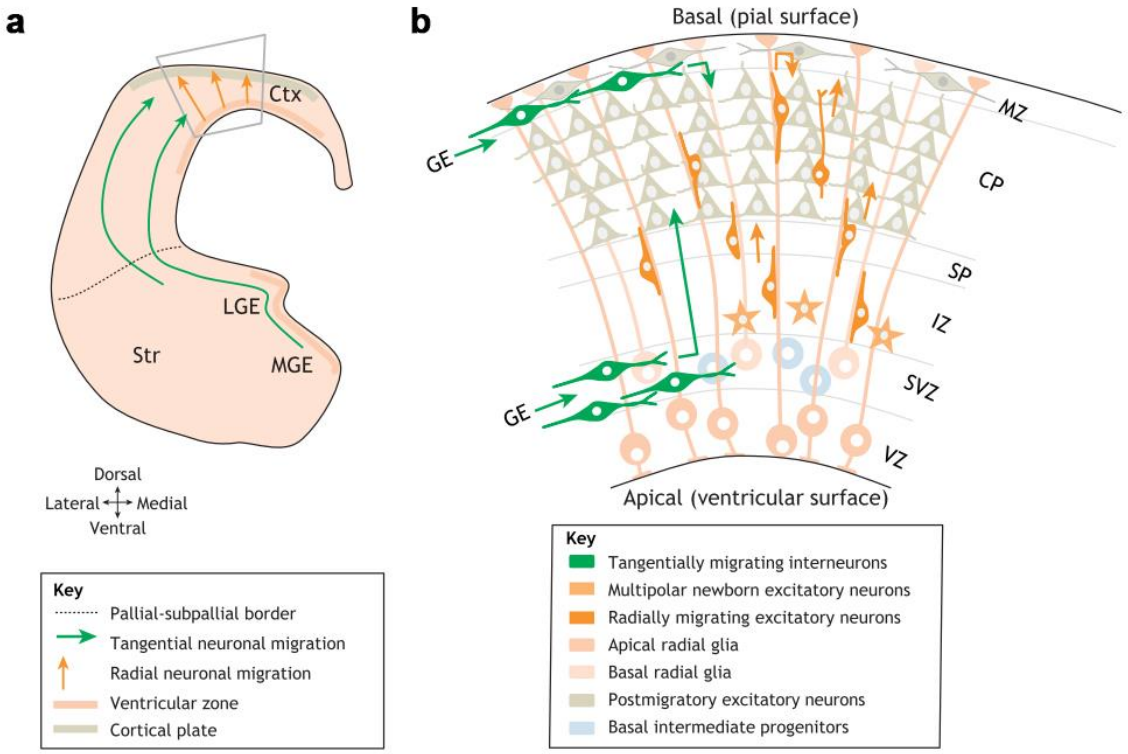

Figure 1. Distinct cell types and migration routes during cortical development
(a) Schematic figure of anterior telencephalon visualizes the distinct migration routes of inhibitory (green arrows) and excitatory neurons (orange arrows). Grey trapezoid is magnified in panel b. (b) Schematic representation of the cortical cellular organization on embryonic day 14. Projection neurons are migrating radially (dark orange cells) by using the radial glia scaffold (elongated cell with light orange color). Interneurons (green cells) are coming from the subpallial ganglionic eminencies via tangential migration and invade the cortical layers radially through the SVZ and CP migration routes. MGE medial ganglionic eminence; LGE: lateral ganglionic eminence, Str: striatum; Ctx: cortex; GE: ganglionic eminence; VZ: ventricular zone, SVZ: subventricular zone, IZ: intermediate zone; SP: subplate, CP: cortical plate; MZ: marginal zone. Figure was adapted from Buchsbaum and Cappello, 2019.

Despite this, they still preserve NSC attributions such as apico-basal polarity (Götz and Huttner, 2005) albeit with a unique bipolar morphology and they attach to the pial surface with their elongated radial fiber (Rakic, 1972). In the neurogenic phase of cortical development between embryonic day 11 to 17, most aRGPCs divide asymmetrically and produce one radial glia progenitor and a basal progenitor cell (BP) or a neuron (Götz and

Huttner, 2005; Noctor et al., 2004; Tamamaki et al., 2001). During asymmetric division the apical ciliary membrane together with the mother centriole and some important regulatory molecules (eg. Par3) are also inherited asymmetrically, which actually determine the fate of daughter cells (Kosodo et al., 2004; Wang et al., 2009).

1.1.2.2. Basal progenitor cells

Two types of basal progenitor cells exist: the basal intermediate progenitor cells (bIPs), which are the most abundant BPs in the rodent embryonic cortex and the basal radial glia progenitor cells (bRGPCs), which are more abundant in primates than in rodents. bIPS are fate-restricted, symmetrically dividing, transient amplifying cells and produce most of the pyramidal cells (Haubensak et al., 2004; Kowalczyk et al., 2009; Vasistha et al., 2015). They do not have a polarized cell body or attachments to the cortical surfaces (Arai and Taverna, 2017), but they have neurites and filopodia which are important to guide the radially or tangentially migrating cells in the SVZ (Hevner, 2019; Kowalczyk et al., 2009). In contrast, bRGPCs are located at the VZ-SVZ border and have unipolar morphology with a basal fiber connecting to the pial surface (Miyata et al., 2001). They have similar proliferative potential as bIPS and responsible for the majority of neuronal production in primates (Ostrem et al., 2017). In contrast to rodents, human SVZ is thick and split into the inner and outer SVZ (iSVZ and oSVZ, respectively, Miller et al., 2019). The oSVZ contains mostly bRGPCs, also called outer radial glia-like cells in humans (Miller et al., 2019). They divide asymmetrically to increase the progenitor pool in the oSVZ (Hansen et al., 2010).

1.1.3. Gliogenic proliferative stage (E17-P3)

At the end of neurogenesis around embryonic day 17.5, the ventricular zone disappears and the SVZ takes over its proliferative function. Progenitor cells in the SVZ mainly produce astrocytes and oligodendrocytes until early postnatal stages (Murao et al., 2016). Recently, it was reported that these progenitor cells are actually present at the beginning of cortical development (around 9.5) but become dormant during the neurogenic phase and get reactivated postnatally (Furutachi et al., 2015).

1.2. Transcriptional regulation of proliferation and differentiation in the pallium

Cell fate is mostly genetically determined and gets directed by sequential waves of transcription factors (Telley et al., 2016). The fluctuation of Notch signaling is one of the key pathways to maintain the NSC self-renewal (Kageyama et al., 2008; Shimojo et al., 2008). Activation of Notch receptor by a single-pass transmembrane protein such as Deltalike-1 (Dll1) instructs progenitor cells to remain in neuronal stem cell state (Andersson et al., 2011; Yoon et al., 2008). Consequently, the expression of Hes1, a Notch-target member of the basic helix-loop-helix (bHLH) transcription factor family, is oscillating in parallel with Notch signaling (Shimojo et al., 2008; Telley et al., 2016). Hes1 is a stem cell marker and inhibits neurogenic commitment via repressing the proneural gene neurogenin 2 (Ngn2) and Dll1 (Shimojo et al., 2008). The fate of the neighbor cell is changed towards differentiation due to repression of Dll-Notch signaling generated lateral inhibition, creating a salt-and-pepper pattern-like distribution of progenitors and differentiating cells (Ohtaka-Maruyama and Okado, 2015).

After the asymmetric division, other transcriptional waves control the further fate of the daughter cells. One example is the sequential expression of PAX6, TBR2 and TBR1 which determine the aRGPCs to BP to differentiated pyramidal cell process (Englund et al., 2005; Hevner, 2019). Paired box protein 6 (PAX6) expression is restricted to RGPCs and this factor is an important regulator of cell division (Asami et al., 2011; Götz et al., 1998) but it is also able to activate the expression of the basal progenitor cell marker, Eomesodermin or T-box brain protein 2 (TBR2) in a dose-dependent manner (Quinn et al., 2007; Sansom et al., 2009). TBR2 is a transcriptional repressor responsible for BP production, specification and necessary for pyramidal cell differentiation (Bulfone et al., 1999; Englund et al., 2005; Mihalas et al., 2016). However, TBR2 also functions as a negative feedback signal as it directly downregulates the expression of PAX6 (Elsen et al., 2018). Finally, T-box brain protein 1 (TBR1) is expressed by postmitotic neurons in the cortical plate (Bulfone et al., 1995) and its activation is regulated by TBR2 (Englund et al., 2005). TBR1 function is related

to the differentiation of pyramidal cells and it regulates several genes partaking in this process (Bedogni et al., 2010).

1.3. Glutamatergic cell migration

At the beginning of cortical development, the first wave of excitatory cells forms the so-called preplate above the VZ. These early born neurons utilize their bipolar morphology and migrate to the MZ by somal translocation (Hirota and Nakajima, 2017). Additionally, another cell type appears in the embryonic MZ, the Cajal-Retzius cells (CRs). In rodents between E10.5 and E12.5, glutamatergic CRs tangentially invade the marginal zone from multiple extra-neocortical sources in a complementary manner (Barber and Pierani, 2016) including the pallial septum, the developing hippocampus (cortical hem; Griveau et al., 2010; Yoshida et al., 2006) and the pallium-subpallium border (Bielle et al., 2005; Griveau et al., 2010). The main function of CR cells is to coordinate radial and tangential migration events. They are transient in nature and get eliminated by programmed cell death during postnatal development (Chowdhury et al., 2010).

Excitatory projection neurons find their final position in the cortical network due to the tightly regulated radial migration process from the VZ to the CP (Rakic, 1972, 1988; Shoukimas and Hinds, 1978). Four subsequent phases of pyramidal cell migration have been described:

1. After asymmetric division daughter cells are delaminated and migrate to the VZ-SVZ border (Shoukimas and Hinds, 1978).
2. Here, postmitotic cells become multipolar and remain for approximately 24 hours, then undergo multipolar-bipolar transition before leaving towards the cortical plate (Nadarajah et al., 2001; Tabata and Nakajima, 2003).
3. Multipolar cells establish their leading and trailing processes (De Anda et al., 2010; Hatanaka et al., 2004; Namba et al., 2014) and migrate to the CP guided by the radial glia scaffold (O'Rourke et al., 1992).
4. Once in the cortical plate the final phase of migration is carried out by terminal translocation (Franco et al., 2011; Noctor et al., 2004).

1.3.1. Delamination and leaving the VZ

To start the migration process, daughter cells need to lose their inherited apical and basal connections and delaminate from the mother cell. They achieve this by downregulating the molecular complex of the adherens junction belt containing Cdh1 and Cdh2 (E- and N-cadherin, respectively; Itoh et al., 2013; Rogers et al., 2018; Rousso et al., 2012). In parallel with neural differentiation, Ngn2 upregulates the levels of Scratch 1 and Scratch 2 transcription factors of the Snail family which induce cell movement via the repression of E-cadherin (Itoh et al., 2013). In addition, it was shown, that repression of Numb proteins, regulators of Notch signaling (Berdnik et al., 2002), also decreases the level of both E- and N-cadherins and causes delamination in parallel with differentiation (Rasin et al., 2007).

Loss of the cell adhesion complexes leads to a change in polarity along with the reorganization of the whole cytoarchitecture (Das and Storey, 2014). Shh (Sonic Hedgehog) signaling via primary cilium and the activation of Ngn2 together regulate the apical fiber abscission and cilium disassembly in daughter cells (Das and Storey, 2014). Meanwhile, intracellular actin dynamics are regulated by the Rho family of GTPases (Ridley, 2015). This family contains three members: Cdc42, Rac1 and RhoA, which are coordinating the connection between cytoskeleton and cell adhesion via cycling between their active (guanosine triphosphate – GTP) and passive (guanosine diphosphate) phases (Hodge and Ridley, 2016).

1.3.2. Morphological transitions during radial migration

During radial migration cell shape and the movement direction can rapidly change. After a short migration from the VZ cells arrive to the SVZ and become multipolar with several neurites extending in every direction (Tabata and Nakajima, 2003). Multipolar cells (MP) can migrate laterally which is independent from the radial glia scaffold (Tabata and Nakajima, 2003). Horizontal movement of MPs is controlled by cell-surface binding ephrin signaling (Dimidschstein et al., 2013; Torii et al., 2009) in particular EfnA (Ephrin-A) ligands and EphA (Ephrin Type-A Receptor) receptors which are both expressed in the SVZ/IZ in a spatial gradient.

It has been reported that two distinct postmitotic populations of daughter cells travel through the SVZ in a different manner. After division, postmitotic neurons accumulate at the apical part of the SVZ while basal progenitor cells immediately migrate to the basal side of the SVZ, where they transform to multipolar cells and undergo further proliferation (Tabata et al., 2009). MP to BP transition is established by transcriptional activation of small GTPases. Activation of Rac1 (Ras-related C3 botulinum toxin substrate 1) promotes the exit from the multipolar stage (Kawauchi et al., 2003) and its interaction with several scaffold proteins properly localizes the activated Rac1 at the basal part of the leading process (Yang et al., 2012). Cdc42 on the other hand, is mainly localized next to the centrosome and is connected to the microtubule organizing center (MTOC) via microtubules. Cdc42 moderates actin dynamics via MTOC, thereby identifying the direction of migration (De Anda et al., 2010; Konno et al., 2005). Rnd2 (Rho-related GTP-binding protein RhoN) is a unique member of the RhoA GTPase family as it lacks intrinsic GTPase activity and regulates neurite extension by the repression of RhoA signaling (Xu et al., 2019). Ngn2 directly activates Rnd2, therefore promotes the MP-BP transition (Heng et al., 2008). Accordingly, modulation of microtubule dynamics by small GTPases is also essential in the elongation of migrating cells, they determine the basal (future dendrite) and apical (future axon) processes (De Anda et al., 2010; Konno et al., 2005; Namba et al., 2014).

1.3.3. Glial-guided locomotion

After MP-BP transition, bipolar cells follow their route to the CP in a glia fiber-guided manner (Noctor et al., 2001; Tabata and Nakajima, 2003). This phenomenon operates coordinated adhesions between the scaffold and the bipolar cell, alternatively utilizing contractile and pulling activity (Dogterom and Koenderink, 2019). Saltatory movement of bipolar cells is achieved via a cyclic two-step process: the centrosome moves forward in the direction of the leading process then the nucleus follows (Tsai et al., 2007). Microtubules are pointing their plus ends towards the leading process and encompass the soma as a cage-like network (Tsai et al., 2007; Xie et al., 2003). Microtubule minus-end associated proteins such as dynein and lissencephaly-1 (Lis1) are located at the dilation zone of the leading process and behave like motors (Dantas et al., 2016; Tsai et al., 2007). Upon contraction from the

lateral regions caused by the activation of the actin-myosin system, microtubule motor proteins pull towards the centrosome followed by the movement of the nucleus and the trailing process (Jiang et al., 2015; Tsai et al., 2007).

Connection between the postmitotic neuron and the radial glia scaffold is crucial for the proper migration process. Gap junction protein, Connexin 43 (Cx43) has an important role in intercellular communications through chemical or electrical coupling of the cells (Valiente and Marín, 2010). However, Cx43 also functions as an adhesion molecule to stabilize the leading process on the radial glial cell fiber and helps nuclear translocation (Elias et al., 2007). Moreover, further experiments showed that Cx43 regulates microtubule dynamics and promotes cell motility via of p27 signaling (Liu et al., 2012).

1.3.4. Terminal translocation

In the final phase, migrating neurons enter the cortical plate and switch to terminal translocation in a radial glia-independent manner (Nadarajah et al., 2001; Sekine et al., 2011). They anchor their leading process to the MZ and move their soma rapidly to their final destination (Hirota and Nakajima, 2017). Cajal-Retzius cells are coordinating the final translocation of migrating neurons by secreting an extracellular glycoprotein, reelin. Mutations in the Reelin gene can cause several pathological symptoms, such as ataxia, locomotion deficits and developmental disorders (Caviness and Sidman, 1973; D'Arcangelo et al., 1995; Magdaleno et al., 2002). In mouse, the spontaneous mutant reeler has inverted cortical layering suggesting that the function of reelin is to coordinate the proper radial migration which maintains the inside-out pattern (D'Arcangelo et al., 1995; Hirotsune et al., 1995; Kubo et al., 2010).

1.4. Progenitor pool in the subpallium, generation of GABAergic cells

Although INs represent only 20-30% of the total neurons in the adult cortex, they are the most diverse population in the brain. Recently, high-throughput RNA-sequencing data identified more than 20 distinct molecular classes of GABAergic cells (Tasic et al., 2016; Zeisel et al., 2015). INs are mostly locally projecting inhibitory cells with different morphological and electrophysiological characteristics. Their main function is to regulate pyramidal cell activity and to control neuronal networks (Tremblay et al., 2016).

DOI:10.14753/SE.2020.2378

Around embryonic day 10 in rodents, the neuroepithelium in the ventral part of the telencephalon starts to protrude into the third ventricle and forms three distinct anatomical parts, called the ganglionic eminences (GEs). The dorsal-most area of the GE is the lateral ganglionic eminence (LGE) which also determines the boundary between the pallial and subpallial regions (Guillemot, 2005). The ventral part of the subpallium is the medial ganglionic eminence (MGE) which produces most of the future cortical interneurons (Miyoshi and Fishell, 2011). The LGE and MGE fuse together at the dorso-caudal part of the GE and establish a common third region, called caudal ganglionic eminence (CGE). This area gives the second highest proportion of interneurons located mostly in the upper cortical layers of the adult cortex (Miyoshi, 2019). The ventral-most part of the GEs is the preoptic region, which is the birthplace of a small amounts (approximately 5-10%) of highly diverse cortical interneurons (Gelman et al., 2009).

The GE contains two germinal zones (VZ, SVZ) but also a molecularly mapped progenitor subdomain structure which produce the different interneuronal subtypes (Figure 2; Martynoga et al., 2012). As in the dorsal telencephalon, subpallial neuroepithelium is composed of neuronal stem cells, which transform into radial glia progenitors (Anthony et al., 2004). However, due the expansion of the ventral telencephalon, radial glia fibers can only reach the pial surface at the beginning of the neurogenic phase (Tamamaki et al., 2001). In order to maintain the radial glia scaffold and enable cell migration at later stages they attach to blood vessels with their basal endfeet (Tan et al., 2016). Subpallial RGPCs have dynamically changing basal endfeet structure, with several protrusions, which are continuously searching for vascular anchoring possibilities (Tan et al., 2016). Four different progenitor cell types were described with distinct proliferative potentials: there are VZ located short neuronal progenitors which undergo symmetric division and generate aRGPCs with the same function as in the pallium (Gal et al., 2006; Turrero García and Harwell, 2017). There are subapical progenitors at the basal part of the VZ which produce more intermediate or basal progenitor cells in the SVZ (Petros et al., 2015; Pilz et al., 2013). Postmitotic inhibitory neurons are mainly produced by the SVZ-located basal progenitor cells and each progenitor subdomain determines the future cell-type specific progeny in the future (Brown

et al., 2011; Harwell et al., 2015). The proliferative capacity and activity differ between the parts of the GE. In the LGE and MGE cell cycles are shorter and they provide more progenitor cells than those in the CGE (Ross, 2011).

The dorsal part of the LGE (dLGE) is an important regulatory region during cortical development because dLGE defines the pallial-subpallial boundary (PSB). This area is characterized by the gradient expression of PAX6 and GSH2 (Genetic-screened homeobox 2) genes and regulates the pallial or subpallial cell fate (Toresson et al., 2000; Yun et al., 2001). Transgenic mouse models showed that PAX6 and GSH2 can cross-repress each other, which is an important molecular mechanism in the positioning of the PSB and the establishment of correct patterning during early telencephalic development (Carney et al., 2009; Corbin et al., 2000).

Similarly to the pallium, cell fate determination in the subpallium is also highly dependent on transcriptional cascades. However, the transcription cascades between the two parts of the telencephalon are suppressing each other, thus stabilizing regional progenitor pool fate (Chouchane and Costa, 2019; Kovach et al., 2013). Ngn2 outlines the glutamatergic regions in the dorsal telencephalon, meanwhile another proneural factor from the bHLH family, Ascl1 (Achaete-Scute-like family bHLH transcription factor 1) promotes GABAergic engagement. At the next level, members of another transcription factor family are expressed sequentially during cell transition in all parts of the GE, called Dlx genes (distal-less homeobox). Dlx2 is expressed by NSCs and RGPCs in the VZ, Dlx1/2/5 appear in SVZ cells and Dlx5/6 visualize postmitotic differentiating cells (Eisenstat et al., 1999; Long et al., 2009; Wang et al., 2010). Dlx genes regulate one another (Lindtner et al., 2019; Zhou et al., 2004) and maintain cell differentiations by repressing proneural genes (Yun et al., 2002). Sequential expression of Dlx genes promotes GABAergic cell fate commitment by direct transcriptional activation of glutamic acid decarboxylase genes (Gad, Le et al., 2017), Gad1 which encodes Gad67 protein and Gad2 which produces Gad65 (Erlander et al., 1991). Their expression in different interneuron populations vary but both proteins synthesize GABA from glutamate (López-Bendito et al., 2004; Rowley et al., 2012; Tamamaki et al., 2003). Although, distinct parts of the GE share common features at the early phase of differentiations, later they acquire

individual transcription factor sets involved in determining interneuron subtype specificity (Mayer et al., 2018).

The MGE produces the majority of cortical neurons, approximately 60-70% of the total cell population that are classified into two main groups (Figure 2): somatostatin-positive (SST) interneurons originating from the dorsal part of the MGE, and parvalbumin-expressing (PV) inhibitory cells rising from the ventral part (Gelman and Marín, 2010). Using single-cell RNA-sequencing, 7 classes of MGE interneurons were determined in total at embryonic stage; 4 subclasses of PV cells and 3 subclasses of SST-positive interneurons (Mi et al., 2018). PV-positive interneurons possess fast-spike firing characteristic and consist of morphologically three different cells types in the adult brain. The chandelier cells or axo-axonic cells have extended axonal arbors and they form synapses on the axon initial segment of the pyramidal cells (Taniguchi et al., 2013). The second group consist of basket cells, which are the most abundant interneuron type. As their name suggests, they form synapses on the soma and proximal dendrites of the excitatory cells, completely surrounding them like baskets (Freund and Katona, 2007). Members belonging to the third group of PV interneurons, the translaminar interneurons have a single elongated axon and establish synapses with several pyramidal cells from the upper layers (Lim et al., 2018). SST-positive interneurons are sorted into three groups: Martinotti cells, which located in layer 2/3 and 5 and arborize with cells in the layer 1, meanwhile non-Martinotti cells are abundant in layer 2 to 6 and they project locally. Finally, GABAergic projection neurons are situated in the deep layers and form inter-regional connections in the neocortex (Lim et al., 2018).

The CGE is the source of a more heterogenous interneuron population, giving 30-40% of all cortical interneurons (Figure 2). CGE-driven interneurons are all Htr3a-positive and divided into six subclasses based on specific protein markers. VIP (vasoactive intestinal peptide) interneurons can be cholecystokinin (CCK) – positive basket cells or CCK-negative/calretinin (CR)-positive bipolar cells. (Tremblay et al., 2016). Neurogliaform and single bouquet cells are located mainly in layer 1 and both express reelin (Lim et al., 2018). NPY (neuropeptide Y) – positive cells are multipolar and restricted to layer 1 and 2 (Tremblay et al., 2016). There is a recently identified new group of 5Ht3aR interneurons

settled under the subplate cells on the edge of the white matter. They have been named as Meis2 – positive (Myeloid Ecotropic viral Integration Site 1 homolog 2) cells (Frazer et al., 2017).

The LGE does not participate in the production of cortical interneurons rather it provides GABAergic cells for the olfactory bulb and medium spiny neurons for the striatum (Bandler et al., 2017; Marín et al., 2000).

The preoptic region consists of two distinct parts: the medially situated preoptic area (PoA) and the most caudally located preoptic-hypothalamic border (PoH, Figure 2). PoA produces a small proportion (approx. 10%) of cortical interneurons (Gelman et al., 2011, 2009) and shares transcriptional codes with MGE, like Nkx2.1(Gelman and Marín, 2010). These transcription factors might regulate the cell fate of this heterogenous population and differentiate these cells from MGE-driven progeny. To corroborate this notion, PoA-produced PV- and SST-positive interneurons are located solely in deep cortical layers, suggesting that these cells may have different electrophysiological characteristics than their MGE-driven relatives (Gelman et al., 2011). In contrast, PoH has molecular and cellular similarities with CGE, furthermore some neurogliaform and multipolar NPY-positive interneurons are originated possibly from this preoptic region (Flames et al., 2007).

1.5. Interneuron migration to the cerebral cortex

The exit of newborn GABAergic cells from the GE is followed by the process of tangential migration which can be divided into three different stages. First, postmitotic cells are detached from the radial scaffold, migrate through the subpallial areas and arrive to the PSB. Second, they invade the cortex tangentially via different cortical migratory streams (Figure 1) and third, they integrate into the cortical layers and differentiate (Marín, 2013).

1.5.1. Tangential migration

Postmitotic interneurons rearrange their morphology (become bipolar and form a leading process) and leave the radial glia scaffold in the GEs, which process is regulated by both intrinsic and environmental signals (Nadarajah et al., 2002). The leading process contains several branches each possessing a growth-cone like structure.

DOI:10.14753/SE.2020.2378

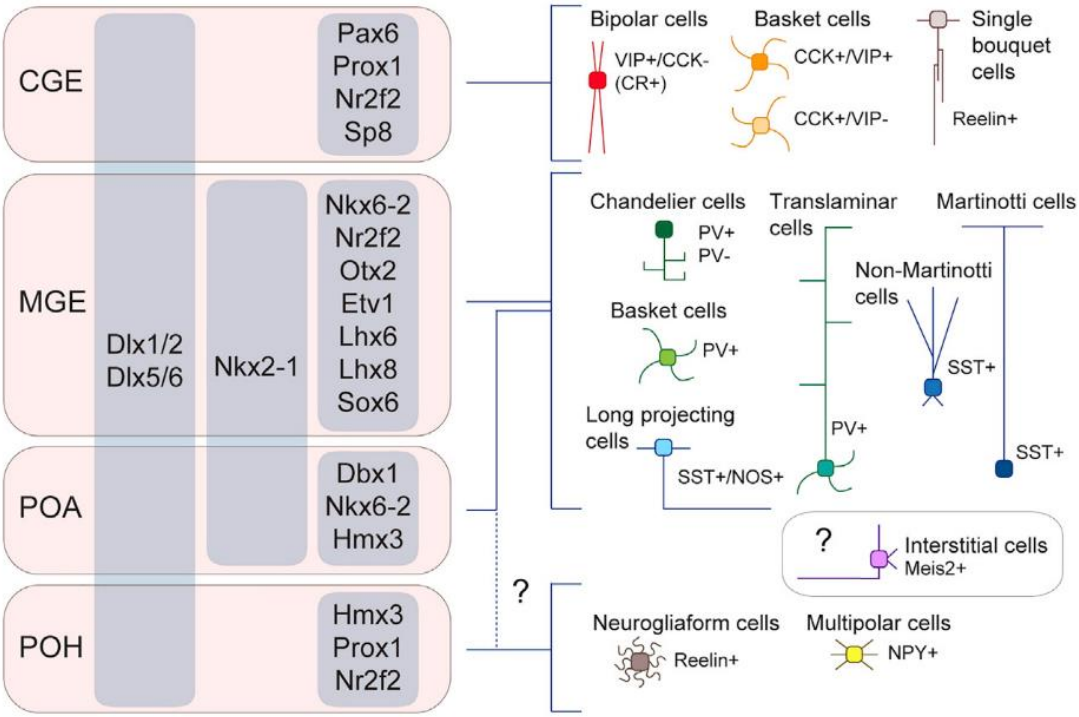

Figure 2. Cortical interneuron subtypes and their developmental origin
This schematic figure displays the distinct parts of the embryonic subpallium and their interneuron derivates. On the left side, regional transcription factors are indicating the different molecular regulation of each subpart of the ganglionic eminences (grey columns). The right side displays the distinct interneuron subtypes with their specific protein profile and morphology. Developmental lineages are represented with blue connecting lines. The precise lineage of Meis2-positive interstitial cells (purple), reelin-positive neurogliaform cells and multipolar cells (brown) is unclear (dashed lines), they might originate from the CGE or/and the preoptic region. CGE: caudal ganglionic eminences; MGE: medial ganglionic eminence; POA: preoptic area; POH: preoptic-hypothalamic border domain; VIP: vasoactive intestinal peptide; CCK: cholecystokinin; PV: parvalbumin; SST: somatostatin; NOS:, NPY: neuropeptide Y; Meis2: myeloid ecotropic viral integration site 1 homolog 2. Figure is adapted from Lim et al., 2018.

Upon chemo-attractive signaling, one of the branches stabilizes and the cell body moves towards that direction. Physiologically this movement is very similar to radial migration mentioned earlier. The regulation of tangential migration is region-specific (Marín, 2013) and is driven by chemoattractant and chemorepulsive signaling including the Ephrin, Semaphorin-neuroligin and Slit-Robo signaling pathways (Rudolph et al., 2014; Steinecke et al., 2014; Zimmer et al., 2008). MGE-driven interneurons leave the germinative niche upon

sensing a chemorepulsive signal provided by the Eph/ephrin family (Steinecke et al., 2014). Semaphorin 3A and semaphorin 3F are membrane-targeted proteins, expressed by striatal cells. Migrating interneurons detect the repulsive signal via semaphorin receptors such as neuropilins and they avoid the striatum during tangential migration (Marín et al., 2001). Another guiding molecular complex, the protein Slit (Slit guidance ligand) and its receptor Robo (Roundabout homolog) which is also responsible for striatal avoidance (Hernández-Miranda et al., 2011). Activation of both semaphorin and Slit/Robo signaling results in the actin-dependent collapse of the leading process, through small GTPAses (Peyre et al., 2015). In contrast to all the repulsive signals, the dorsal cortex secretes chemoattractive signals, such as brain-derived neurotrophic factor (BDNF) and neuregulins (Flames et al., 2004; Polleux et al., 2002). Different isoforms of neuregulins are expressed along the migration paths, which activate the ErbB4 (Erb-B2 receptor tyrosine kinase 4) receptor on the leading processes of interneurons (Flames et al., 2004).

1.5.2. Cortical invasion

Once migrating neurons reach the PSB, they enter the cortex through two distinct migration streams carefully avoiding the cortical plate (Marín, 2013). Instead, they use the MZ and SVZ tracks (Lavdas et al., 1999; López-Bendito et al., 2004). The choice of migratory stream is based on the subtype and origin of the interneuron. Although fluorescently labelled GABAergic cells of all kinds of origins migrate through the SVZ stream, researchers found that half of the SST-positive interneurons, especially future Martinotti cells and PV-positive translaminar cells, preferentially use the MZ route (Lim et al., 2018).

Cortical tangential migration is regulated by chemokine signaling. SVZ and MZ migratory tracks contain high concentration of the chemoattractant Cxcl12 (C-X-C Motif Chemokine Ligand 12) which is secreted by TBR2-positive intermediate progenitor cells and the leptomeninges (López-Bendito et al., 2008; Sessa et al., 2010). The activation of chemokine receptors Cxcr4 and Cxcr7 on the surface of leading protrusion by Cxcl12 promotes the locomotion of interneurons (Wang et al., 2011). Moreover, ablation of both

receptors results in an altered laminar and regional distribution of interneurons (López-Bendito et al., 2008; Wang et al., 2011).

1.5.3. Laminar allocation

The different types of interneurons share the same cortical layers albeit with different connectivity (Tremblay et al., 2016). Previously, it was thought that interneurons, like pyramidal cells, populate the cortical layers in an inside-out manner (Kriegstein and Noctor, 2004), however it was shown that CGE-driven interneurons preferentially populate the superficial layers, therefore the origin or birthdate do not determine the layering distribution of interneurons (Miyoshi and Fishell, 2011). Nevertheless, GABAergic cells from different parts of the GE arrive to the cortex at different timepoints. First, the MGE-driven SST-positive cells enter the cortex, followed by the PV-positive population (Wonders and Anderson, 2006). Later, the VIP- and the NPY-positive cells invade the cortex from the CGE and lastly the reelin-positive CGE-driven cells arrive and localize the cortical layer 1 (Yozu et al., 2004). The laminar allocation of interneurons is regulated by several factors. Chemokine signaling is important during tangential dispersion, but when cells change to radial migration they lose their responsiveness to Cxcl12 (Li et al., 2008). Parallel to this, developing excitatory cells control the position of interneurons in a subtype specific manner (Lodato et al., 2011). This idea is proven by the fact that aberrant cortical layering modifies the locations of inhibitory cells (Lodato et al., 2011; Pla et al., 2006). Moreover, pyramidal cells secrete neuregulin 3 during tangential migration, which guides allocating interneurons via the ErbB4 signaling (Bartolini et al., 2017). Once interneurons change to radial migration, they start to express Cx43, which establishes tight connections between the radial glia fibers and the cells (Elias et al., 2010).

The two main neurotransmitters, GABA and glutamate, are both promoting neuronal migration as excitatory signals, through depolarizing the plasma membrane and evoking Ca^{2+} mediated transients in the cells (Wang and Kriegstein, 2009). Interneurons begin to express KCC2, a potassium-calcium exchanger during their final phase of migration. Upregulation of KCC2 reverses the chloride potential in the migrating interneurons and makes GABA as hyperpolarizing signal (Ben-Ari, 2002; Bortone and Polleux, 2009). This phenomenon is

termed as “GABA switch” is indispensable for the proper maturation and differentiation of interneurons (Bortone and Polleux, 2009; Miyoshi and Fishell, 2011).

1.6. Developmental cell death during cortical development

In the process of brain development, a lot more cells are born than get utilized in the final neuronal circuits. In addition, transient cell populations like Cajal-Retzius cells and subplate cells also have to be eliminated for normal postnatal development. Accordingly, a complex cell death mechanism is developed to maintain the balance between the cell production and the functionally active cell number (Wong and Marín, 2019). Three classical cell death types are responsible for maintaining this balance: apoptosis, necrosis and autophagy (Galluzzi et al., 2018). Programmed cell death or apoptosis is the most common mechanism in the developing brain (Wong and Marín, 2019).

Programmed cell death is achieved in two different manners, the intrinsic and the extrinsic signaling pathways. The intrinsic apoptotic pathway is initiated by endogenous processes, which can change the permeability of the mitochondrial membrane, therefore pro – and anti-apoptotic proteins can be released from the outer membrane space and interact with each other (Hollville et al., 2019). After pro – apoptotic proteins, such as cytochrome c (CytC) is released to the cytoplasm, they interact with apoptosome forming proteins and trigger initiator and effector caspases. The cleavage of caspase-3 (CC3) is the last step in this pathway, functioning as a point of no return, causing irreversible DNA and mitochondria fragmentation which leads to the ultimate disruption of cell morphology (Kondratskyi et al., 2015). In contrast, the extrinsic pathway is mediated by death receptors. Upon ligand binding, these receptors undergo conformational changes and establish a complex with initiator caspases which in turn are activating the effector caspases (Galluzzi et al., 2018).

Three typical cell death waves are present during corticogenesis. The first occurs in the VZ and SVZ during the proliferation and controls the number of progenitors. The second is responsible for the elimination of dispensable pyramidal cells, and the third wave is the disposal of inactive interneurons (Wong and Marín, 2019). A recent study using stereological methods found that approximately 13% of pyramidal cells undergo programmed cell death between postnatal day 2 and 5 (Wong et al., 2018). It is important to note that pyramidal cell

death is different between cortical layers and it is highly dependent on neuronal activity (Blanquie et al., 2017). Approximately 30% of interneurons die the first two weeks of postnatal development (Southwell et al., 2012), however the elimination pathway and its time window differs between interneuron subtypes. The survival of interneurons from the MGE is mostly determined by local pyramidal cell activity. In the absence of pyramidal synaptic transmission, inactive interneurons upregulate the AKT pathway inhibitor PTEN (Phosphatase And Tensin Homolog) which triggers cell death between postnatal day 5 and 10 (Wong et al., 2018). Meanwhile, CGE-driven interneurons undergo programmed cell death later than MGE interneurons, around P12-22 (Priya et al., 2018). The survival of these cells is also activity-dependent, and regulated by a calcium-dependent phosphatase, called calcineurin (Priya et al., 2018). Conclusively, subtype-specific interneuron cell death seems to proceed based on their neurogenic sequence (Wong and Marín, 2019).

1.7. Cadherin superfamily

Cadherins are Ca^{2+}-dependent adhesion proteins that are responsible for establishing cell to cell connections. The first cadherin-like ancestor appeared approximately 600 million years ago in early metazoans. Since then, the cadherin superfamily evolved and expanded greatly, owing the emergence of multi-layered tissues and functionally highly specialized organs (Gul et al., 2017). The human genome encodes 114 different cadherin proteins, which are classified into three functionally and structurally different groups. The major cadherin class includes 32 members, the protocadherin branch has 65 proteins and the cadherin-related subfamily contains 17 molecules (Gul et al., 2017). Despite the high diversity of cadherin molecules, they also share structural similarities. With the exception of Cdh13, they all have a transmembrane domain which is connected to cadherin motifs or extracellular (EC) domains at the N-terminal. The number of EC domains shows high variation between cadherin subgroups (Hirano and Takeichi, 2012). EC domains maintain the connection with the partner cell through a conserved tryptophan residue settled in the so-called adhesion arm. Cadherin molecules usually are connected in a homophilic manner however evidence shows that different types of cadherins can also interact in a heterophilic way (Katsamba et al.,

2009). At the cytoplasmic side of the transmembrane domain cadherins interact with several different proteins to regulate adhesion-based intracellular signaling (Gul et al., 2017).

1.7.1. Cadherin subfamilies

The major cadherin branch consists of the classic cadherins, desmosomal cadherins, T-cadherin, Flamingo or Celsr cadherins and the 7D family (Hirano and Takeichi, 2012). The classical cadherins, such as E-cadherin and N-cadherin have five EC domains which provide the platform for Ca^{2+} binding. Once Ca^{2+} attaches, grooves between the EC domains, it stabilizes the cadherin EC structure and allows it to interact with the connection partner (Loh et al., 2019). The Flamingo/Celsr has seven transmembrane domains and a long complex extracellular part which is important in the formation of cell polarity. T-cadherin is a unique member of the cadherin family as it lacks the cytoplasmic domain, instead it is connected to the extracellular surface via a GPI (Glycosylphosphatidylinositol) anchor (Hirano and Takeichi, 2012).

The protocadherin family is divided into two subclasses, the clustered and non-clustered groups. Clustered protocadherin encoding genes are located in chromosome 5 in three clusters, each including more than ten genes. Meanwhile non-clustered protocadherins are translated from different chromosomes (Mountoufaris et al., 2018). Although protocadherins and classic cadherins share some common features, protocadherin-based adhesion is weaker, therefore the general view is that protocadherins act as specific “bar codes” on the plasma membrane and mediate cellular signaling in a cell type specific manner (Rubinstein et al., 2017).

The cadherin-related family is the most diverse group. Proteins from the calsyntenin subfamily have two EC domains and they have a major role in kinesin dependent vesicular transport. Calsyntenin was reported as an important molecular player of axonal branching, synaptogenesis and synaptic plasticity (de Ramon Francàs et al., 2017). Dachsous (DCHS1,2) and FAT (Protein Fat Homolog 1-4) are the longest of the cadherins, with more than 20 EC domains. They interact with each other in a heterophilic manner. Mutations in DCHS1 and FAT4 cause the Van Maldergem syndrome with serious developmental deficits such as cortical migration defects and increased proliferation which lead to periventricular

heterotopia, the displacement of neurons below the white matter (Cappello et al., 2013). Cadherin-related 15 (Cdhr15) and cadherin-related 23 (Cdhr23) bind to each other and have an important regulatory role in inner-ear mechanotransduction (Araya-Secchi et al., 2016).

1.7.2. Cadherin-binding proteins

The cytoplasmic domain of classic cadherins is connected to cadherin-associated proteins with diverse cellular functions. p120catenin (or CTNND1, Catenin Delta 1) and β-catenin directly bind to the juxtamembrane region and the C-terminal of cadherins, respectively. Both proteins contain armadillo repeats, a repetitive amino acid sequence which includes the cadherin-catenin binding site (Gul et al., 2017). Secondary catenin-binding proteins are the α-catenin and the vinculin, both of which link the adhesion complex to the actin cytoskeleton (Figure 3; Shapiro and Weis, 2009). This cadherin-catenin molecular complex allows the control of cell fate determination by direct transcriptional regulation via β-catenin/Lef binding and cell motility through p120 which accesses to the microtubular system (Hirano and Takeichi, 2012; Stocker and Chenn, 2015). In vertebrates, β-catenin is duplicated and its paralogue gamma-catenin or plakoglobin creates an adhesion complex called desmosome or macula adherens with the two desmosomal cadherins, desmocollin and desmoglein (Schmidt and Jäger, 2005).

Cadherin based adhesion positively regulates the canonical Wnt (Wingless-Type MMTV Integration Site Family) signaling pathway (Figure 3; Gao et al., 2014). Wnt ligands are approximately 400 amino acid long glycoproteins. In the classical view, Wnt ligands bind to the seven transmembrane receptor Frizzled (Fzd) and its co-receptor the lipoprotein receptor related protein 6 (LRP6) which together interact with the intracellular scaffold protein dishevelled (DVL; Acebron and Niehrs, 2016). This interaction leads to the phosphorylation of LRP6 by glycogen synthase kinase 3β (GSK3β) and casein kinase 1 (CK1). The phosphorylated LRP6 accretes the scaffold proteins, axin and APC (Adenomatous Polyposis Coli Protein) to the plasma membrane and allows the cytoplasmic accumulation and nuclear transport of β-catenin where it can activate gene transcription through the LEF1/TCF transcription factor complex. In the absence of a Wnt ligand, β-

DOI:10.14753/SE.2020.2378

catenin is associated with a destruction complex composed of axin, APC and phosphorylated by GSK3β and CK1 for final degradation by the proteasome (Acebron and Niehrs, 2016).

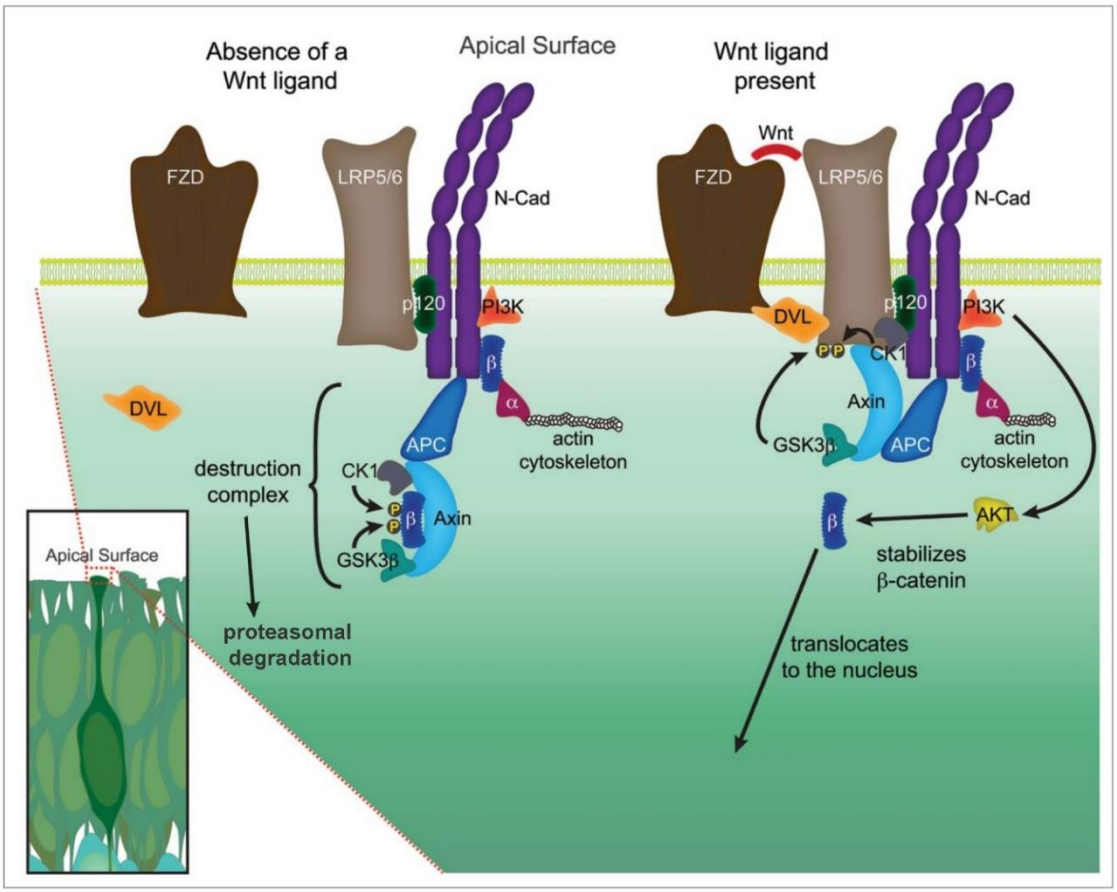

Figure 3. Canonical Wnt/ β-catenin signaling

The adherens junction is built up by cadherin dimers (here N-cadherin) and its associated molecules localized at the apical surface of neural progenitor cells. In the absence of Wnt ligand, β-catenin (β) undergoes phosphorylation by the destruction complex which leads to its ubiquitination and proteasomal degradation. In contrast, in the presence of Wnt ligand, FZD (Frizzled) and LPR5/6 (lipoprotein receptor related protein 5/6) are connected by DVL (Dishevelled) and the phosphorylated by glycogen synthase kinase 3β (GSK3β) and casein kinase 1 (CK1). This leads to the attachment of scaffold protein axin and APC (Adenomatous Polyposis Coli Protein) to the plasma membrane. In this case the destructive complex is unable to eliminate β-catenin, therefore it can regulate gene expression after nuclear translocation. In addition, N-cadherin also triggers β-catenin transcriptional activation through the phosphorylation of AKT by PI3K (Phosphoinositide 3-kinases). β-catenin mediated signaling regulates the actin cytoskeleton via α-catenin (α). Figure was adopted and modified from Stocker and Chenn, 2015.

1.8. N-cadherin function during embryonic cortical development

During the neurogenic phase of the developing embryonic cortex, N-cadherin is highly expressed in the adherens junction belt at the ventricular surface of both the pallium and subpallium, as well as in the intermediate zone and in the cortical plate (Kadowaki et al., 2007; László et al., 2019). Interestingly, these layers include mainly polarized cells, which suggest the functional importance of cadherin in regulating morphological changes. N-cadherin is vital in progenitor maintenance and identifies the apical side of progenitor cells (Zhang et al., 2010). After asymmetric cell division the position of N-cadherin also directs the formation of the leading process to face the basal surface (Gärtner et al., 2015). Moreover, N-cadherin at the basal side regulates the recruitment of the centrosome and the Golgi apparatus, which are indispensable for neuronal migration. This dual cellular distribution of the protein highlights its diverse function in every step of cortical development (Hansen et al., 2017).

1.8.1. N-cadherin in the neuroepithelium and in progenitor pools

After neuronal tube closure, classic epithelial cells downregulate the tight junction protein, so-called occludin and upregulate N-cadherin resulting in a rosette-like shape at the ventricular surface of the developing cortex (Aaku-Saraste et al., 1996; Gänzler-Odenthal and Redies, 1998). The role of N-cadherin-based adhesions and signaling during progenitor pool expansion is highly investigated in different animal models. Blocking N-cadherin function in chicken embryos resulted in the disruption of proper neuroepithelial organization (Gänzler-Odenthal and Redies, 1998). In addition, zebrafish and murine models revealed, that mutations in the *Cdh2* gene cause neuronal displacement, increased mitosis and embryonic lethality at approximately 72 hours and 10 days post-fertilization respectively (Lele et al., 2002; Radice et al., 1997). Later, a conditional knockout study using a neocortical selective promoter showed gross morphological changes in the developing cortex, clusters of cells protruded into the lateral ventricles and the radial glia organization was also disrupted. Furthermore, mispositioned progenitor cells, increased proliferation and an overall thicker cortex was observed in these animals (Gil-Sanz et al., 2014; Kadowaki et al., 2007).

1.8.2. N-cadherin as a regulator of cell fate commitment

N-cadherin-connected catenins not only support cell-cell connections but are also able to recruit several molecules to form a multi-functional signaling hub (Figure 3). This network is crucial in progenitor pool maintenance in the developing telencephalon (Stocker and Chenn, 2015). N-cadherin homophilic binding activates protein kinase B (PKB, also known as AKT) thereby inducing pro-survival signaling through the phosphorylation of β-catenin (Zhang et al., 2010). In addition, activation of Wnt signaling also promotes progenitor state maintenance and stabilizes cell-cell connections via PAX-6 mediated positive feedback regulation (Gan et al., 2014; Gao et al., 2014) therefore progenitor cells are able to inhibit their own differentiation (Zhang et al., 2010, 2013). Accordingly, loss of β-catenin causes progenitor pool disassembly and brain malformations, in contrast gain-of-function experiments reveal increased progenitor pool and gyrification-like phenotypes in the embryonic mouse brain (Chenn and Walsh, 2003; Junghans et al., 2005). It has been proposed that Notch signaling-associated Numb proteins are important regulators of N-cadherin localization. Numb is localized primarily in the proximity of N-cadherin and interacts with p120catenin to maintain the N-cadherin-based intercellular connections thereby preserving the progenitor state (Rasin et al., 2007). N-cadherin connections also contribute to neurogenesis via Notch signaling (Hatakeyama et al., 2014). In contrast, the proneural gene, Ngn2 negatively regulates the levels of N-cadherin via the expression of Foxp2 and 4 (forkhead domain protein 2 and 4) transcription factors, in this way promoting differentiation and delamination (Rousso et al., 2012). During physiological delamination, the downregulation of N-cadherin fosters the cilium disassembly and apical abscission (Das and Storey, 2014). Finally, the localization of the remaining N-cadherin determines the origin of the future leading trail for radial migration by repositioning and stabilizing centrosomes (Gärtner et al., 2012).

1.8.3. N-cadherin role during cell migration

Neuronal migration is a dynamic and well-regulated process, and without proper adhesion it cannot be completed (Franco et al., 2011; Luccardini et al., 2013). Both excitatory and inhibitory cell migration are regulated by cadherin-based adhesion (Kon et al., 2017;

Luccardini et al., 2015). However, it is important to note, that the role of N-cadherin-mediated signaling during glutamatergic cell development has been more thoroughly investigated than in migration of interneuron precursors.

During glial-guided locomotion of glutamatergic precursors, N-cadherin is expressed in the leading process and maintains a reversible adhesion between the radial glia scaffold and the postmitotic cell. The turnover of N-cadherin is mediated by endocytic vesicle-associated Rab-GTPases (Hor and Goh, 2018; Kawauchi et al., 2010; Linford et al., 2012). Internalized proteins can undergo lysosomal degradation or they can get recycled into the plasma membrane (Cadwell et al., 2016). In addition, metalloproteases ADAM9 and 10 (disintegrin and metalloprotease domain 9 and 10) directly control the shedding of N-cadherin in a Rab14-dependent manner (Linford et al., 2012). Cleavage of the extracellular domains of N-cadherin by ADAM proteins results in the redistribution of β-catenin from the cell membrane to the cytoplasmic pool and initiates β-catenin-mediated gene expression (Linford et al., 2012; Reiss et al., 2005).

MZ-derived reelin promotes neuronal migration through Rap1 GTPase and triggers the AKT signaling pathway to enhance N-cadherin-based connection forming (Jossin and Cooper, 2011; Matsunaga et al., 2017). Once bipolar cells arrive to the CP, they peel off from the radial fiber by lysosomal degradation of N-cadherin in a Rab7-dependent manner (Kawauchi et al., 2010). This process is also induced by reelin, which regulates cytoskeletal dynamics through the phosphorylation of Dab1 (disabled homolog 1). Activation of Dab1 promotes the direct phosphorylation of cofilin and inhibits the actin-depolymerization, causing the leading process attachment to the MZ (Chai et al., 2009). Activation of Dab1 recruits Rap1 GTPase which has a dual function. It stabilizes the growth cone of the leading process via integrin – fibronectin connections (Sekine et al., 2012) and helps to establish homophilic N-cadherin connections between the neurons and Cajal-Retzius cells (Franco et al., 2011; Gil-Sanz et al., 2013; Jossin and Cooper, 2011). This tight connection allows postmitotic neurons to translocate their soma and begin their integration into the cortical layers (Franco et al., 2011).

In case of interneuron migration, *in vivo* data showed that selective elimination of N-cadherin from MGE-driven cells causes tangential migration delay and the disruption of cortical invasion (Luccardini et al., 2013). Accordingly, *in vitro* results refer that the presence of N-cadherin promotes IN migration, as its downregulation leads to impaired cell motility and leading process formation. These changes are mainly caused by defects in the polarization and the centrosome localization in these cells (Luccardini et al., 2013, 2015).

1.9. The endocannabinoid system

1.9.1. Endocannabinoid mediated retrograde neuronal transmission

Endocannabinoids are plasma membrane-derived lipid molecules, which mediate specific retrograde signaling in the mature synapses via cannabinoid receptors. These molecules have similar molecular architecture to the psychoactive compound of *Cannabis sativa*, called THC (Δ9-tetrahydrocannabinol). The two main endocannabinoids present in the brain are 2-arachydonoyl-glicerol (2-AG) which has high affinity to the G protein-coupled cannabinoid receptor 1 and 2 (CBR1, CBR2) and anandamide (AEA) which serves as a partial agonist of CBRs (Di Marzo, 2018) but binds to TRPV1 (transient receptor potential vanilloid receptor 1) and PPAR (peroxisome proliferator-activated receptor) receptors (Di Marzo, 2018) with higher affinity. The endocannabinoid system is evolved to control neuronal network activity (Figure 4) as a negative feedback regulator of synaptic transmission (Katona and Freund, 2008). Briefly, Ca^{2+} influx into the boutons during neuronal activity triggers neurotransmitter-containing vesicle release at the synapse. Receptors at the postsynaptic density bind these neurotransmitters and transmit the signal via secondary messenger molecules (Piomelli, 2003). These GABA or glutamate receptors are connected to the so-called postsynaptic machinery which includes a molecular cascade carrying out the synthesis of 2-AG. Then, the postsynaptically released endocannabinoid travels back to the presynapse through the synaptic cleft and activates the CBR1, which in turn inhibits the voltage-gated calcium channels via G-proteins thereby decreasing synaptic transmission (Katona and Freund, 2012). 2-AG is mainly synthesized by DGLα or β (diacylglycerol-lipase α or β) and is degraded in the presynapse by MAGL (monoacylglycerol lipase) to arachidonic acid and glycerol (Figure 4; Wang and Ueda, 2009).

In contrast, AEA is mainly produced by NAPE-PLD (N-acyl phosphatidylethanolamine phospholipase D) and is cleaved by FAAH (fatty acid amide hydrolase) to arachidonic acid and ethanolamine (Figure 4,Hussain et al., 2017). It is important to note, that meanwhile 2-AG synthesis is dependent on DGL availability, AEA can be produced via several pathways incorporating many other lipases (Tsuboi et al., 2018).

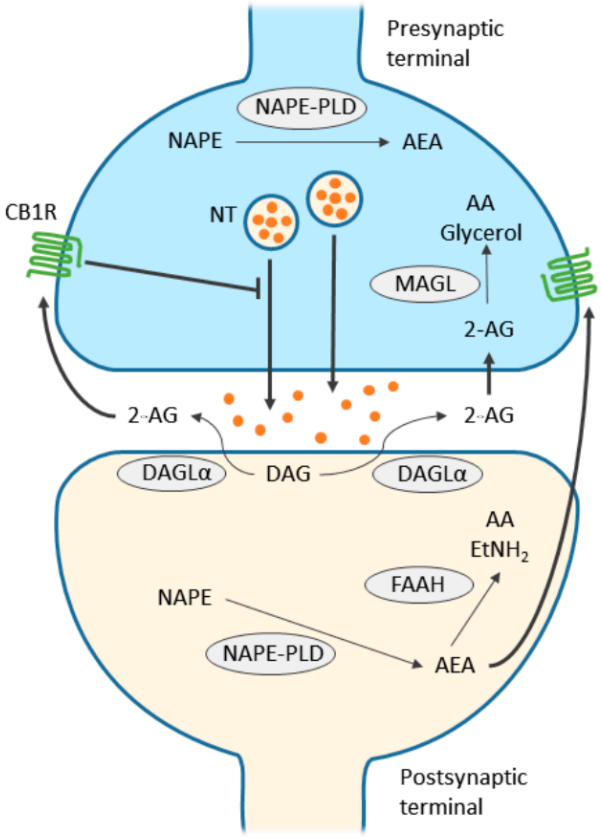

Figure 4. CB1 receptor-mediated endocannabinoid signaling
Schematic figure shows the main synaptic functions of endocannabinoids. 2-AG (2-arachydonoyl-glicerol) is synthesized by DGLα (diacil-glycerol lipase α) from diacil-glycerol (DAG) at the postsynaptic region, diffuses through the synaptic cleft and binds to presynaptic CB1 receptors (cannabinoid receptor 1). Activation of CB1 receptor leads to the termination of neurotransmitter release. Then, 2-AG is cleaved by MAGL (monoacylglycerol lipase) to arachidonic acid and glycerol. NAPE-PLD (N-acyl phosphatidylethanolamine phospholipase D) is responsible for the synthesis of AEA (anandamide) both pre- and postsynaptically. AEA might have both autocrine and paracrine effect on CB1 receptors. Finally, fatty acid amide hydrolase (FAAH) degrades AEA to AA and ethanolamine. Figure was adapted from Zou and Kumar, 2018.

DOI:10.14753/SE.2020.2378

1.9.2. The function of the endocannabinoid system during cortical development

1.9.2.1 Endocannabinoid function during proliferation and differentiation

The level of the two main endocannabinoids is increased during embryonic development in rodents and peaks in the first two weeks of postnatal development. Accordingly, enzymes which are responsible for the metabolism of 2-AG display the same expressional tendency (Maccarrone et al., 2014). However, the AEA synthesizing enzyme NAPE-PLD becomes enzymatically active only in the first postnatal week (Morishita et al., 2005), hence the enzyme responsible for embryonic production of AEA is still unknown.

In the embryonic brain CB1 receptor shows gradual expression along the apico-basal axis of the embryonic cortex with the lowest levels being displayed in the ventricular zone (Berghuis et al., 2007; Galve-Roperh et al., 2013). Genetical ablation of CBR1 causes the disappearance of SVZ progenitors and the decrease of proliferating cells in the VZ. In contrast, more progenitor cells were found in the embryonic cortex of FAAH knockout animals, which reveals a function of AEA in proliferation (Mulder et al., 2008). Moreover, not just FAAH and CBR1 knockout animals display radial migration defects but using CBR1 and FAAH antagonists also produces the same effect (Mulder et al., 2008). In addition, prenatal exposure to the CBR1 agonist WIN 55,212-2 impairs the radial and tangential migration, furthermore increases the number of TBR2-positive intermediate progenitor cells (Saez et al., 2014). Another study used transient silencing of the CBR1 via *in utero* electroporation of small interfering RNA, which resulted in the overall impairment of radial migration (Díaz-Alonso et al., 2017). Overall, these *in vivo* experiments propose the existence of an endocannabinoid regulatory pathway which controls embryonic cortical proliferation and migration. Additionally, *in vitro* studies claimed that activation of CB1- and CB2- receptor mediated signaling promotes neuronal progenitor cell proliferation and differentiation (Díaz-Alonso et al., 2012) through the activation the AKT-pathway, which leads to the phosphorylation of Gsk3β and triggers the nuclear translocation of β-catenin (Trazzi et al., 2010).

AEA was shown to inhibit neuronal differentiation by inactivating the ERK-(extracellular-signal regulated kinase) pathway, thereby disrupting cytoskeletal dynamics via small GTPases (Rueda et al., 2002). Controversially, CB1 receptor agonist such as THC, AEA, 2-AG and other chemical compounds could promote the phosphorylation of ERK signaling, which is important in cell growth and survival (Berghuis et al., 2007; Derkinderen et al., 2003). Despite that several *in vitro* studies couple the endocannabinoid signaling with other pathways, more experiments are required to unfold their precise mechanism of action.

1.9.2.2 Endocannabinoid signaling in axonal guidance and behavior

The function of endocannabinoid signaling in neurite outgrowth and synaptogenesis was highly investigated in the last decades. Although the paracrine endocannabinoid signaling is crucial for fine-tuned neuronal communication in the mature brain, in the embryonic brain this is done in an autocrine manner (Keimpema et al., 2011). The CBR1-mediated 2-AG signaling was reported to regulate axonal growth in the cortex. The corticofugal axons target subcortical regions, meanwhile deep layer pyramidal cells establish connections with the thalamus through thalamocortical axons. During axonal growth these trans-regional connections are grown facing each other and use the endocannabinoid signaling to differentiate themselves from each other (Keimpema et al., 2011). Corticofugal axons express CBR1 and DGLα in the growth cone and MGL in the stabilized axonal part, in contrast thalamocortical axons express only MGL. During neurite outgrow, 2-AG acts as an autocrine signal for corticofugal axons and promote their elongation through CBR1, meanwhile 2-AG also behaves as a paracrine signal and triggers corticofugal axonal fasciculation (Keimpema et al., 2010). Thalamocortical axons perceive 2-AG and break it down via MGL, therefore these axons can limit endocannabinoid signals for corticofugal axons and regulate their normal fasciculation and distribution (Maccarrone et al., 2014). In addition, these axonal tracks maintain the migratory route of CB1 receptor-positive interneurons (Morozov et al., 2009). An *in vitro* study using interneuron culture claimed that CBR1 is located at the tip of the axonal filopodia and regulates the growth cone motility. Application of AEA triggered the translocation of CB1 receptors from the tip to the center of

the growth cone, which promoted the phosphorylation of ERK and the repulsion of neurites by the activation of RhoA (Berghuis et al., 2007). Additionally, other receptor families can transactivate CBR1 and regulate endocannabinoid mediated cell viability and cytoskeletal changes in an autocrine manner (Berghuis et al., 2005; Williams et al., 2003). Activation of receptor tyrosine kinases (RTK) including FGFR (fibroblast growth factor receptor) or TrkB and TrkA (tropomyosine receptor kinase A and B) enhances the synthesis of 2-AG which acts cell-autonomously and regulate cell motility and microenvironment (Berghuis et al., 2005; Zhou et al., 2019). On the other hand, upon ligand binding, RTK receptors dimerize and support cell survival through AKT and ERK signaling cascades (Keimpema et al., 2013; Williams et al., 2003; Zhou et al., 2019).

1.9.3. The medical relevance of cannabinoids

Medical marihuana, regularly used in treating morning sickness and nausea during pregnancy is related to long-term behavioral changes, mental disorders and higher vulnerability to drug addiction and alcoholism in adulthood (Frau et al., 2019; de Salas-Quiroga et al., 2015). Moreover, this effect is inherited in transgenerational manner due to epigenetic mechanisms (Szutorisz and Hurd, 2018). Therefore, better understanding of endocannabinoid-mediated signaling during brain development could help in the establishment of novel therapeutics or preventive medicine for neuropsychiatric problems caused by prenatal cannabis exposure.

DOI:10.14753/SE.2020.2378

2. Aims

Mammalian cortical complexity is a result of tightly regulated combination of proliferation, differentiation and migration processes. The comprehensive role of N-cadherin (*Cdh2*) during proliferation and radial migration in the dorsal telencephalon has been highly investigated in the last decades. In contrast, almost nothing is known about its *in vivo* regulatory function of cell death processes. Also, the role of N-cadherin during interneuron precursor migration, particularly in its postmitotic stage has not been investigated in detail, either. Considering the complex role of N-cadherin during glutamatergic cell development, its malfunction likely to increase the risk of various cortical developmental disorders. Therefore, the examination of cadherin-based cell connections and signaling during pathophysiological circumstances, such as abnormal delamination or teratogenic insults, is fundamental. Thus, our specific aims in this study were the following:

1. To investigate the role of N-cadherin in postmitotic interneuron migration and differentiation
    - Establish a mouse model in which N-cadherin-deficient migrating postmitotic interneurons can be monitored
    - Describe the interneuron migration phenotype in the absence of N-cadherin
    - Investigate the consequences of N-cadherin abolishment from postmitotic neurons in the early postnatal and adult mouse brain
2. To examine the outcome of adherens junction disruption and its mechanism during cortical development
    - Evaluate and characterize the effect of dominant-negative model of cadherin-based adherens junction disruption on glutamatergic cell development
    - Examine the role of endocannabinoid signaling in the molecular mechanism of pathophysiological delamination
    - Investigate the signaling of potential teratogenic insult which is known to initiate delamination and migration defects in the embryonic cortex

DOI:10.14753/SE.2020.2378

3. Material and Methods

3.1. Animals

All animals were kept in standard laboratory conditions and were maintained according to protocols approved by the Hungarian Committee of the Scientific Ethics of Animal Research (license numbers: XIV-1-001/2332-4/2012 and PE/EA/354-5/2018). Experiments were carried out according to the Hungarian Act of Animal Care and Experimentation (1998, XXVIII, Section 243/1998), in accordance with the European Communities Council Directive of 24 November 1986 (86-609-EEC; Section 243/1998). C57BL/6 mouse line was ordered from Charles River Laboratories. The Abhd4 transgenic line was made and validated by Benjamin Cravatt's laboratory (Lee et al., 2015). The triple transgenic Dlx5/6i-Cre/Cdh2-floxed mouse line was made by crosses of Dlx5/6i-Cre mouse line (kind gift of J. Rubenstein, UCSF) with $Cdh2^{fl/fl}$ (from Jaxmice strain #07611) then bred with Gad65-GFP mice (López-Bendito et al., 2004). In this study +/+ (wild type) and -/- (knock out) refers to *Dlx5/6i-Cre*$^{+/+}$*;Cdh2*$^{fl/fl}$ and *Dlx5/6i-Cre*$^{Cre/+}$*;Cdh2*$^{fl/fl}$, respectively.

3.2. Genomic DNA extraction and genotyping

Minimal amount of tail tissue was digested with Proteinase K (Thermo Fisher Scientific) in TE-NS buffer (10mM Tris-Hcl at pH10.5; 1mM EDTA; 150 mM NaCl and 0.5% SDS) at 55°C. After tissue was dissolved, solution was separated by centrifugation. Genomic DNA was extracted with ice-cold isopropanol and 70% EtOH from the flow through, and DNA pellet was resolved in autoclaved water. Genotyping was performed by RT-PCR, using BioMix Red (Bioline) PCR mix with the appropriate primers (Table 1.) and template according to the manufacturer's instructions. After DNA amplification, PCR products were separated on 2% agarose gel by gel electrophoresis and visualized by ethidium bromide in UV chamber.

3.3. Sample preparation and sectioning

Adult and postnatal day 8 and 10 (P8-10) animals were anesthetized with a suitable dose of 1,25% avertin (2,2,2, -tribromoethanol and 2-methyl-2-butanol in autoclaved water, Sigma) intraperitoneal injection, perfused transcardially with 4%PFA/ 0,1M PB and brains were postfixed overnight in the same solution. Next day brains were washed in PBS and were

sectioned at 40µm for in situ hybridization and immunohistochemistry on a Leica1000 vibratome (Leica). Sections were collected in 24-well cell culture plates and stored at 4°C until the experimental procedures. Embryonic (E14.5-E18.5) and early postnatal (P1, P3) animals were decapitated, brains were removed from the skull and fixed overnight in 4%PFA/ 0,1M PB solution. To prepare free-floating sections, embryonic and early postnatal brains were embedded in 2% agarose (Sigma) and sliced 50 µm thin sections with vibratome. For cryostat sectioning embryonic heads were cryoprotected in 15 and 30% sucrose/PBS solution overnight. Afterwards, tissue was embedded in Tissue-TEK OCT compound (Sakura) and 20 µm thick cryosections were collected on Superfrost Ultra Plus glass slides (Thermo Fisher Scientific) with MICROM HM 550 cryostat (Thermo Fisher Scientific) and stored at -20°C until further experiments.

3.4. DNA constructs and cloning protocols

Mouse N-cadherin was cloned via RT-PCR using embryonic and adult cDNA as template with Long-template PCR mix according the manufacturer's instructions (Roche) (Table 1.). The clone was sequenced then a dominant negative version of N-cadherin was created (ΔnCdh2) by OliI-HindIII digestion, followed by Klenow fill-in of the HindIII-overhang and religation of the plasmid. This creates a molecule which lacks all EC domains but contains the signal sequence followed by the transmembrane and intracellular domains essentially reproducing the molecule used earlier by others (Fujimori and Takeichi, 1993; Kintner, 1992; Nieman et al., 1999). Mouse Abhd4 was also cloned via RT-PCR from E16 embryonic cDNA as template using the same way as described above. A shorter, 418bp fragment of Abhd4 was cloned separately to use as a template for in vitro transcription of the probe used in situ hybridization experiments. The hydrolase dead version of Abhd4 (inactive Abhd4) was created by site-directed mutagenesis of serine 159 into glycine via PfuI PCR and DpnI digestion of the template plasmid. All the fragments were cloned into pGEMTEasy plasmid (Promega) and sequenced. ΔnCdh2, Abhd4 and Inactive-Abhd4 was then subcloned from pGEMT into the pCAGIG mammalian expression vector (Addgene # 11159; Matsuda and Cepko, 2004), and purified with NucleoBond Xtra Plus EF kit (Macherey-Nagel) based on the manufacturer's protocol. For in situ hybridization on adult mouse brain, RNA was

prepared by Ambion RNAqueous-4PCR kit (Thermo Fisher Scientific). Reverse transcription was performed by Maxima RT Kit (Thermo Fisher Scientific) and fragments were amplified via RT-PCR, using appropriate primers (Table 1.), then cloned into a pGEMT-Easy vector (Promega). Orientation of the incorporated fragment was checked using competent restriction enzymes.

3.5. *In vitro* transcription and in situ hybridization

To generate riboprobes, plasmid was linearized by the 5' end of the insert with proper restriction enzyme and the product was separated with agarose gel electrophoresis followed by fragment isolation (GeneJET Gel Extraction Kit, Thermo Fisher Scientific). *In vitro* transcription was performed by DIG-UTP labeling mix (Roche) and the appropriate RNA polymerase (T3, T7, SP6, Promega). After Dnase treatment RNA probes was purified by RNA Clean & Concentrator kit (Zymo Research). The riboprobes encoded by *Slc17a7* (encoded vGlut1protein) and *Gad1* (encoded Gad67 protein) were made before, see for more details Mayer et al., 2010. Before hybridization, sections were washed with PBSTw (PBS+0.1%Tween20) repeatedly, then change to hybridization buffer without t-RNA (50% formamide, 25% 20XSSC, 0,1 % Tween20 at pH6 by citric acid) for several washes. Prehybridization were done using hybridization buffer with t-RNA(1mg/10ml). RNA probe hybridization was carried out in the same buffer with distinct probes overnight on different temperature (approximately between 60-65°C). Next day slices were washed with serial dilution of SSC/Tween20 solutions: formamide/SSCT, 2xSSCT and 0.2xSSCT, all at 65°C then sections were rinsed in PBSTw at room temperature (RT) and incubated in blocking solution (2% FBS, 2mg/ml BSA in PBSTw). To label the hybridized probes, slices were incubated with the anti-DIG Fab fragment (Roche 1:4000) in the blocking solution overnight at 4°C. After extensive (5x15 mins) washes in PBSTw and (3x10mins) TBSTw (0.1M TrisHCl, pH:9.5, 100mM NaCl, 50mM Mg2Cl, 0.1% Tween20) staining was done by using NBT/BCIP solution (Roche) dissolved in TBSTw (1µl NBST+3.5µlBCIP/1mlTBSTw). Signal development was continuously monitored and staining was stopped with PBSTw washes and 4% PFA in PBSTw. Sections were pulled onto glass slides (Thermo Fisher Scientific), mounted with Aqua-Poly/Mount (Polysciences, Inc.) and sealed with nail polish.

DOI:10.14753/SE.2020.2378

Table 1. Primers used for cloning and genotyping

Gene	Primers	Annealing temp.	Fragment Size
Abhd4 genotyping	-GCTGCTATTGGCCGCTGC -GTGCTCTCAGGAAGCATTCTT -GGCACTCAGTGAATCCATGTT	62 °C	+/+: 220 bp -/-: 399 bp
GFP genotyping	-GCACGACTTCTTCAAGTCCGCCATGCC -GCGGATCTTGAAGTTCACCTTGATGCC	57°C	268 bp
Ncad genotyping	-CCAAAGCTGAGTGTGACTTG -TACAAGTTTGGGTGACAAGC	61 °C	290 bp
Cre genotyping	-GCATTACCGGTCGATGCAACGAGTGATGAG -GAGTGAACGAACCTGGTCGAAATCAGTGCG	68 °C	408 bp
Cdh2	-ATGTGCCGGATAGCGGGAGCGC -TCAGTCGTCACCACCGCCGTACATG	57°C	896 bp
Abhd4	-ATGGGCTGGCTCAGCTCGACCCG -TCAGTCAACTGAGTTGCAGATCTCT	57°C	1068 bp
Abhd4 in situ fragment	-CGGCAGGGCTTGTTTACTAT -TCTCCCGCCATGTCTCTATT	57°C	418 bp
Inactive Abhd4	-CCGTGCACCTCCAACCTGGGTCAGGGCTG TGGCATCTGTCC -GGACAGATGCCACAGCCCTGACCCAGGTT GGAGGTGCACGG	62 °C	1068 bp
VIP	-CCTGGCATTCCTGATACTCTTCAG -TTCTCTGATTTCAGCTCTGCCCAG	52°C	527 bp
NPY	-AGAGGCACCCAGAGCAGAG -AATGGGGCGGAGTCCAGCCTAGTG	55°C	471 bp
Reln	-TCGCACCTTGCTGAAATACACAGTG -GCCGCATCCCAAATTAATAGAAAAC	55°C	1176 bp
Calb2	-GATGCTGACGGAAATGGGTACATTG -CCTACCAGCCACCCTCTCTCCATC	55°C	893 bp
Slc1a3 (Glast1)	-TAGGGGCAGGCTGTGTGTGGCTCAC -TCGTTTCTTTGGGGGCTGATTAGGGAC	55°C	406 bp
SST	-TGAAGGAGACGCTACCGAAGCCG -TGCAGGGTCAAGTTGAGCATCG	52°C	544 bp
Cnr1 (CBR1)	-ATGAAGTCGATCTTAGACGGCCTTG -TCACAGAGCCTCGGCAGACGTGTCTG	55°C	14227 bp

3.6. In utero electroporation

Timed-pregnant mouse females were anesthetized (embryonic day 14.5) with 1,25% avertin intraperitoneal injection or isoflurane vaporization. Abdominal cavity was opened next to the linea alba and uterine horns were exposed. Using glass capillary and mouth pipette, approximately 1 µl of expression vector (1-3 µg/µl for all of the constructs, dissolved in endotoxin-free water) with or without the general caspase inhibitor Z-VAD-FMK (5 µM final concentration; BD Biosciences) in endotoxin-free water containing Fast Green (Roth 1:10000 dilution) was injected into the lateral ventricle of the embryo. Electroporation was performed by SP-3c electroporator (Supertech) and tweezer electrodes with 5 pulses of 50 V for 50 millisecond duration with 950 millisecond intervals. After the electrical pulses, uterine horns were returned into the abdominal cavity, muscle walls and skin were sutured, embryos were allowed to develop for the required time (1-3days).

3.7. Fluorescent single-cell mRNA detection (RNAscope)

In order to visualize the plasma membrane of the cells in the ventricular zone, ChR2-GFP (Addgene #26929, Boyden et al., 2005) was electroporated in the embryos. One day later (E15.5) embryos were sacrificed by decapitation and heads were immediately frozen on isopentane/dry ice combination. Frozen embryonic heads were equilibrated in the cryostat at -20°C for 2-3 hours, then embedded in OCT and 20 µm thick cryosections was cut as described above. Cryosections were held in the cryostat until the sectioning was finished. Sections were fixed immediately with cold 10% PFA solution for 30 minutes at 4°C. After fixation, slides were washed with PBS and treated with series of alcohol solution, 50% EtOH/PBS, 75% EtOH/PBS, 100% EtOH each for 5 mins, then slides were incubated in absolute alcohol overnight at -20°C. Next day RNAscope assay (Advanced Cell Diagnostic, Manual Fluorescent Assay AP-FastRed) was performed based on the manufacturer's instructions. Briefly, slides were taken out from the freezer and dried at room temperature (RT) until alcohol was vaporized. Liquid barrier was drawn around the sections and Protease IV digestion was carried out for 10 mins (shorter than recommended in order to preserve the GFP signal). Meanwhile, HybEZ oven was adjusted to 40°C, filter paper was rinsed in distilled water and laid into the cassette to obtain appropriate humidity. *Abhd4* RNAscope

probe was custom designed for Abhd4 full sequence (Mm-Abhd4-O1; 524551; channel 1; 1x dilution) and used with *Tbr2* (Mm-Eomes-C2; 429641-C2; channel 2; 50x dilution) or *Glast1* (Mm-Slc1a3-C2; 430781-C2; channel 2; 50x dilution) separately. After protease treatment, slides were washed in water then treated with the preheated mixed probes in the Hybez oven for 2 hours. Meanwhile, 1x wash buffer was diluted and used in every washing step for 2x2 mins. Altogether 4 amplification steps were done and at the final amplification step *Abhd4* was amplified with Atto-550 dye, *Tbr2* and *Glast1* with Atto-674. After the last washes slides were fixed with 10% PFA for 10 mins and immunohistochemistry was performed to improve the electroporated GFP signal with anti-GFP antibody and Alexa-488 secondary antibody. Finally, slides were washed in PBS and mounted with Vectashield Hard Set (Vector Labs) and sealed with nail polish.

3.8. Immunohistochemistry

Embryonic cryosections, adult free-floating samples or free-floating embryonic sections for STORM imaging were permeabilized by different concentration of Triton X-100/PBS solution and/or with 10mM sodium-citrate at 65 °C depending on the antibody (Table 2., permeabilization column). Sections were then blocked with 5% Normal Donkey Serum (NDS; Sigma) in PBS for one hour. After several washes with PBS, sections were incubated in primary antibody (Table 2.) at 4°C, overnight. The following day samples were treated with secondary antibodies in PBS for 4 hours at room temperature. Finally, sections were washed with PBS and mounted with Vectashield Hard Set and sealed with nail polish. For STORM super-resolution microscopy, sections were mounted onto coverslips and stored uncovered at 4°C until the day of imaging. The primary and secondary antibodies which were used in this study and their properties are listed in Table 2. and Table 3, respectively.

3.9. Cell death detection - TUNEL assay

Cell death was detected by terminal deoxynucleotidyl transferase dUTP nick end labeling (TUNEL) assay according to the official protocol (Millipore, Apoptag Red In Situ Apoptosis Detection Kit). Briefly, free floating sections or slides were permeabilized with 2:1 (v:v) ethanol and acetic acid mixture at -20°C. After PBS washes, equilibration buffer then TDT enzyme solution was applied at 37°C for an hour, then reaction was stopped and

anti-digoxigenin conjugate (rhodamine) was used to visualize the signal of the fragmented DNA. After final washes, slides or sections were mounted as described before.

3.10. BrdU (5-bromo-2'-deoxyuridine) treatment and staining

BrdU in 0.9% saline solution (200 mg/kg –Sigma) was prepared (pH7.4), passed through on a 0.2-μm pore size filter (Millipore) then intraperitoneally injected in the pregnant female mouse at day 14. Two hours later the embryos were decapitated, and heads were fixed with 4% PFA overnight. Next day embryonic brains were sliced in a free-floating manner as described before. Slices were washed quickly in autoclaved water to remove excess PBS and were incubated in 2M HCl solution for 1 hour at 37 °C. HCl treatment is necessary for the antibody to recognize the incorporated BrdU in the DNA. After this, sections were washed for a minimum of an hour with PBS to re-equilibrate the floating slices to pH7.4. After blocking step with 5% NDS blocking solution, sections were incubated in anti-BrdU antibody solution overnight at 4°C (Table 2.). Next day, sections were incubated in secondary antibody and mounted as described before.

3.11. *In vitro* studies

HEK-293 cells were a kind gift from Balázs Gereben (IEM-HAS) and were maintained under normal conditions in plastic dishes with Dulbecco's Modified Eagle Medium (4.5 g/L glucose, L-glutamine & sodium pyruvate, Corning) containing 10% heat inactivated Fetal Bovine Serum (Biosera) in a 5% CO_2 incubator at 37 °C. Cells were seeded a day before transfection, on poly-D-lysine coated coverslips in 24-well cell culture plate. The cells were held in Opti-MEM Media (Gibco) for an hour then transfection was made by using 2 μl Lipofectamine 2000 Reagent (Invitrogen) mixing with1 μg plasmid DNA in Opti-MEM Media. After 20 hours, the transfected cells were washed with PBS and fixed with 4% PFA for 10 minutes. Fixed cells were treated with 0.2 % Triton X 100 for 15 mins in room temperature, and block with 1% Human Serum Albumin (HSA, Sigma) in PBS for 30 mins. Primary antibodies were diluted as listed below (Table 2.) for 1.5 hours at RT. After PBS washing, cells were incubated in secondary antibody solution for an hour. Then cells were washed with PBS and mounted on coverslips with Vectashield Hard Set (Vector Labs). In

case of STORM super-resolution microscopy coverslips were stored in PBS at 4°C until the day of imaging.

Table 2. Used primary antibodies and their properties

Name	Raised in	Dilution	Manufacturer	Permeabilization
Paired box protein-6 (PAX6)	Rabbit	1:300	Biolegend (901301)	10 mM sodium-citrate (60 mins) and 0.1% TritonX/PBS (30 mins)
Cleaved Caspase-3 (CC3)	Rabbit	1:500	Cell signaling (9661S)	0.3% TritonX/PBS (30 mins)
Laminin subunit alpha 1 (LAMA1)	Rabbit	1:500	Sigma (L9393)	0.2% TritonX/PBS (30 mins)
Transcription factor T-box brain 1 (TBR1)	Rabbit	1:500	Abcam (ab31940)	
Transcription factor T box brain 1 (TBR2)	Rabbit	1:500	Abcam (ab23345)	
Phospho-histone H3 (PHH3)	Rabbit	1:500	Millipore (06-570)	
Nestin	Mouse	1:200	Millipore (MAB353)	
5-bromo-2'-deoxyuridine (BrdU)	Mouse	1:400	Sigma (B8434)	2 M HCl (60 mins)
Catalase	Rabbit	1:3000	Abcam (ab1877)	TBS/Tween20 (60mins)
Green fluorescent protein (GFP)	Goat	1:1000	Abcam (ab5450)	0.2% TritonX/PBS (30 mins)
Translocase of outer mitochondrial membrane 20 (TOM20)	Rabbit	1:1000	Santa Cruz (s-11415)	
Cytochrome C (CytC)	Mouse	1:2000	Biolegend (612302)	
Abhydrolase domain containing 4 (Abhd4)	Rabbit	1:500	ImmunoGenes Ltd	TBS/Tween20 (60mins)
Calretinin (Calb2)	Mouse	1:1000	Millipore (MAB1568)	0.3% TritonX/PBS (60 mins)
Somatostatin (SST)	Goat	1:1000	Santa Cruz (sc-7819)	0.3%TritonX/PBS (60 mins)
Parvalbumin (PV)	Goat	1:3000	Swant (PVG214)	0.2% TritonX/PBS (30 mins)

Table 3. Secondary antibodies used in the experiments.

Name	Raised in	Dilution	Company	Cat. number
Anti-Rabbit Alexa 488	Donkey	1:400	Jackson ImmunoReserach Ltd	711-545-152
Anti-Rabbit Alexa 594	Donkey	1:400		711-585-152
Anti-Mouse Alexa 488	Donkey	1:400		715-545-150
Anti-Mouse Alexa 594	Donkey	1:400		711-585-150
Anti-Mouse Alexa 647	Donkey	1:400		715-605-150
Anti-Goat Alexa 488	Donkey	1:400		705-545-147
Anti-Goat Alexa 594	Donkey	1:400		705-545-147
Anti-Goat Alexa 647	Donkey	1:400		705-605-147
Anti-Rabbit CF568	Donkey	1:1000	Biotium	20098-1
DAPI		1:2000	Millipore	508741
Anti-Rabbit IgG, HRP-linked antibody	Goat	1:3000	Cell Signaling	7074
Alexa Fluor 568 Phalloidin		1:500	Thermo Fisher Scientific	A12380

3.12. Western blot

Embryonic telencephalon from *Abhd4* +/+ and -/- animals and Abhd4 transfected HEK-293 cells (as positive control) were homogenized in RIPA lysis buffer (50mM Tris-HCl, 150mM NaCl, 1% Tx-100, 0.1% SDS, 1mM DTT) containing 1x Protease inhibitor cocktail (Roche). Samples were denatured in Laemmli sample buffer (Bio-Rad) at 95°C for 5 mins and immediately loaded onto a 12% SDS-polyacrylamide gel. The amount of 15 μg protein was separated with PowerPac HC High-Current Power Supply (Bio-Rad) at 160 V, 400 mA then transferred to nitrocellulose membrane electrophoretically (Bio-Rad). For immunoblotting, we used 5 % Bovine Serum Albumin (BSA, Sigma) in TBST to block nonspecific binding sites, then incubated with primary antibodies in TBST overnight at 4°C. Washes with TBST were followed by horseradish peroxidase labeled secondary antibodies (1:3000; Cell Signaling) for 2 hours at RT, then membranes were developed by Supersignal West Dura Extended Duration Substrate Kit (Thermo Fisher Scientific).

The transgenic rabbit line used for Abhd4 antibody generation has an elevated neonatal Fc receptor (FcRn) activity which provides enhanced specificity (Baranyi et al., 2013). The rabbits were intramuscularly immunized with KLH-conjugated (keyhole limpet hemocyanin) polypeptide corresponding the amino acid residues 50-69 (N'-PNQNKIWTVTVSPEQKDRT-C') of mouse Abhd4. Immunization, antiserum selection, affinity purification was made by ImmunoGenes Ltd. Antibody validation was carried out in Abhd4-transfected HEK-293 cells as a first step. Antisera, which showed high specificity to ectopic Abhd4 were used further experiments. Antibody validation was carried out using Western-blots and immunohistochemistry with knockout control.

3.13. Maternal alcohol consumption model

Abhd4 littermate embryos came from heterozygous breeding and were identically exposed to ethanol *in utero*. In the subchronic model, timed-pregnant mice received daily two vehicle or 2.5g/kg ethanol in saline intraperitoneal injections for two days (E13.5-E15.5) then embryos were collected at E16.5. The acute model was performed with a single 5g/kg vehicle or ethanol in saline injection at E14.5 and embryos were fixed 12 hours later. Maternal blood ethanol content was determined enzymatically, mother animals were decapitated, 0.1 ml blood was collected and immediately mixed with 900 ul of 6.25% trichloroacetic acid and centrifuged at 2000 rpm for 2 min to obtain the supernatant. The sample was then mixed with an alcohol reagent using the Synchron System Ethanol assay kit (Beckman) and assayed at 340 nm wavelength. Blood ethanol standards were created by mixing alcohol standards (0,1 ‰; 0,5 ‰; 1 ‰; 1,5 ‰; 2‰) with the reagent and immediately assayed. Maternal blood alcohol levels were between 0.5‰-1‰ in the subchronic model and it reached 1.5‰-2‰ in the acute model.

3.14. Phylogenetic tree

Protein sequences of species representing various phylogeny levels were collected from UniProt (https://www.uniprot.org/) and NCBI (https://www.ncbi.nlm.nih.gov/gene). Sequence similarities were determined using protein alignment by Mega7 software (Kumar et al., 2016), and the evolutionary history was inferred by using the Maximum Parsimony method. The analysis involved 12 amino acid sequences which are: Q8TB40, H2Q7Z0,

G1T725, Q8VD66, Q5EA59, D3ZAW4, Q8WTS1, NP_001017287.1, NP_001017613.1, Q7JQU9, H2KZ86, Q04623. All positions containing gaps and missing data were eliminated. There was a total of 310 positions in the final dataset.

3.15. Image acquisition and editing

In situ hybridization samples were imaged by Nikon Eclipse Ti80 upright microscope equipped with a Nikon DS-Fi1 CCD camera or a Zeiss Axioscope with an Axiocam Hrc digital camera. Fluorescent images were taken with Nikon A1R laser-scanning confocal system built on a Ti-E inverted microscope and operated by Nikon NIS-Elements AR software. STORM images with correlated confocal stacks were acquired via a CFI Apo TIRF 100x objective (1.49 NA) on a Nikon Ti-E inverted microscope with a Nikon C2 confocal scan head and an Andor iXon Ultra 897 EMCCD. The setup was controlled by Nikon N-STORM module in NIS-Elements AR software. Prior to imaging, sections were covered with imaging medium containing 0.1 M mercaptoethylamine and components of an oxygen scavenging system (5 m/v% glucose, 1 mg/ml glucose oxidase, 2.5 µl/ml catalase), and the coverslips were sealed with nail polish. Correlated confocal and STORM image acquisition and analysis were done as described earlier by Dudok et al., 2015. Briefly, confocal z-stacks were taken from Nestin filaments located either in the ventricular zone or in the cortical plate to determine the best focal plane for subsequent STORM imaging. In case of cell culture, confocal z-stack were taken from the focal plane of TOM20-positive mitochondira. For single channel 3D direct STORM (dSTORM) imaging, 2.500-10.000 cycles were captured using 647-nm excitation. Continuous illumination with the 405 nm laser line was used in order to reactivate the fluorophores and get more localization events. Peak detection was done using the Nikon N-STORM module in NIS-Elements AR software. Pictures were always made and edited by equal settings between +/+ and -/- samples. Figure compositions were done by Photoshop CS5 (Adobe).

3.16. Image analysis

Correlated confocal and STORM images, pixel-based confocal images and 3D-coordinates of molecular localizations were aligned and analyzed by VividSTORM software (Barna et al., 2016). To investigate the nanoarchitecture of Nestin-bundles, segments of the

filament bundles were selected based on the confocal pixel intensities and the number of localization points in the given region of interest (ROI) was calculated. To measure the 3D extent of the Nestin filament bundles, segments with identical lengths were selected by drawing circular ROIs with a diameter of 1 µm on the filaments. A convex hull was fitted onto the outermost localization points and the volume and surface area of the convex hulls were measured. To determine the width of the filament bundles, localization data were first loaded into the N-STORM module and captured. Intensity profiles perpendicular to the bundles were measured on the captured image, and the full width at half maximum (FWHM) values were calculated in Nis-Elements by fitting a Gaussian distribution onto the intensity profiles. Localization data were visualized in the N-STORM module using Gaussian rendering, where localization events with higher localization accuracies are represented by brighter dots. Only density filtering was applied on the raw data. The visualization of the convex hull and 3D rendering was obtained by using the Visual Molecular Dynamics software. The nanoscale distribution of cytochrome c and the size of mitochondria (related to the pixel number of TOM20) were determined by a custom Python script. First, transfected cells were freehand selected as ROIs and cytochrome c localization points were counted over the TOM20-positive and TOM20-negative pixels to determine the distribution of CytoC inside and outside of mitochondria respectively. The ratio of cleaved caspase-3 and GFP double positive cell ratio was counted manually, $CC3^{+}/GFP^{-}$ and also CC3-positive cell number, which was normalized to the GFP total number/quadrate (($GFP^{+}CC3^{+}/GFP^{+}$) * 100).

Cellular distribution in equal bins, morphology or cell death assays were quantified from confocal microscopy images with ImageJ software using different custom plug-ins. RNAscope dots were measured by manual counting inside the GFP based ROI, and dot numbers were normalized to group averages. Spearmann's rank correlation was made between Abhd4/Glast and Abhd4/Tbr2. In the migration assays or in case of Gad65-GFP and TUNEL distributions in the cortex, cell positions (X, Y coordinates) were measured by ImageJ plug-in and the Y values were differentiated in 5 or 10 equal bins. PAX6 positive cell distributions were measured by pixel intensities in 5 equal bins. The quantification of TBR1-, TB2-, PHH3-, BrdU- and TUNEL-positive cell density was made by ImageJ cell counter

plug-in. In morphological analysis after distinct electroporations, whole electroporated cell number was counted by ImageJ cell counter plug-in, then rounded shaped cells were selected manually, finally the ratio of rounded to all electroporated cell number gave the cell percentage. Calb2/SST colocalization was counted manually in the same quadrates, where the Calb2 counting was assessed. To investigate the interneuron migration in the embryonic brain, GFP-positive cells were counted by manually in the pallium from the pallium-subpallium border. To statistically compare the adult in situ hybridization results and the Gad65-GFP cell density in WT and KO, images was converted to black and white pictures and cell number was counted by custom-made ImageJ cell counter plug-ins. Laminar distribution of different cell types in Abhd4 +/+ and -/- animals was quantified by Fiji. First, images were auto-thresholded by the following settings: vGlut1- Otsu; Gad67 - Li; Glast1 – Triangle, then images were converted to binary images. Laminar distribution of the pixels was measured in 5 equal bins and their percentages were counted. Throughout the dissertation "cell density" corresponds to actual counted cell numbers in each analyzed image.

3.17. Statistical analysis

Experimental results were tested for statistical significance by Statistica 13.1 (TIBCO) and Prism5.0 (Graphpad) programs. All experiments were repeated at least in 3 independent cases on different animals. Shapiro–Wilk normality test or in case of low item number, Kolmogorov–Smirnov test was used to measure the normality of the samples. To determine the poolability of the raw datasets Kruskal-Wallis test was used. Unpaired comparisons were tested using two-tailed unpaired Student's t-tests in case of normal distribution and Mann–Whitney tests based on nonparametric results. Multiple comparisons were examined by Kruskal-Wallis test followed by post hoc Dunn's Multiple Comparison Test. Statistical significance with standard classification star system is shown on the figures (* means $p<0.05$, **means $p<0.01$ and *** means $p<0.001$).

3.18. Personal contributions for the results

All the presented data in this study based on teamwork, with many excellent people, especially from the Momentum Laboratory of Molecular Neurobiology. The projects were

conceived by Dr. István Katona and Dr. Zsolt Lele. My contribution was central in performing in utero electroporations, animal breeding, fluorescent single-RNA detection, western blots, phylogenetic analysis, data analysis and planning experiments, validate the Abhd4 antibody *in vitro* and on tissue samples, genotyping Abhd4 animals with the help of Erika Tischler and finally, supervising the work of students. The *Dlx5/6i-Cre*$^{Cre/+}$*;Ncad*$^{fl/fl}$ mouse line was created by Dr. Zsolt Lele in the Laboratory of Molecular Biology and Genetics led by Dr. Gábor Szabó. Molecular cloning, embryonic and adult in situ hybridization (Figure 7, 8, 15, 23) were planned and performed by Dr. Zsolt Lele. *Cdh2 in situ* hybridization and PHH3 staining on triple transgenic animals were planned by Dr. Zsolt Lele and performed by Kinga Bercsényi (Figure 5). HEK cells were maintained and transfected by Fruzsina Mógor (Figure 20), she recorded most of the STORM images of HEK cells with the help of Miklós Zöldi and the data were analyzed by Vivien Miczán and Fruzsina Mógor. Nestin STORM images were taken and analyzed by Miklós Zöldi (Figure 11 and 16). I and Dr. Zsolt Lele have planned and carried out all the immunofluorescence- and TUNEL stainings and confocal microscopy. Abhd4 antibody was made by ImmunoGenes Ltd. The genotyping of triple transgenic animals was made by Dr. Zsolt Lele. Everyday laboratory assistance was provided by Erika Tischler and Balázs Pintér.

DOI:10.14753/SE.2020.2378

4. Results

4.1. The role of N-cadherin (*Cdh2*) during tangential migration and interneuron differentiation in the somatosensory cortex

4.1.1. Lack of *Cdh2* in postmitotic interneurons effects their tangential migration but not proliferation in the ganglionic eminences

N-cadherin is highly expressed by several parts of the embryonic brain including the germinative zones of the pallium and subpallium (Figure 5a). To investigate its role during tangential migration however, we eliminated *Cdh2* in postmitotic neurons via activation of Cre by the *Dlx5/6i* regulatory element (Ghanem, 2003; Ghanem et al., 2007; Monory et al., 2006). As a result, *Cdh2* expression was completely absent in all postmitotic interneurons and striatal cells in the subpallium, meanwhile other regions most importantly the subpallial ventricular zone as well as the thalamus or pallial structures were not influenced (Figure 5b). In order to visualize tangentially migrating interneurons in the absence of N-cadherin, *Dlx5/6i*-Cre/*Cdh2*-floxed animals were crossed to a GABAergic cell-type specific Gad65-GFP mouse line (López-Bendito et al., 2004). Examining the pallium of these embryos showed that significantly less interneurons were able to migrate past the pallium – subpallium border (Figure 5c-e; +/+: n = 3, -/-: n = 3; two-sided Mann-Whitney U test; ***$P < 0.0001$). These data corroborate an earlier report (Luccardini et al., 2013) indicating that *Cdh2* is necessary for proper tangential migration. Previously, several studies showed (Gil-Sanz et al., 2014; Luccardini et al., 2015; Zhang et al., 2010) that N-cadherin has a role in the regulation of proliferation and its absence could be an explanation behind the decreasing number of Gad65-GFP-positive interneurons in the pallium. To test this hypothesis, we performed phospho-histone H3 immunostaining (mitosis M phase marker) on the embryonic cortices at E14, however we could not detect any changes in proliferation between the genotypes (Figure 5f-h; +/+: n = 3, -/-: n = 3; two-sided Mann-Whitney U test; $P = 0.1389$). These data show that lack of *Cdh2* in postmitotic interneurons cause only a migration delay without affecting progenitor proliferation.

DOI:10.14753/SE.2020.2378

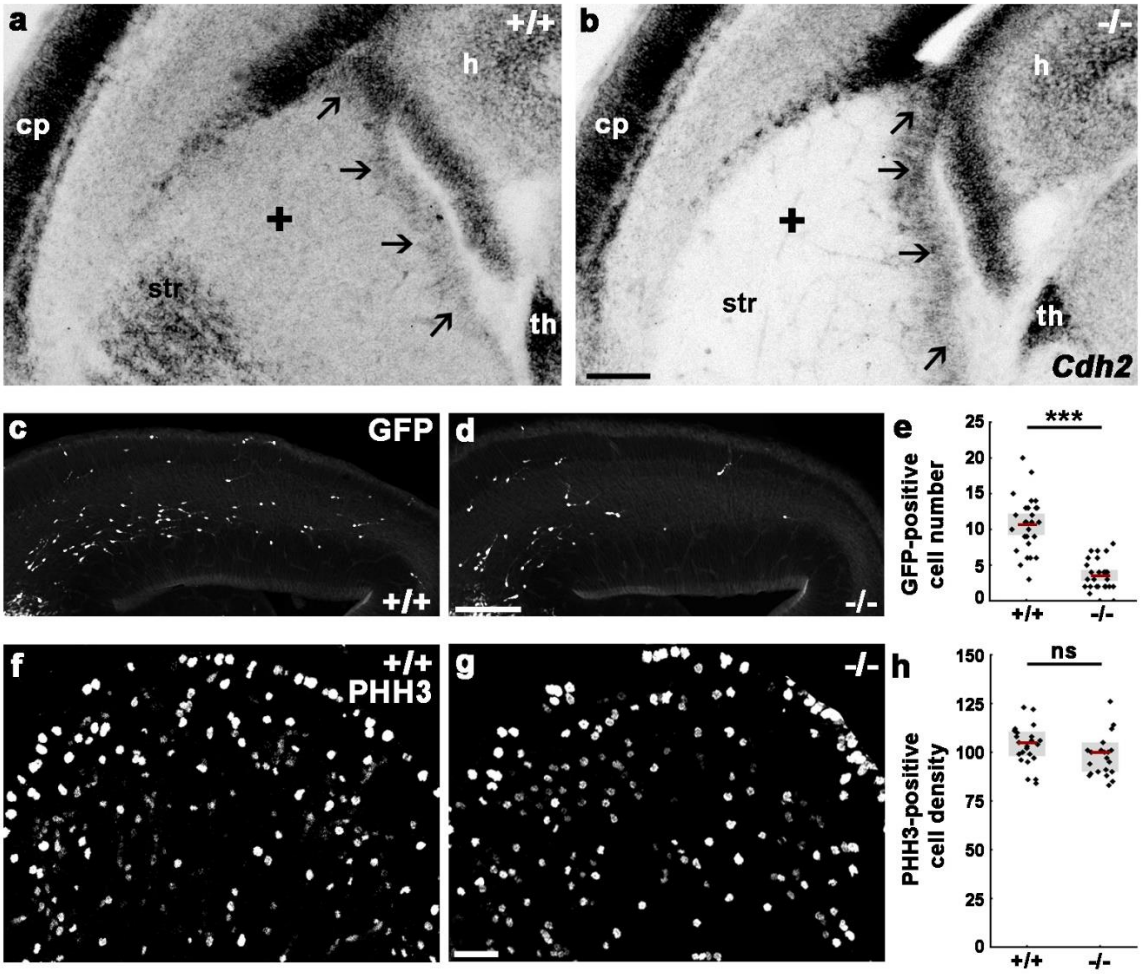

Figure 5. Elimination of *Cdh2* from postmitotic interneurons affects tangential migration but not proliferation.

(a, b) *Cdh2* mRNA is highly expressed in the ganglionic eminences (GE) of E14 +/+ embryos (black arrows mark the ventricular zone of subpallium). In contrast *Cdh2* expression is missing from the postmitotic zone and striatum of -/- animals. Note that expression in the VZ of the GE, the thalamus and the pallial SVZ is still intact. (c, d) Migration delay of GFP-positive precursors in *Cdh2-/-* embryos at E14.5. (e) Quantification of GFP-positive interneurons in the pallium shows decreased cell numbers in the -/- animals (two-sided Student's t test; ***$P < 0.0001$; +/+: n = 3, 10.7 ± 0.74; -/-: n = 3, 3.552 ± 0.38; t = 8.645, df = 54). Graph shows raw data points and mean ± 2 × standard error. (f-h) Lack of *Cdh2* does not influence the proliferation in the GE of -/- littermates at E13.5 (two-sided Mann-Whitney U test; ns = not significant; $P = 0.1389$; +/+: n = 3, 104.5 ± 13.3; -/-: n = 3, 100 ± 15; U: 206). Graph shows raw data points and median ± interquartile range. n indicates the number of mice per groups. Scale bars show (a-d) 100 µm and (f, g) 25 µm. cp: cortical plate, h: hippocampus, th: thalamus, str: striatum. Modified figure from László et al., 2019.

DOI:10.14753/SE.2020.2378

4.1.2. Gad65-GFP-positive cell number is changed in the triple transgenic adult brain

Our previous experiments demonstrated a migration delay of GFP-positive interneurons in the embryonic dorsal telencephalon of knock out animals, which might also have a long-term consequence. To confirm this, we counted the GFP-positive interneurons in the primer somatosensory cortex of adult transgenic animals and indeed found significantly less cells in the -/- mice compared with +/+ littermates (Figure 6a-c; +/+: n = 6, -/-: n = 6; two-sided Student's t-test; ***$P < 0.0001$).

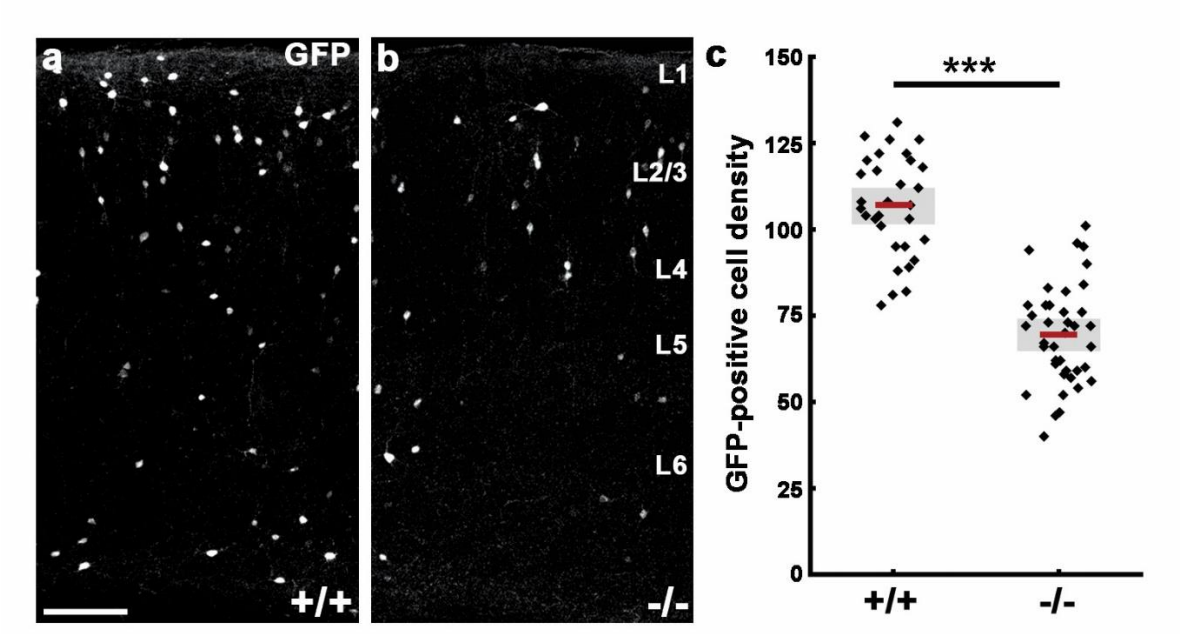

Figure 6. Gad65-GFP-positive interneuron number reduction in the adult somatosensory cortex caused by loss of *Cdh2*.
(a, b) Decreased GFP-positive interneuron numbers in triple transgenic -/- animals when compared with +/+ littermates. (c) Quantification of GFP-positive cell density (two-sided Student's t-test; ***$P < 0.0001$; +/+: n = 6, 106.8 ± 2.625; -/-: n = 6, 69.44 ± 2.335; t = 10.63, df = 68). Graph shows raw data points and mean ± 2 × standard error. n indicates the number of mice per group. Scale bar show (a, b) 100 µm. L1-6 mark the cortical layers. Modified figure from László et al., 2019.

4.1.3. N-cadherin regulates interneuron composition of the adult primer somatosensory cortex

It was previously described, that main interneuron subtypes are originated from distinct parts of the ganglionic eminences (Lim et al., 2018). To understand which cell population is affected by the loss of N-cadherin, we analyzed the interneuron densities in the adult cortex with widely accepted markers of different GABAergic interneuron subtypes (Klausberger and Somogyi, 2008; Tremblay et al., 2016). We did not detect any changes in the number of parvalbumin (PV; Figure 7a-c; +/+: n = 6, -/-: n = 6; two-sided Mann-Whitney U test; P = 0.8182) – or *reelin (Reln)* – positive interneurons between genotypes (Figure 7d-e; +/+: n = 7, -/-: n = 7; two-sided Mann-Whitney U test; P = 0.2086). Furthermore, these experiments did not reveal any changes in the cell densities of *VIP*- and *NPY*-expressing cell types, either (Figure 7g-l; both experiments: +/+: n = 7, -/-: n = 7; two-sided Mann-Whitney U test; P = 1). In order to mark VIP-negative and cholecistokinin (CCK)-positive interneuron population, we chose *cannabinoid receptor 1 (Cnr1)* as a marker, considering its perfectly overlapping expression with CCK (Marsicano and Lutz, 1999), but excluding the CCK-positive glutamatergic population (Zeisel et al., 2015). However, this comparison also did not show any alteration between +/+ and -/- (Figure 7m-o; +/+: n = 8, -/-: n = 8; two-sided Mann-Whitney U test; P = 0.9591).

In contrast to the results described above, there was a sharp decrease in the number of *calretinin (Calb2)* – positive interneurons (Figure 8a-c; +/+: n = 7, -/-: n = 7; two-sided Student's t-test; ***$P <$ 0.0001), not just in RNA, but in protein level as well (Figure 8g-i; +/+: n = 6, -/-: n = 6; two-sided Mann-Whitney U test; ***$P < 0.0001$). Moreover, we also detected a significant decrease in the number of *somatostatin (SST)* – expressing interneurons in the adult somatosensory cortex of triple transgenic -/- animals (Figure 8d-f; +/+: n = 11, -/-: n = 11; two-sided Mann-Whitney U test; **P = 0.0041). Furthermore, double immunostaining against Calb2 and SST revealed that the number of double – positive cells in the -/- animals was altered as well (Figure 8g, h, j; +/+: n = 6, -/-: n = 6; two-sided Mann-Whitney U test; **P = 0.0024). Taken together, these results indicate that loss of *Cdh2* affects postmitotic interneuron development in a cell-type specific manner.

DOI:10.14753/SE.2020.2378

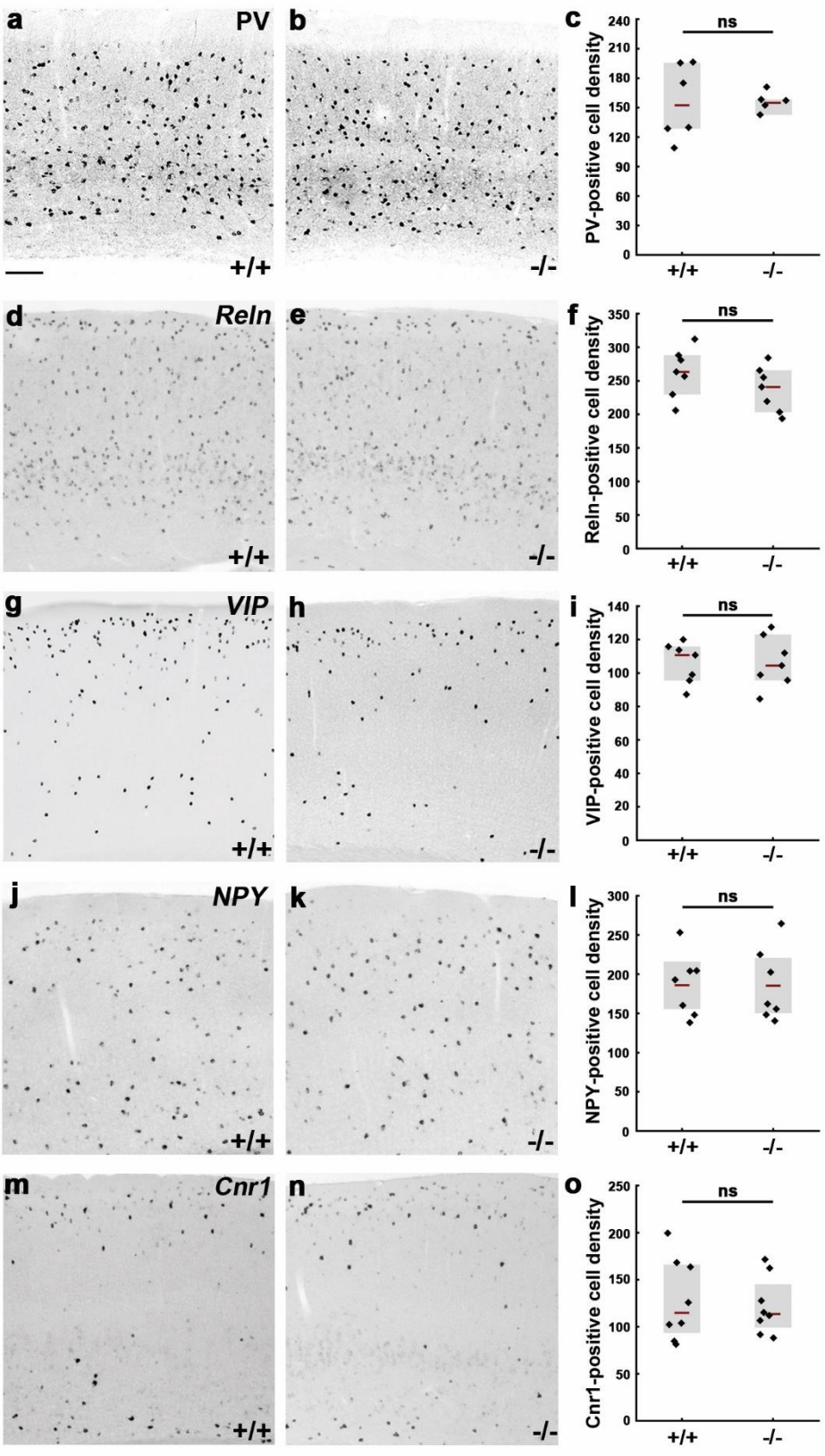

Figure 7. Comparative analysis of distinct interneuron subtypes in the somatosensory cortex of triple transgenic animals.
(a, b) Parvalbumin (PV) expression in the cortex of +/+ and −/− offsprings. (c) Quantification of PV-positive cell density (two-sided Mann-Whitney U test; *P*=0.8182; +/+: n=6, 154.4 ± 72.5; -/-: n=6, 154.9 ± 34.3; U: 16). (d-f) *Reelin (Reln)*-expressing cells in the somatosensory cortex. (f) Statistical analysis of Reln-positive cell density (two-sided Mann-Whitney U test; *P*=0.2086; +/+: n=7, 263.3 ± 58.2; -/-: n=7, 240.8 ± 62.2; U: 14). (g-i) *Vasoactive Intestinal Peptide (VIP)* expression and its quantification (two-sided Mann-Whitney U test; *P*=1; +/+: n=7, 110.8 ± 20.3; -/-: n=7, 104.8 ± 27.35; U: 24). (j, k) *Neuropeptide Y (NPY)*-expressing cells in the somatosensory cortex. (l) Statistical analysis (two-sided Mann-Whitney U test; *P*=1; +/+: n=7, 185.86 ± 56.5; -/-: n=7, 185.5 ± 76.7; U: 24).(m–o) *Cannabinoid receptor 1 (Cnr1)*-positive cell numbers in triple transgenic animals also show no significant differences between genotypes (two-sided Mann-Whitney U test; *P*=9591; +/+: n=8, 114.8 ± 77.95; -/-: n=8, 113.6 ± 58.19; U: 31). Graphs show median ± interquartile range. n indicates the number of mice per group. ns = not significant. Scale bar shows 100 μm. Modified figure from László et al., 2019.

DOI:10.14753/SE.2020.2378

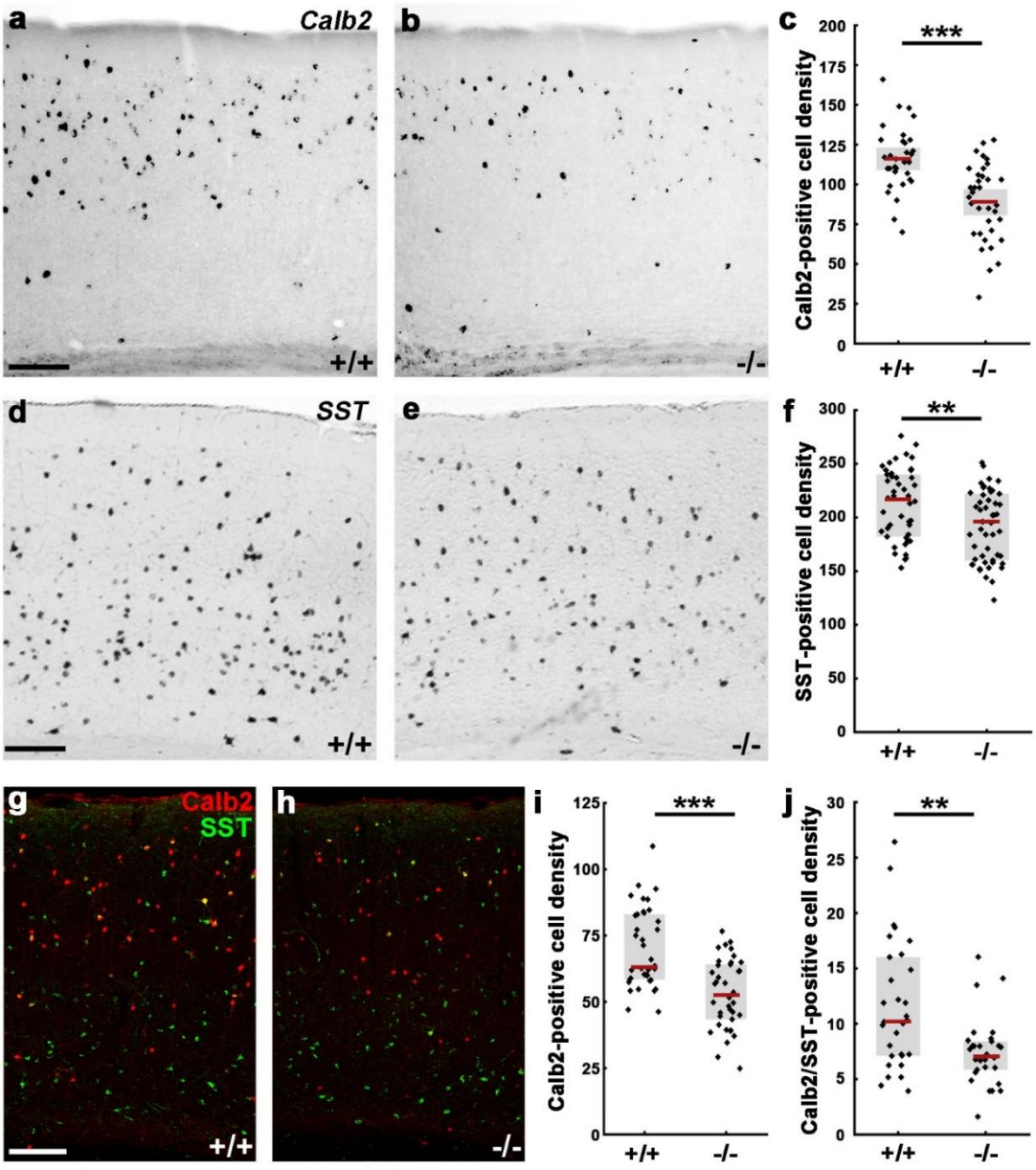

Figure 8. Lack of *Cdh2* from postmitotic GFP-positive cells reduces calretinin and somatostatin interneuron cell numbers in the adult somatosensory cortex.
(a-c) *Calretinin (Calb2) in situ* hybridization and its statistical analysis (c; two-sided Student's t-test; ****P* < 0.0001; +/+: n = 7, 116 ± 3.542; -/-: n = 7, 88.8 ± 4.065; t = 5.021, df = 65). (d, e) *Somatostatin (SST) in situ* hybridization +/+ (d) and -/- (e) animals. (f) Statistical analysis of SST-positive cell density shows significant difference between +/+ and -/- (two-sided Mann-Whitney U test; ***P* = 0.0041; +/+: n = 11, 216.5 ± 58.5; -/-: n = 11, 195.5 ± 62.8; U: 758.5). (g, h) SST and Calb2 double immunostaining on triple transgenic adult animals. (i, j): Statistical analysis demonstrates a significant decrease in both Calb2-

positive and Calb2/SST double-positive cell density in -/- littermates (two-sided Mann-Whitney U test; Calb2-positive cell density: ***$P < 0.0001$; +/+: n = 6, 63.11 ± 24.76; -/-: n = 6, 52.6 ± 21.43; U: 314; Calb2/SST-positive cell density: **$P = 0.0024$; +/+: n = 6, 10.25 ± 8.9; -/-: n = 6, 7.1 ± 2.64; U: 244). Graphs show raw data points and mean ± 2 × standard error (c) or median ± interquartile range (f, i, j). n indicates the number of mice per group. Scale bars indicate 100 µm. Modified figure from László et al., 2019.

4.1.4. Disruption of N-cadherin signaling in postmitotic cells causes a migration delay in the somatosensory cortex

Beforehand, we observed migration delay in the embryonic cortex (Figure 5) and fewer SST/Calb2-positive interneuron number in the adult somatosensory cortex (Figure 8). To investigate the fate of these cells between the embryonic migration delay and the adult phenotype, first we measured the number of GFP-positive cells at an early postnatal age (P8) where we found significantly less GFP-positive interneurons in the cortices of the -/- littermates (Figure 9a-b, d; +/+: n = 4, -/-: n = 4; two-sided Mann-Whitney U test; ***$P <$ 0.0001). Moreover, we found that not only the cell number changed, but so did the laminar allocation of the GFP-positive cells in -/- mice (Figure 9a-c). Distribution analysis also demonstrated a shift in the localization of these cells from the upper towards the deeper layers indicating that their migration has been arrested in the subventricular zone of the postnatal cortex (Figure 9c; +/+: n = 4, -/-: n = 4; Bin4 and Bin10: two-sided Mann-Whitney U test; ***$P < 0.0001$).

Next, we considered if the absence of *Cdh2* could cause a migration route change and a missing of their target cortical area. To test this hypothesis, we analyzed other brain areas, which can serve as alternative destinations, such as the more lateral, supplementary somatosensory cortical area and the striatum. Interestingly, the number of GFP–positive interneurons was also decreased in both of these areas (Figure 9e-f; +/+: n = 4, -/-: n = 4; two-sided Mann-Whitney U test; supplemental somatosensory area (S2) ***$P < 0.0001$; striatum ***$P = 0.0002$), which indicates, that the precursors did not alter their migration route, rather probably got arrested before radial migration. All together these results show that loss of N-cadherin from subpallial postmitotic interneuron precursors affects various brain areas.

DOI:10.14753/SE.2020.2378

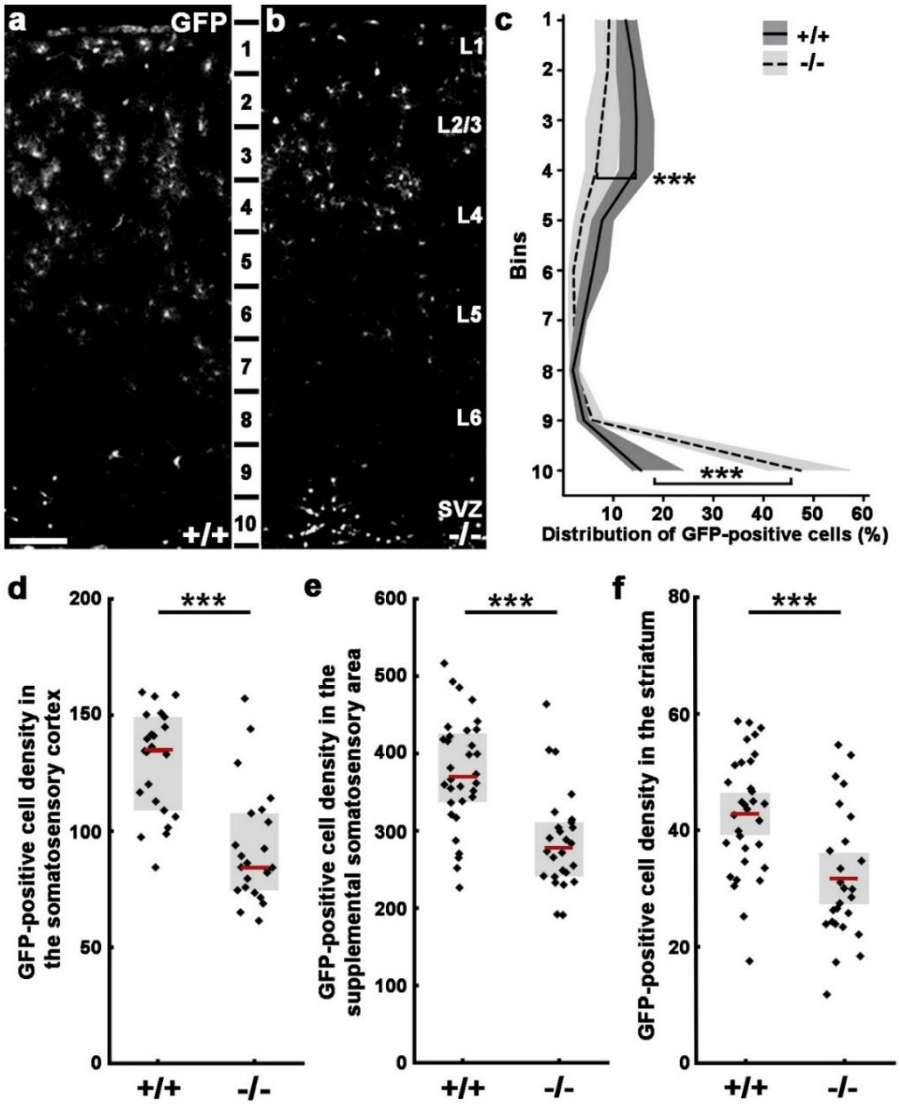

Figure 9. Reduced GAD65-GFP-positive interneuron numbers are found in both cortical and subcortical areas of early postnatal triple transgenic animals.
(a, b) GFP-positive interneuron distribution in P8 littermates. (c) Distribution analysis in 10 equal cortical bins illustrates cell density changes in the -/- animals compared with +/+ littermates (Bin4: two-sided Mann-Whitney U test; ***$P < 0.0001$; +/+: n = 4, 14.24 ± 6.52; -/-: n = 4, 6.58 ± 5.9; U: 51; Bin10: two-sided Mann-Whitney U test; ***$P < 0.0001$; +/+: n = 4, 15.54 ± 9.9; -/-: n = 4, 47.42 ± 15.75; U:28). Graph shows median (line) ± interquartile range (transparent band). (d, f) Statistical analysis of GFP-positive cell density in different brain regions. Significant reduction in cell numbers occurs between +/+ and -/- animals in the somatosensory cortex (d; two-sided Mann-Whitney U test; ***$P < 0.0001$; +/+: n = 4, 134.6 ± 40.3; -/-: n = 4, 85.33 ± 34.03; U: 95), in the supplemental somatosensory area (S2; e; two-sided Mann-Whitney U test; ***$P < 0.0001$; +/+: n = 4, 369.8 ± 91; -/-: n = 4, 278.5

± 70.7; U: 144), as well as in the striatum (f; two-sided Student's t-test; ***P = 0.0002; +/+: n = 4, 42.82 ± 1.8; -/-: n = 4, 31.72 ± 2.2; t = 3.942, df = 56). Statistical figures show raw data points and median ± interquartile range (d, e) or mean ± 2 × standard error (f). n indicates the number of mice per group. Scale bars indicate 100 µm (a, b); L1-6 mark the cortical layers; SVZ: subventricular zone. Modified figure from László et al., 2019.

4.1.5. The fate commitment of the arrested cells in the postnatal SVZ

In the developing neocortex, pyramidal neuron activity can influence the fate and number of local interneurons. In an early critical period (P7-10) excitatory inputs to distinct interneuron cell-types can decide their survival or death (Wong et al., 2018). We assumed that the missing cells from the adult somatosensory cortex in triple transgenic -/- mice were eliminated at some point, because they did not change their fate or get misdirected to other possible target areas. In order to establish the fate of the arrested cells, we performed TUNEL assays at embryonic and early postnatal stages to visualize cell death (Figure 10a). At embryonic day 14, we analyzed two regions of the caudal ganglionic eminences, in a quadrate next to the ventricular surface and in the future striatal area. However, this analysis didn't show any difference between genotypes at embryonic age (Figure 10b, c; +/+: n = 3, -/-: n = 3; two-sided Mann-Whitney U test; CGE P = 0.7535; striatum P = 0.5429). In contrast, at P8 when we observed the migration arrest before, we also measured higher level of TUNEL-positive cell numbers in the somatosensory cortex (Figure 10d-f; +/+: n = 5, -/-: n = 5; two-sided Student's t-test; ***P < 0.0001). Moreover, the laminar distribution of the TUNEL-positive cells reveals, that most of the dead cells were in the area where the migration was arrested (Figure 10g; +/+: n = 5, -/-: n = 5; Bin1 and 10: two-sided Mann-Whitney U test; ***P < 0.0001).

In summary, we showed evidence, that loss of *Cdh2* from postmitotic interneurons causes not just migration arrest but also the elimination of the cells stuck in the postnatal SVZ.

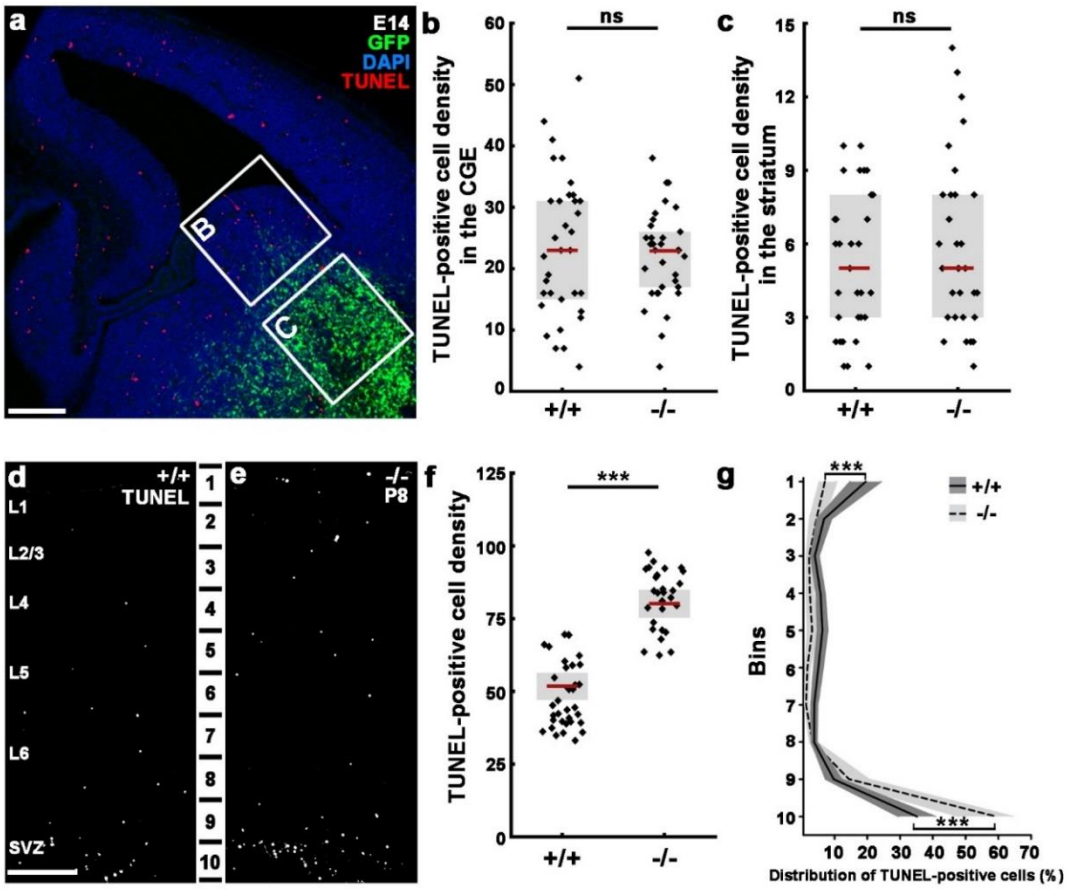

Figure 10. Absence of *Cdh2* causes increased cell death in the postnatal somatosensory cortex.

(a) Visualization of cell death by TUNEL assay in E14 embryos. Example quadrates indicate statistical analysis from CGE (b; two-sided Mann-Whitney U test; ns = not significant, P = 0.7535; +/+: n = 3, 23 ± 16.5; -/-: n = 3, 23 ± 10; U: 535.5) and developing striatum (c; two-sided Mann-Whitney U test; ns = not significant, P = 0.5429; +/+: n = 3, 5 ± 5; -/-: n = 3, 5.9 ± 5; U: 437). Graphs show raw data points and median ± interquartile range. (d, e) TUNEL-stained brain slices from triple transgenic animals at P8. (f) Statistical analysis of TUNEL-positive cell density in the somatosensory cortex (two-sided Student's t-test; ***P < 0.0001; +/+: n = 5, 51.74 ± 2.3; -/-: n = 5, 80.09 ± 2.4; t = 8.465. df = 76). Graph shows raw data points and mean ± 2 × standard error. (g) Distribution analysis of TUNEL-positive cells in 10 equal bins (Bin1: two-sided Mann-Whitney U test; ***P < 0.0001; +/+: n = 5, 17.57 ± 15.61; -/-: n = 5, 7.07 ± 5.32; U: 163; Bin10: two-sided Mann-Whitney U test; ***P < 0.0001; +/+: n = 5, 33.3 ± 24.58; -/-: n = 5, 59.32 ± 16.5; U: 113). Graph shows median (line) ± interquartile range (transparent band). n indicates the number of mice per group. L1-6 mark the cortical layers. SVZ: subventricular zone. Scale bars indicate 100 µm (a) and 50 µm (d-e). Modified figure from László et al., 2019.

4.2. The consequences of abnormal delamination in the developing mouse cortex

4.2.1. *In vivo* cadherin-based adherens junction disruption model

N-cadherin function during pallial development is highly investigated in physiological circumstances (Gärtner et al., 2015). However, much less known about its potential contributions to cortical malformations. In order to examine the outcome of abnormal delamination we utilized an *in vivo* cadherin disruption model in the embryonic telencephalon. N-cadherin is one of the major molecular components of the adherens junction belt, which anchors radial glia progenitor cells to each other forming the ventricular wall (Kadowaki et al., 2007). In utero electroporation of a dominant-negative form of N-cadherin (ΔnCdh2-GFP) was able to disconnect classic cadherin-based connections, therefore we could avoid the potential functional redundancy between N-cadherin and E-cadherin (Cdh1;Kintner 1992; Fujimori and Takeichi 1993; Nieman et al. 1999). Perturbation of N-cadherin connections resulted in a specific adherens junction destruction around the targeted aRGPCs, as indicated by decreased expression of the fibrillar actin marker phalloidin (Figure 11a-b').

Next, we performed STORM super-resolution imaging on the radial glia scaffold. Reconstruction of the nanoscale architecture of Nestin intermediate filaments however showed unaltered radial glia scaffold following *ΔnCdh2-GFP* electroporation (Figure 11c-h). Previously it was shown, that elimination of integrin-laminin connections at the pial surface influences the morphology and survival of progenitor cells (Radakovits et al., 2009), nevertheless the basal endfeet-basal lamina connections of the aRGPCs, visualized by the electroporated GFP and laminin subunit alpha 1 (LAMA1) respectively, were also intact (Figure 11i-k").

As a result of adherens junction belt elimination 48 hrs after electroporation, the PAX6-positive progenitor cells dispersed from the VZ and accumulated at the SVZ (Figure 12; n = 3; two-sided Mann-Whitney U test; ***P = 0.0004 in Bin4 and *** P = 0.0003 in Bin5).

Taken together, these results demonstrate, that elimination of cadherin-based cell-to-cell connections at the ventricular surface leads to abnormal delamination of aRGPCs.

DOI:10.14753/SE.2020.2378

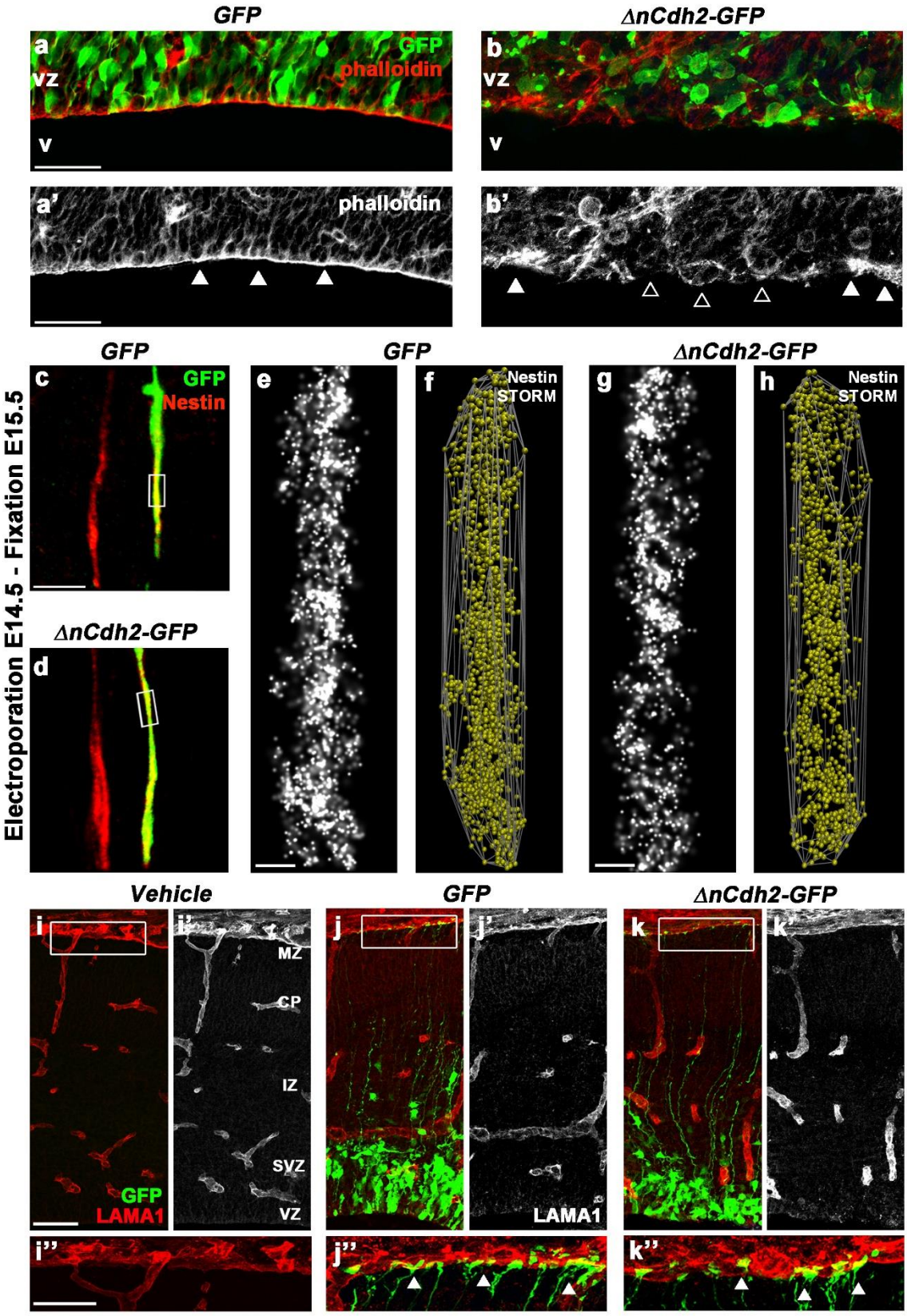

Figure 11. ΔnCdh2-GFP eliminates the adherens junction connections between aRGPCs, but does not affect the nanoscale structure of radial glia scaffold or their connections to the pial surface

(a-b') High resolution images of phalloidin staining show a continous adherens junction belt in control samples (a, a') which gets disrupted around ΔnCdh2-GFP electroporated cells. (c, d) Example image of GFP and ΔnCdh2-GFP electroporated Nestin-positive filaments. (e, g) Nestin immunostaining visualized by STORM microscopy. (f, h), Three-dimensional convex hull fitted onto the outermost localization points of STORM coordinates. (i-k") Lamininα1 (LAMA1) visualize the pial surface of vehicle-, GFP- and ΔnCdh2-GFP-electroporated cortices. (i',j',k') Laminin staining only. (i"-k") High power images of the basal end feet of electroporated radial glia cells. MZ: marginal zone; CP: cortical plate; IZ: intermediate zone; SVZ: subventricular zone; VZ: ventricular zone. Scale bars indicate 50 µm (a-b', i-k'), 25 µm (i"-k"), 5 µm (c, d), 200 nm (e-h).

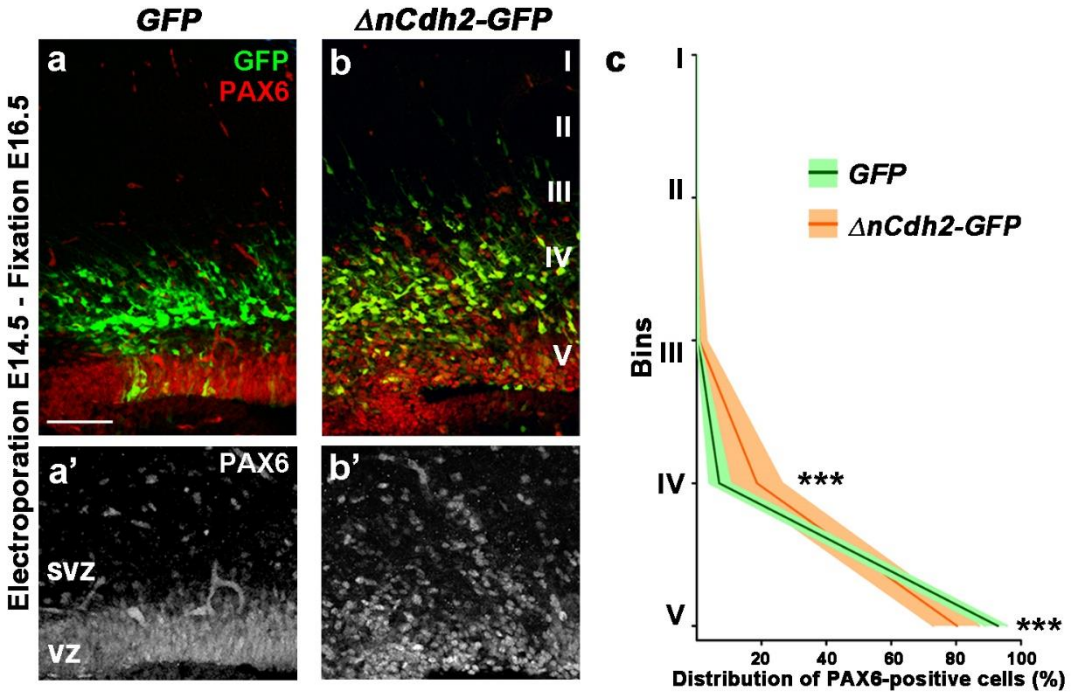

Figure 12. Cadherin-based adhesion loss obtains aRGPC dispersion.

(a-b'), Electroporation of ΔnCdh2-GFP but not GFP only causes dispersion of PAX6-positive aRGPCs. (c) Quantification of PAX6 immunofluorescence distribution between the five identical size cortical bins (Roman numerals) displays significant difference between GFP and ΔnCdh2-GFP electroporated samples with a shift of ΔnCdh2-expressing cells from the 5th to the 4th bin (two-sided Mann-Whitney U test; Bin4: ***P = 0.0004; GFP: 6.957 ± 6.398; ΔnCdh2-GFP: 18.06 ± 15.59; Bin5: ***P = 0.0003; GFP: 92.92 ± 6.71; ΔnCdh2-GFP: 80.31 ± 13.99; n = 3 from each conditions). Data are shown as median (line) and interquartile range (transparent band in the same colour). n indicates the number of mice per group. SVZ: subventricular zone; VZ: ventricular zone. Scale bar represents 25 µm (a-b').

4.2.2. Pathophysiological delamination causes apoptosis and migration defect in the embryonic dorsal telencephalon

Based on the fact that abnormally delaminated cells are generally eliminated via apoptosis to prevent possible malformations in an epithelial tissue environment, we asked whether a similar mechanism evolved to remove abnormally dispersed progenitor cells in the developing cortex? To test this hypothesis, we performed TUNEL assay to visualize cell death. Two days after ΔnCdh2-GFP electroporation, we found approximately 2- fold cell death increase in the electroporated area compared with control conditions (Figure 13a-b'). This phenomenon was prevented by co-injection of the general caspase inhibitor, Z-VAD-FMK (Figure 13c-e; GFP and GFP+Z-VAD-FMK n = 3-3; ΔnCdh2-GFP and ΔnCdh2-GFP+Z-VAD-FMK n = 4-4 animals; Kruskal-Wallis test with post hoc Dunn's Multiple Comparison Test; ΔnCdh2-GFP vs all the controls and treatments: ***$P < 0.0001$; between controls: $P \approx 1$). Moreover, the observed migration defect, also shown previously by others (Kawauchi et al., 2010) was rescued by the presence of the caspase inhibitor, indicating that disrupted cell migration is a consequence of the apoptotic process caused by the breakdown of adherens junctions (Figure 13f-i; n = 3 in each group; Kruskal-Wallis test with post hoc Dunn's Multiple Comparison Test , Bin1 and 4: GFP vs ΔnCdh2-GFP, ΔnCdh2-GFP vs ΔnCdh2-GFP + Z-VAD-FMK ***$P < 0.0001$; Bin2: GFP vs ΔnCdh2-GFP: ***$P = 0.0002$; ΔnCdh2-GFP vs ΔnCdh2-GFP + Z-VAD-FMK **$P = 0.0031$; Bin5: GFP vs ΔnCdh2-GFP, ΔnCdh2-GFP vs ΔnCdh2-GFP + Z-VAD-FMK: ***$P = 0.0001$).

These results confirm our hypothesis, that there is a protective caspase-dependent cell death mechanism which eliminates inappropriately delaminating cells in the developing cortex.

DOI:10.14753/SE.2020.2378

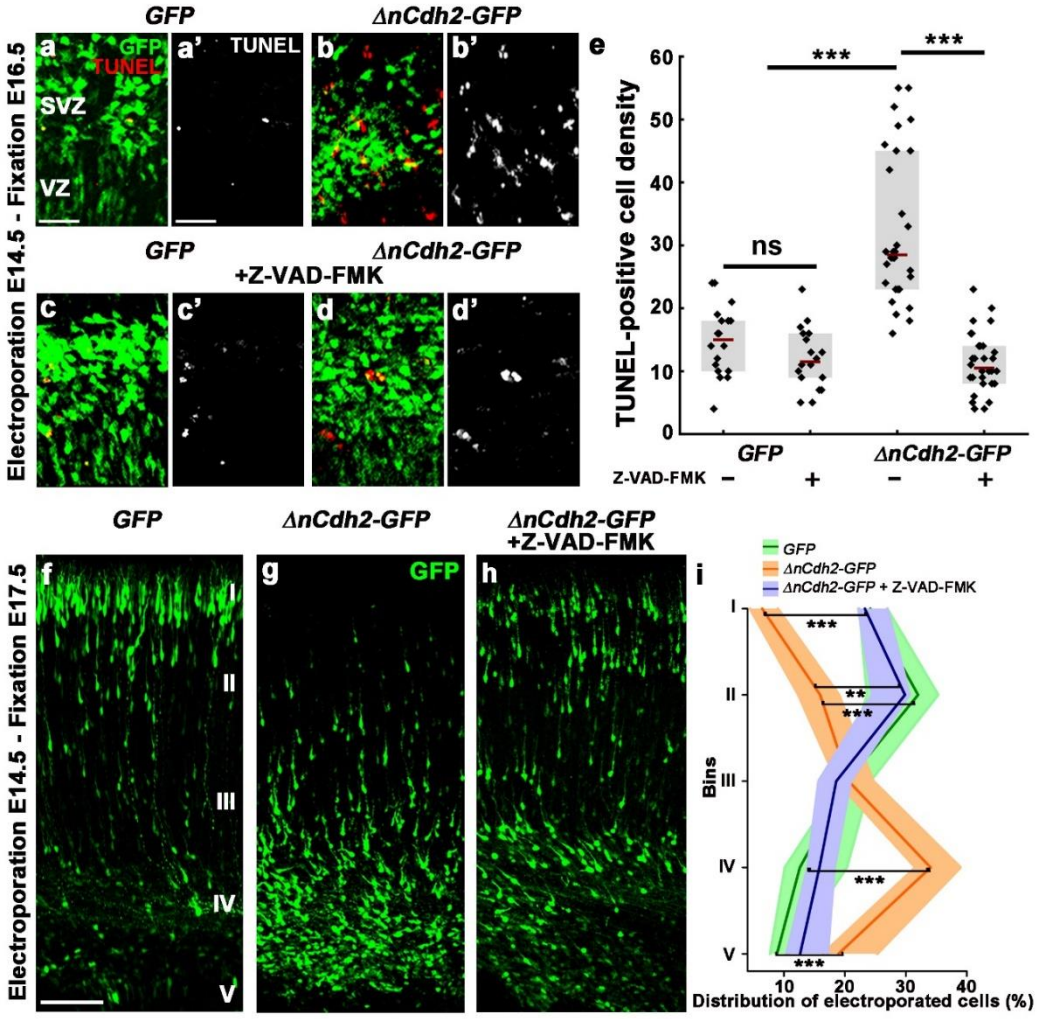

Figure 13. Adherens junction disruption increases caspase-dependent cell death and delays radial migration of postmitotic neuroblasts.

(a-b') Confocal images show elevated cell death after ΔnCdh2-GFP electroporation compared with GFP. (c-d') Z-VAD-FMK general caspase inhibitor could largely prevent the ΔnCdh2-GFP induced cell death. (e) Quantification of TUNEL-positive cell density from electroporated and treated samples (Kruskal-Wallis test with post hoc Dunn's Multiple Comparison Test; ***$P < 0.0001$; ns = not significant, $P \approx 1$; GFP and GFP+Z-VAD-FMK n = 3, ΔnCdh2-GFP and ΔnCdh2-GFP+Z-VAD-FMK n = 4). Graphs show raw data and median ± interquartile range. (f, g) ΔnCdh2-GFP, but not GFP expression causes a migration defect. (h) General caspase inhibitor treatment prevents ΔnCdh2-effect on radial migration (i) Laminar distribution analysis in 5 equal bins (Roman numerals) shows significant differences between the groups (Kruskal-Wallis test with post hoc Dunn's Multiple Comparison Test , Bin1 and 4: GFP vs ΔnCdh2-GFP, ΔnCdh2-GFP vs ΔnCdh2-GFP + Z-VAD-FMK ***$P < 0.0001$; Bin1: GFP: 24.1 ± 4.5; ΔnCdh2-GFP: 6.4 ± 4.5; ΔnCdh2GFP +Z-VAD-FMK: 23.3 ± 4.8; Bin4: GFP: 12.6 ± 10.2; ΔnCdh2-GFP: 34 ± 7.4 ; ΔnCdh2GFP

+Z-VAD-FMK: 15.8 ± 4.4; Bin2: GFP vs ΔnCdh2-GFP: ***P = 0.0002; ΔnCdh2-GFP vs ΔnCdh2-GFP + Z-VAD-FMK **P = 0.0031; GFP: 32.01 ± 11.7; ΔnCdh2-GFP: 15.9 ± 6.69; ΔnCdh2GFP +Z-VAD-FMK: 29.84 ± 6.17; Bin5: GFP vs ΔnCdh2-GFP, ΔnCdh2-GFP vs ΔnCdh2-GFP + Z-VAD-FMK: ***P = 0.0001; GFP: 8.8 ± 3; ΔnCdh2-GFP: 18.9 ± 8.9; ΔnCdh2GFP +Z-VAD-FMK: 12.6 ± 6.76; n = 3 animals per each groups). Data are shown as median (line) and interquartile range (transparent band in the same color). Scale bars indicate 50 μm (a-d') and (f-h). SVZ: subventricular zone, VZ: ventricular zone.

4.3. Investigation of the pathological delamination-evoked cell death mechanism

4.3.1. The identification of potential molecular players in cadherin-loss induced apoptosis

To reveal the molecules involved in adherens junction breakdown-induced cell death, we carried out manual *in silico* analysis of available expression databases and single-cell RNA-sequencing studies searching for genes from the endocannabinoid system with ventricular zone restricted expression. Different expression analysis from mouse, human and cerebral organoids revealed a gene called *Abhydrolase domain containing 4* (Abhd4), a serine-hydrolase previously implicated in N-arachidonoyl-ethanolamide (anandamide, AEA) synthesis (Camp et al., 2015; Nowakowski et al., 2017; Simon and Cravatt, 2006; Telley et al., 2016). Chromogenic *in situ* hybridization experiments provided evidence that *Abhd4 mRNA* was specifically restricted to the germinative zones of the embryonic telencephalon during cortical development (Figure 14a-a" and Figure 15a-i), and this expression was absent in *Abhd4 knockout* littermates (Figure 14b, c).

Furthermore, immunoblotting analysis of tissue samples revealed that Abhd4 was present in the E16.5 brain at the protein level as well (Figure 15m-n).

DOI:10.14753/SE.2020.2378

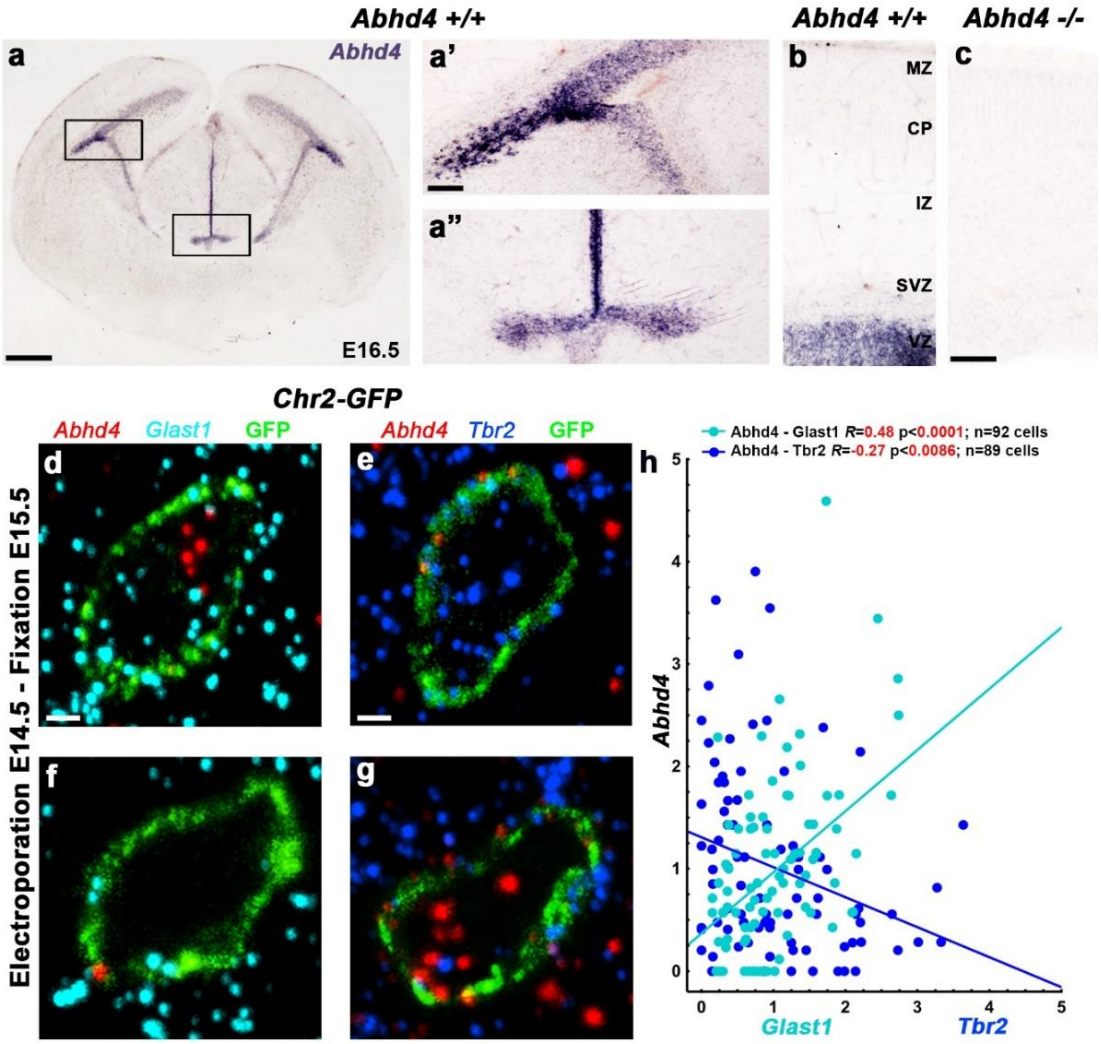

Figure 14. *Abhd4* mRNA expression is restricted to the germinative zones and positively correlates with *Glast1* radial glia marker

(a, b) *Abhd4 mRNA* is expressed exclusively in the ventricular zone of the lateral (a') and third ventricles (a"). (c) Abhd4 mRNA probe was validated on *Abhd4 -/-* animals. (d-g) Single-cell mRNA profile was performed by combination of ChR2-GFP electroporation and fluorescent single-mRNA detection, RNAscope. Representative examples show *Abhd4* and *Glast1* double positive (d) and negative cells (f), *Abhd4 mRNA*-negative and *Tbr2*-positive cell (e) and *Tbr2*-negative but *Abhd4*-positive (g) cell. (h) Quantification of single cell mRNA levels (Spearman's rank correlation, Abhd4/Glast1: R = 0.48, $P < 0.0001$; n = 92 cells from n = 4 mice; Abhd4/Tbr2: R = -0.27, $P = 0.0086$; n = 89 cells from n = 4 mice). The scatter plot shows data from individual cells normalized to the median value of the respective mRNA levels. MZ: marginal zone; CP: cortical plate; IZ: intermediate zone; SVZ: subventricular zone; VZ: ventricular zone. Scale bars indicate 100 μm (a), 25 μm (a', a"), 50 μm (b, c), 2 μm (d-g).

Considering the fact that these germinative niches are the most active, highly proliferative hence very crowded regions of the developing brain, analyzing the expression of Abhd4 at the single-cell level is extremely challenging. To characterize the cell-type specific expression, we combined membrane targeting *in utero* electroporation with fluorescent single-mRNA detection, called RNAscope. Our experiments revealed that *Abhd4* expression correlates positively with the *Glast1* (Slc1a3 gene) radial glia marker. In contrast, inverse correlation was observed with the intermediate progenitor marker *Tbr2* (Eomes; Figure 14d-h; n = 4 mice; Spearman's rank correlation, Abhd4/Glast1: R = 0.48, ***P < 0.0001; Abhd4/Tbr2: R = -0.27, **P = 0.0086).

Next, we wanted to know whether the previously-observed specific expression of *Abhd4* changes during brain development. We found however, that *Abhd4* expression pattern remained confined to the proliferative zones throughout cortical development (Figure 15a-i) and decreased in parallel with the number of proliferating progenitors in postnatal animals. Interestingly, the two main germinative niches, the SVZ of dorsal telencephalon and the subgranular zone (SGZ) of the hippocampus where neurogenesis still occurs in the adult mouse brain also expressed *Abhd4* (Figure 15j-l).

4.3.2. Characterization of Abhd4 knockout animals

Radial glia cells serve two functions during cortical development. They are proliferating multipotent progenitor cells, but also provide a scaffold for postmitotic neuroblasts migration (Marín and Rubenstein, 2003). In the previous section, we presented evidence that *Abhd4* colocalizes with the radial glia marker *Glast1*, so next we examined if it plays a critical role in aRGPC functions. Unexpectedly, neither single-pulse bromodeoxyuridine (BrdU, mitosis S phase marker) labeling of proliferating precursors (Figure 16a-c) nor immunohistochemistry using the M-phase marker, phospho-histone H3 (PHH3, Figure 16d-f) revealed any quantitative differences between E14.5 +/+ and -/- cortices (Figure 16; BrdU, +/+: n = 6; -/-: n = 4; two-sided Student's t-test, P = 0.323; PHH3, +/+: n = 3; -/-: n = 3; two-sided Student's t-test, P = 0.6882).

DOI:10.14753/SE.2020.2378

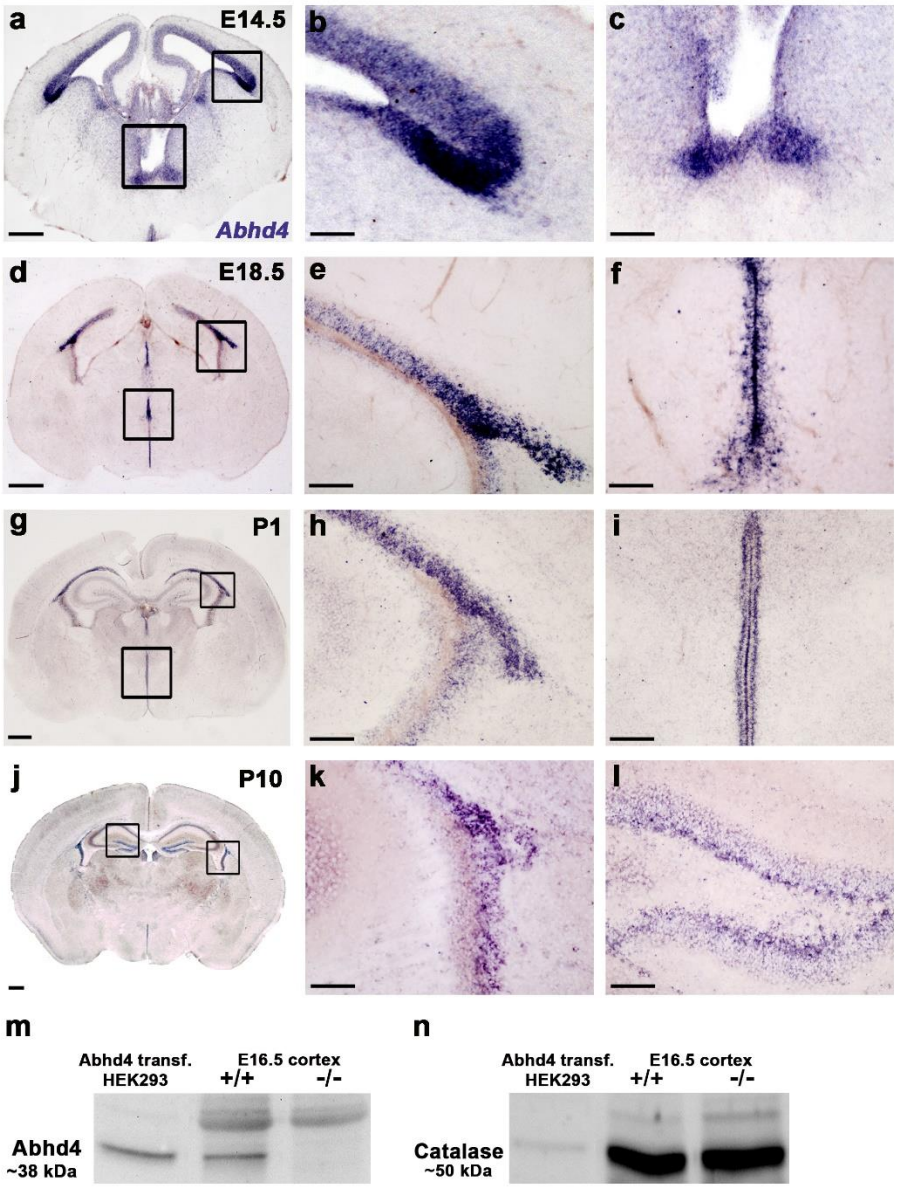

Figure 15. *Abhd4 mRNA* expression in the proliferative zones of the cortex is preserved throughout development.

(a,) Coronal section of an E14.5 cortex shows *Abhd4 mRNA* expression in the germinative zones, through development this pattern is the same in E18.5 (d) and in P1 (g). High magnification images show the proliferative zone of the lateral - (b, e, h) and the third ventricle (c, f, i). During postnatal development *Abhd4* expression remained albeit weaker in the adult neurogenic niches: (j) in the SVZ of telencephalon and in the SGZ of hippocampus (l). (m, n) Abhd4 and control catalase protein is visualized by Western blot in E16 *Abhd4* +/+ and *Abhd4* -/- cortical extracts. Scale bars indicate 200 µm (a), 50 µm (b, c, e, f, h, i, k, l), 500 µm (d, g, j).

DOI:10.14753/SE.2020.2378

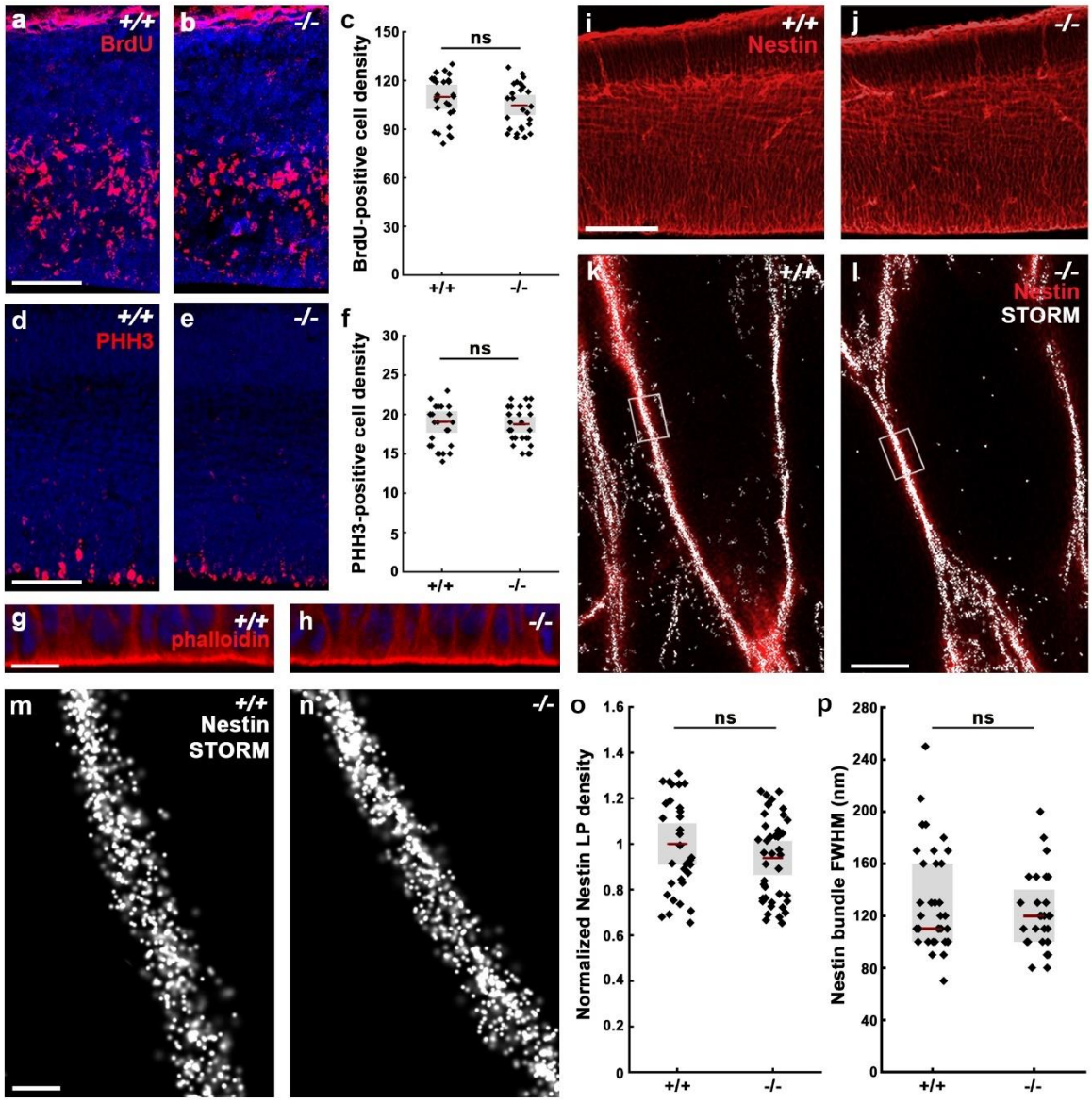

Figure 16. Loss of Abhd4 does not affect the function of radial glia cells.
(a, b) BrdU experiment indicating cell proliferation in the S phase in E14 cortices. (c) Quantification of BrdU-positive cell density (two-sided Student's t-test, *P* = 0.323; +/+: n = 6, 109.9 ± 3.738; -/-: n = 4, 104.8 ± 3.089; t = 0.9959, df = 65). (d, e) Phospho-histone H3 immunostaining visualizes cell proliferation in the M phase. (f) Quantification of phospho-histone H3 cell density (two-sided Student's t-test, *P* = 0.6882; +/+: n = 3, 19.04 ± 0.68; -/-: n = 3, 18.7 ± 0.51; t = 0.4035, df = 54). (g, h) F-actin binding phallodin labels the adherens junction belt at the ventricular surface. (i, j) Example immunofluorescence images for Nestin staining in *Abhd4* +/+ and -/- cortex. (k, l) Correlated confocal and STORM microscopic image of Nestin-positive radial glia scaffold in E15.5. (m, n) High power STORM images of the Nestin bundles. (o) Quantification of Nestin STORM localization point (LP) density

(two-sided Student's unpaired t-test, P = 0.297; +/+: n = 3, 1 ± 0.04; -/-: n = 3, 0.93 ± 0.03; t = 1.05, df = 94). (p) Quantification of full-width-at-half-maximum (FWHM) of Nestin filament bundles (two-sided Mann-Whitney U test, P = 0.684; +/+: n = 3, 0.12 ± 0.045; -/-: n = 3, 0.11 ± 0.06; U: 487). Graphs show raw data and mean ± 2 x standard error (c, f, o) or raw data and median ± interquartile range (p). ns = not significant. n indicates the number of mice per group. Scale bars indicate (a, b, d, e, i, j) 50 µm, (g, h) 20 µm, (k, l) 2 µm, (m, n) 200 nm.

To analyze the nanoscale architecture of the radial glia scaffold, we made STORM super-resolution microscopy and the composition of Nestin intermediate filament was reconstructed. Comparing the *Abhd4* +/+ and -/- cortices however, we could not discover any difference neither in the number of Nestin localization points (Figure 16o) nor the size of the Nestin bundle (Figure 16p; Nestin NLP, +/+: n = 3; -/-: n = 3; two-sided Student's t-test, P =0.297; FWHM, +/+: n = 3; -/-: n = 3; two-sided Mann-Whitney U test, P = 0.6882). Notably, we could not detect any abnormalities in the structure of the adherens junction belt visualized by Alexa568-phalloidin staining in the *Abhd4 -/-* animals, either (Figure 16g, h).

Furthermore, to examine the possible changes in the organization of *Abhd4 -/-* cortex, we measured the cell number and distribution by distinct cell-fate markers. PAX6 the marker of proliferating progenitors showed the same distribution and quantity in both genotypes. (Figure 17a-c; +/+: n = 4; -/-: n = 4; two-sided Student's t-test, P = 0.2598). In addition neither TBR1, which is the marker of deep-layer postmitotic neurons in the cortical plate, nor TBR2, an intermediate progenitor cell marker expressed in the SVZ, revealed significant changes in the embryonic *Abhd4 -/-* cortex (Figure 17d-i; TBR2, +/+: n = 3; -/-: n = 3; two-sided Student's t-test, P = 0.1942; TBR1, +/+: n = 3; -/-: n = 3; two-sided Mann-Whitney U test, P = 0.0741).

These results demonstrate that Abhd4 is not involved in classic radial glia cell functions.

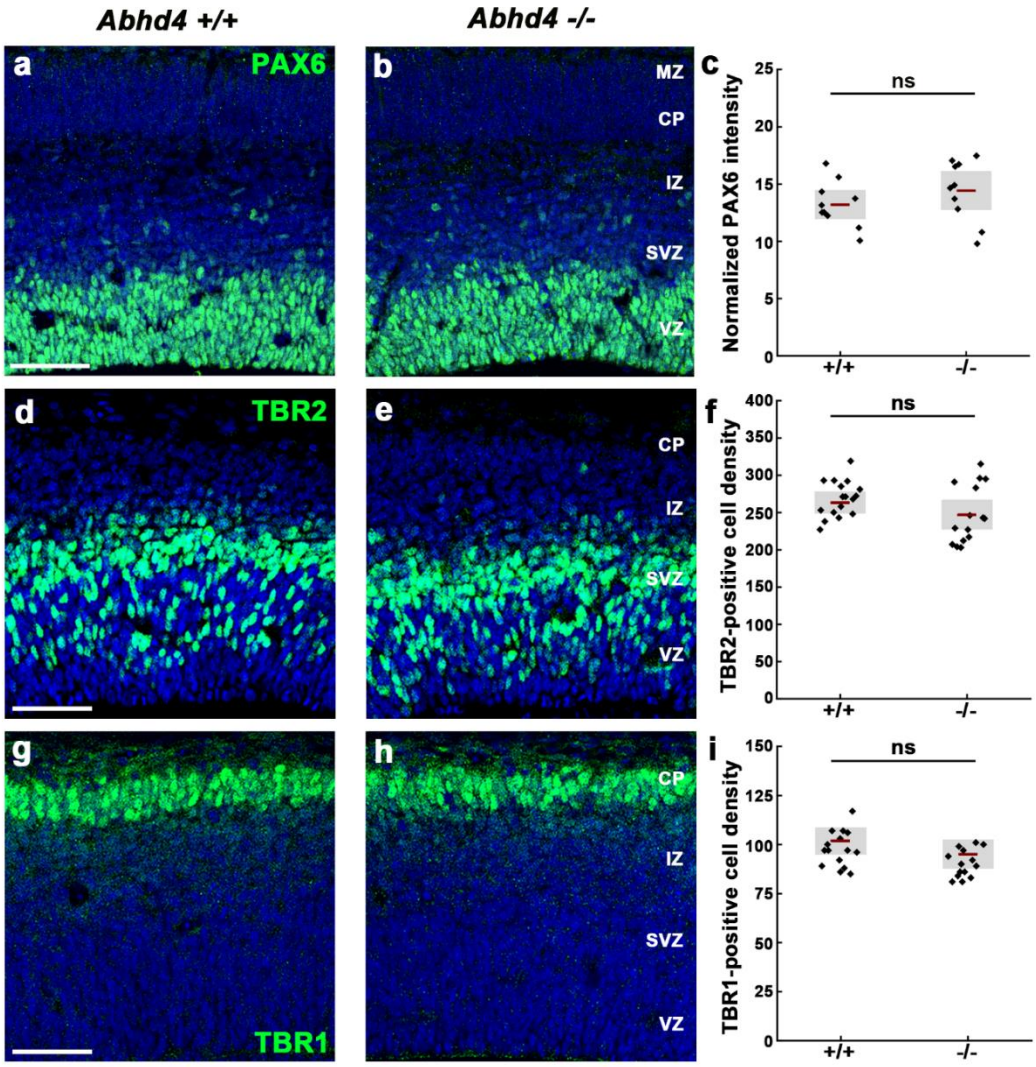

Figure 17. Laminar organization shows no difference between *Abhd4* +/+ and -/- embryos.

(a, b) PAX6-positive progenitor niche in E14 cortex of *Abhd4*+/+ and -/- embryos. (c) Quantification of PAX6 fluorescence intensity (two-sided Student's t-test, $P = 0.2598$; +/+: n = 4, 13.21 ± 0.63; -/-: n = 4, 14.44 ± 0.84; t = 1.163, df = 18). (d, e) Distribution of TBR2-positive intermediate progenitor cells in E14 cortices. (f) Quantification of TBR2-positive cell density (two-sided Student's unpaired t-test, $P = 0.194$; +/+: n = 3, 263.4 ± 7.3; -/-: n = 3, 247.3 ± 9.9; t = 1.327, df = 31). (g-i) Differentiating neurons in the cortical plate by TBR1 staining and its statistical analysis (two-sided Mann-Whitney U test, $P = 0.074$; +/+: n = 3, 97 ± 16.5; -/-: n = 3, 91 ± 15.25; U: 86). Graphs show raw data and mean ± 2 x standard error (c, f) or median ± interquartile range (i). ns = not significant. n indicates the number of mice per group. MZ: marginal zone; CP: cortical plate; IZ: intermediate zone; SVZ: subventricular zone; VZ: ventricular zone. Scale bars represent 50 µm.

4.3.3. Abhd4 is sufficient to trigger caspase-dependent cell death

As described before, we found no visible phenotype in the loss-of-function experiments and considering the specific expression of the enzyme we hypothesized that Abhd4 function must be restricted to the ventricular zone, before postmitotic daughter cells starts their radial migration. To test this idea, we expressed Abhd4 outside of the ventricular zone by using *in utero* electroporation with a plasmid contains strong promoter which remains active outside the ventricular zone and followed its effect at different time points during development. Three days after the surgery, we observed a massive migration defect in the Abhd4-electroporated cortices compared with GFP control (Figure 18a, b, d; n = 4 animals in each conditions; Kruskal-Wallis test with post hoc Dunn's Multiple Comparison Test; Bin1, 2, 4, 5: ***P < 0.0001). To prove that enzymatic function of Abhd4 is responsible for this migration phenotype, we mutated the catalytic serine in the conserved hydrolase domain to glycine (labelled inactive Abhd4-GFP in the figures) for produce a non-functional form of the protein (Figure 19).

Expression of the inactive Abhd4-GFP did not affect radial migration indicating that the enzymatic function of Abhd4 generated the migration arrest (Figure 18c, d; n = 3; Kruskal-Wallis test with post hoc Dunn's Multiple Comparison Test; Bin1, 2, 5: ***P < 0.0001; Bin4: **P = 0.0063). Moreover, ectopic expression of Abhd4-GFP also induced characteristic morphological changes such as shrinkage, loss of extensions and rounded shape. After quantification of the occurrence of the two main morphological states of the cells (bipolar vs. rounded), we found significantly decreased number of bipolar, migrating-cells after Abhd4 perturbation when compared with the controls (Figure 18e-h; n = 3 in each treatment; Kruskal-Wallis test with post hoc Dunn's Multiple Comparison Test, Abhd4-GFP vs GFP or Inactive Abhd4-GFP: *** P <0,0001; GFP vs Inactive Abhd4-GFP: $P \approx 1$).

DOI:10.14753/SE.2020.2378

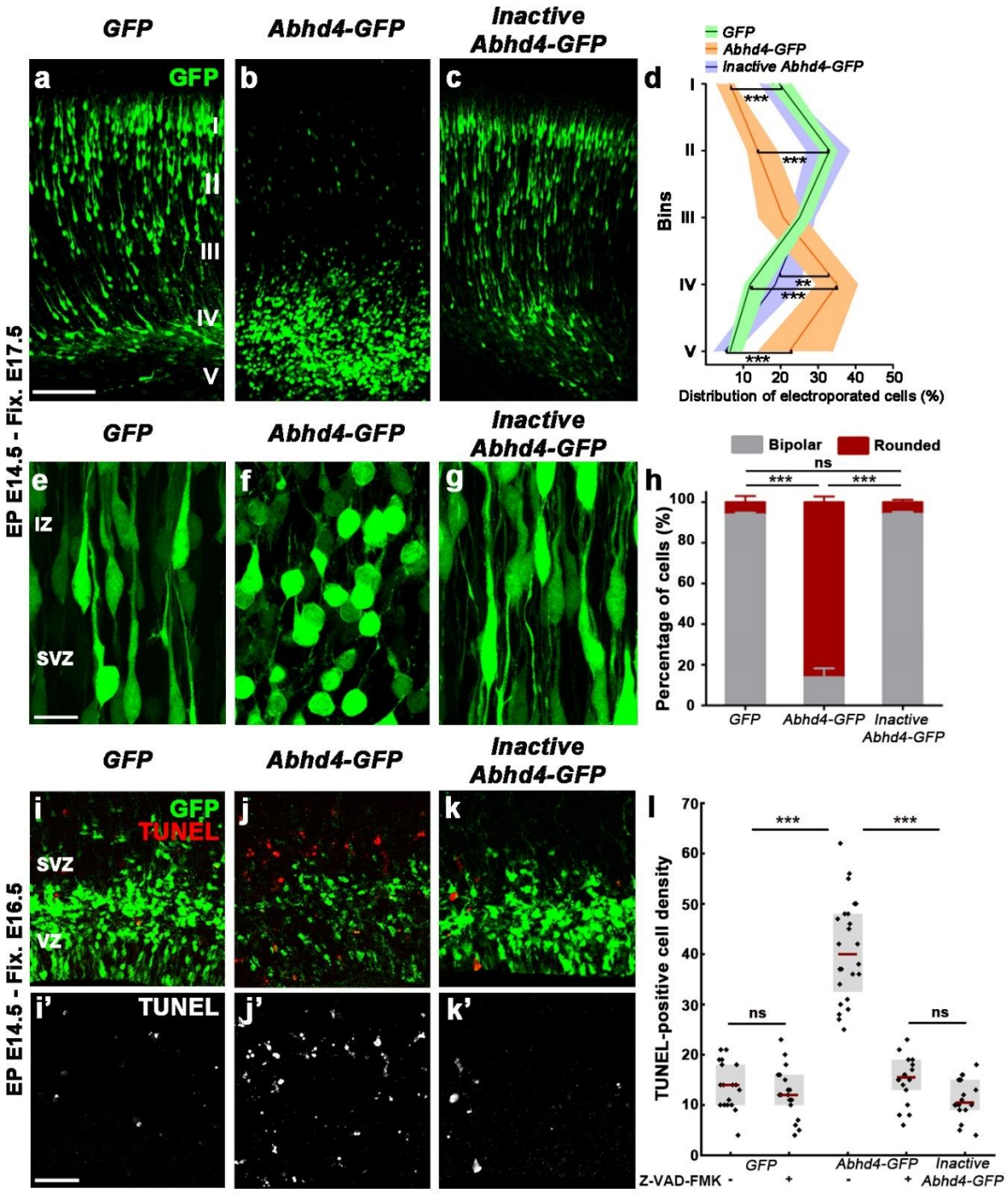

Figure 18. Abhd4 is sufficient to induce a radial migration defect and elevate caspase-dependent cell death.

(a-b) Overexpression of Abhd4-GFP causes radial migration defect when compared with GFP-electroporated control. (c) Electroporation of enzymatically inactive form of Abhd4 does not have a similar effect. (d) Schematic diagram shows layered distribution of electroporated cells in 5 equal bins (Roman numerals; Kruskal-Wallis test with post hoc Dunn's Multiple Comparison Test was made in every bin, Bin1, 2, 4, 5: ***P < 0.0001. Bin4: **P = 0.0063; Bin1: GFP: 19.7 ± 5.67; Abhd4-GFP: 6.511 ± 3.648; Inactive Abhd4-GFP: 17.84 ± 4.99; Bin2: GFP: 33.06 ± 4.01; Abhd4-GFP: 14.02 ± 6.98; Inactive Abhd4-GFP: 31.51 ± 11.21; Bin4: GFP: 111.85 ± 5.84; Abhd4-GFP: 34.75 ± 10.06; Inactive Abhd4-GFP: 18.57 ± 9.1; Bin5: GFP: 6.51 ± 3.506; Abhd4-GFP: 22.97 ± 18.48; Inactive Abhd4-GFP: 5.194 ± 5.301; GFP and Abhd4-GFP n = 4, Inactive Abhd4-GFP n = 3). Data are shown as median (line) and interquartile range (transparent band in the same color). (e-g) High magnification images show distinct morphological changes in Abhd4 overexpressing samples compared with controls. (h) Morphological changes were quantified by determining the percentage of bipolar or rounded cells in each group (Kruskal-Wallis test with post hoc Dunn's Multiple Comparison Test, ***P < 0.0001; ns = not significant, P ≈ 1; bipolar: GFP: 93.9 ± 3.83; Abhd4-GFP: 13.9 ± 7.13; Inactive Abhd4-GFP: 93.82 ± 2.15; rounded: GFP: 6.098 ± 3.87; Abhd4-GFP: 86.1 ± 7; Inactive Abhd4-GFP: 5.714 ± 2; n = 3-3 animals per treatment). Graphs show median ± interquartile range. (i-k') Representative confocal images show the increased TUNEL-positive cell density after Abhd4-GFP electroporation but not in the controls. (l) Quantification of TUNEL-positive cell density after treatments (Kruskal-Wallis test with post hoc Dunn's Multiple Comparison Test, ***P < 0.0001; ns = not significant, P ≈ 1; except Abhd4-GFP-electroporation with Z-VAD-FMK treatment vs Inactive Abhd4-GFP P = 0.607; GFP: 14 ± 8.25, n=3; GFP+ ZVAD-FMK: 12 ± 6.75, n = 3; Abhd4-GFP: 40 ± 16.25, n = 4; Abhd4-GFP+ Z-VAD-FMK: 15.5 ± 6.75, n = 4; Inactive Abhd4-GFP: 10.5 ± 6, n = 3). Graphs show raw data and median ± interquartile range. VZ: ventricular zone; SVZ: subventricular zone. Scale bars show 100 µm (a-c), 20 µm (e-g), 50 µm (i-k').

The morphological changes described above can be a manifestation of a beginning cell death process (Clarke, 1990) so next, we performed TUNEL assay on the electroporated brain slices. Two days after electroporation we found higher level of TUNEL-positive cell density in the Abhd4-expressing samples, which we could prevent using the pan-caspase inhibitor, Z-VAD-FMK or the inactive form of the enzyme (Figure 18i-l; GFP; GFP + Z-VAD-FMK and Inactive Abhd4-GFP n = 3;Abhd4-GFP and Abhd4-GFP + Z-VAD-FMK n = 4; Kruskal-Wallis test with post hoc Dunn's Multiple Comparison Test, Abhd4-GFP vs controls ***P < 0.0001; between controls P ≈ 1; except Abhd4-GFP + Z-VAD-FMK treatment vs Inactive Abhd4-GFP P = 0.607). Altogether, these results provide evidence that ectopic expression of Abhd4 evokes caspase-dependent apoptosis and radial migration defect in the mouse embryonic cortex.

DOI:10.14753/SE.2020.2378

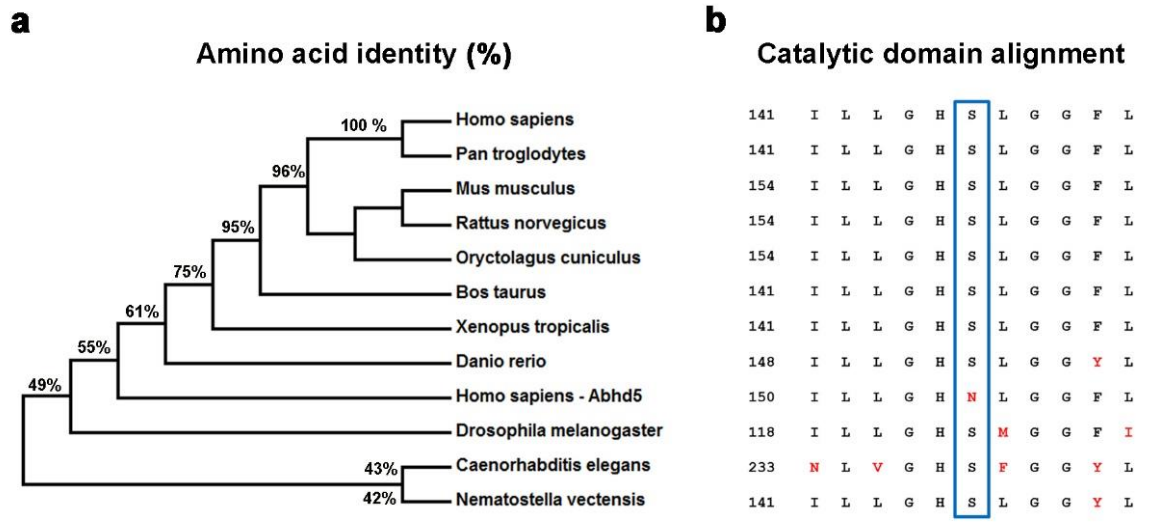

Figure 19. Abhd4 and particularly its hydrolase domain around the catalytic serine is highly conserved during evolution.

(a) The phylogenetic tree of Abh4 was created using the Maximum Parsimony method, percentage values indicate the amino acid identity between animal species and human Abhd4. (b) Highly conserved hydrolase domain contains the catalytic serine residue in the consensus "nucleophile elbow" sequence "GXSXG" (blue box) at all evolutionary level examined.

4.3.4. The mechanism of Abhd4-induced cell death

Our previous experiment using a pan-caspase inhibitor suggested that Abhd4-mediated apoptosis might be processed via the conventional intrinsic apoptotic pathway rather than the death receptor-activated one. To test this hypothesis, we chose the two main apoptosis makers (Cytocrome C: CytC and Cleaved Caspase-3: CC3) of the intrinsic pathway to investigate the cell death signaling induced by Abhd4. We transfected Human Embryonic Kidney-(HEK) 293 cell line, which lacks endogenous Abhd4 and is relatively resistant to apoptotic stimuli (Lin et al., 2014) therefore it is an ideal *in vitro* model for investigating the pro-apoptotic potential of Abhd4.

Using correlated confocal and super-resolution microscopy, we found that pixel intensity of the TOM20 mitochondrial outer membrane protein was significantly decreased after Abhd4 transfection when compared with the enzymatically inactive form (Figure 20a-e; n = 4 experiments; two-sided Mann-Whitney U test, ***P <0.0001). In parallel, the number of cytochrome c STORM localization points was lower after Abhd4 perturbation (Figure 20b-d', f; n = 4 experiments; two-sided Mann-Whitney U test, ***P <0.0001). Taking full advantage of super-resolution imaging, we could also separately quantify the distribution of intra- and extramitochondrial CytC localization points with a custom-made python script. As we expected, the level of CytC NLP was higher in the cytoplasm after Abhd4 transfection then in the control condition, meanwhile in the control the majority of the CytC NLP remained in the mitochondria (Figure 20g, h; n = 4 experiments; two-sided Mann-Whitney U test, ***P = 0.0003). In addition, we examined the level of CC3 after Abhd4 perturbation and we found that the CC3 and GFP double positive cell ratio was higher in these samples than in the inactive Abhd4-GFP transfected ones (Figure 20i-k; n = 3 experiment; two-sided Mann-Whitney U test, ***P <0.0001). Important to note, that GFP-negative CC3-positive cell number was unchanged, conclusively, Abhd4-induced cell death is a cell autonomous phenomenon (Figure 20l; n = 3 experiment; two-sided Student's t-test, P = 0.5972). In summary, we established that Abhd4 triggers the conventional intrinsic apoptotic pathway, which is mediated by CytC release from the mitochondria and the activation of the final effector, caspase-3.

DOI:10.14753/SE.2020.2378

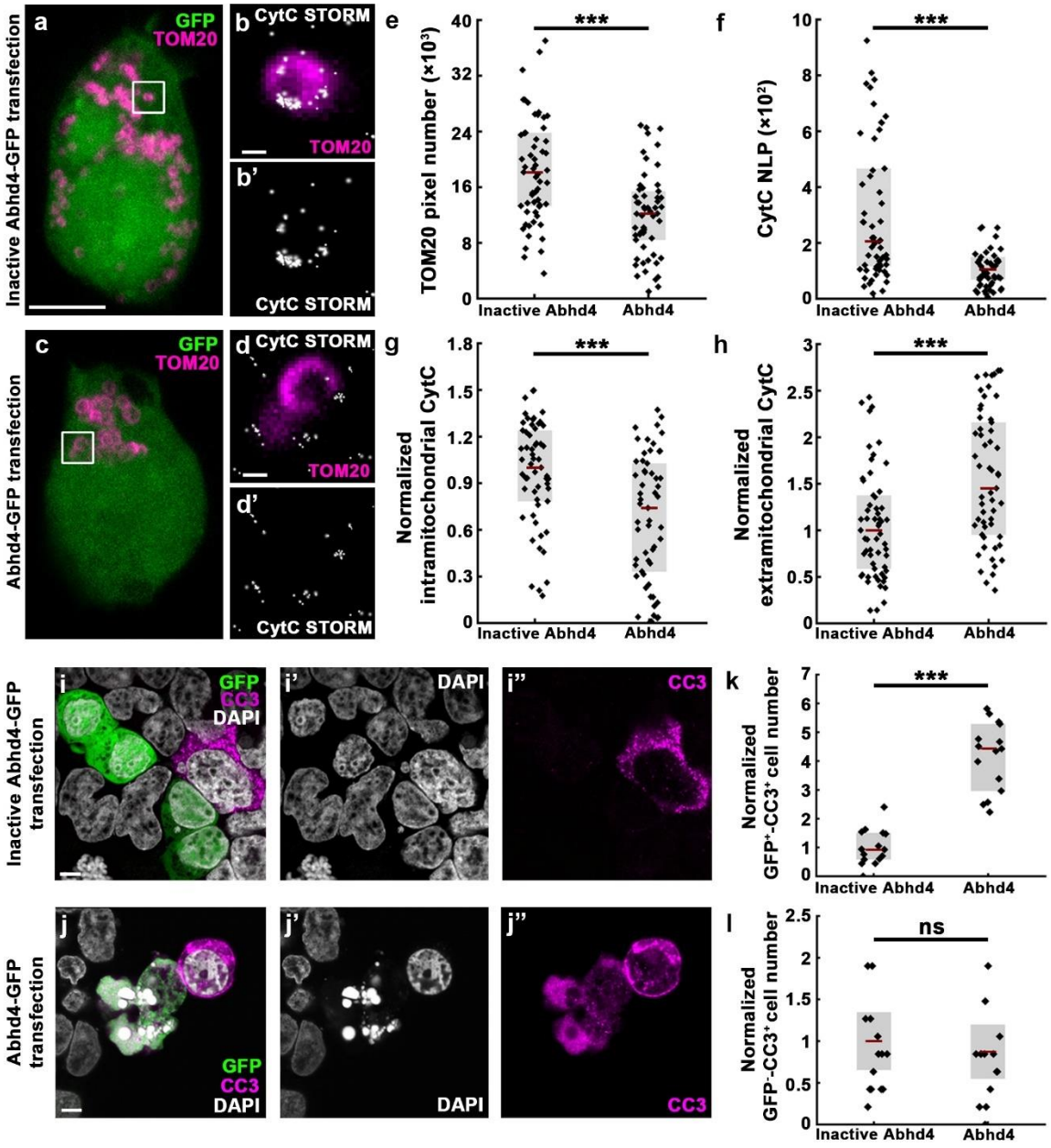

Figure 20. Increased apoptosis of HEK-293 cells after Abhd4 transfection.
(a-b) TOM20 (mitochondrial outer membrane maker) labeling mitochondria in inactive Abhd4- and Abhd4-GFP-transfected HEK-293 cells. (b-d') Representative high power confocal and STORM images of TOM20 and CytoC (cytochrome c) stained mitochondria. (e) Quantification of TOM20-positive pixel numbers in different transfections (two-sided Mann-Whitney U test, ****P* <0.0001; inactive Abhd4-GFP: 18142 ± 10872; Abhd4-GFP: 12209 ± 7617; U: 899). (f) Graph shows CytC number of localization points (NLP) comparison in transfected cells (two-sided Mann-Whitney U test, ****P* <0.0001; Inactive Abhd4-GFP: 2059 ± 4043; Abhd4-GFP: 1049 ± 888; U: 875.5) (g, h) Normalized intra- and

extramitochondrial CytC NLP in transfected groups (two-sided Mann-Whitney U test, ***P = 0.0003; Intramitochondrial: Inactive Abhd4-GFP: 1 ± 0.4728; Abhd4-GFP: 0.7403 ± 0.7115; U: 1070; Extramitochondrial: inactive Abhd4-GFP: 1 ± 0.8189; Abhd4-GFP: 1.450 ± 1.233; U: 1070). (i-j") Cleaved Caspase-3 (CC3) immunohistochemistry in inactive Abhd4-GFP and Abhd4-GFP transfection. (k, l) Quantification of the ratio of cleaved caspase-3 and GFP expressing cells (k: two-sided Mann-Whitney U test, ***P <0.0001; inactive Abhd4-GFP: 1 ± 0.9206; Abhd4-GFP: 4.162 ± 2.33; U:1; l: two-sided Student's t-test, P = 0.5972; inactive Abhd4-GFP: 1 ± 0.17; Abhd4-GFP: 0.87 ± 0.16; t = 1.053; df = 28). Graphs show raw data and mean ± 2 x standard error (l) or raw data and median ± interquartile range (e-k). (e-h) n = 4 experiments and (k, l) n = 3 experiments. Scale bars show 5 µm (a, b, i-j"), 500 nm (b, b', d, d').

4.3.5. Abhd4 is necessary for loss-of adherens junction-induced cell death

Considering the lack of defects in *Abhd4-/-* embryonic cortex (Figures 16-17) and the protein's ability to strongly induce cell death in gain-of-function experiments *in vivo* (Figure 18) and *in vitro* (Figure 20), we hypothesized that Abhd4 might be involved in the cell death process evoked by loss of adherens junctions (Figure 13). So next, we examined if endogenous Abhd4 is required for AJ-loss induced apoptosis *in vivo*. As a preliminary control (Figure 12) we showed that ΔnCdh2-GFP electroporation initiated a similar dispersion of ectopic PAX6-positive aRGPCs in both *Abhd4* genotypes, indicating that Abhd4 is not required for delamination itself (Figure 21a-c; n = 3 in both genotypes; two-sided Mann-Whitney U test, no significant difference between genotypes).

In contrast, cell death levels induced by disruption of ventricular zone adherent junctions via ΔnCdh2-electroporation were much lower in *Abhd4 -/-* than in *Abhd4 +/+* embryos (Figure 21d-e', g; n=4 from each condition; Kruskal-Wallis test with post hoc Dunn's Multiple Comparison Test, ***P < 0.0001). Furthermore, exogenous replenishment of Abhd4 by co-electroporation of the two constructs into knockout animals restored the TUNEL-positive cell density to the *Abhd4 +/+* level (Figure 21f-f', g; n = 4; Kruskal-Wallis test with post hoc Dunn's Multiple Comparison Test, Abhd4 -/- vs +/+ and co-electroporation ***P < 0.0001; Abhd4 +/+ vs co-electroporation $P \approx 1$;).

DOI:10.14753/SE.2020.2378

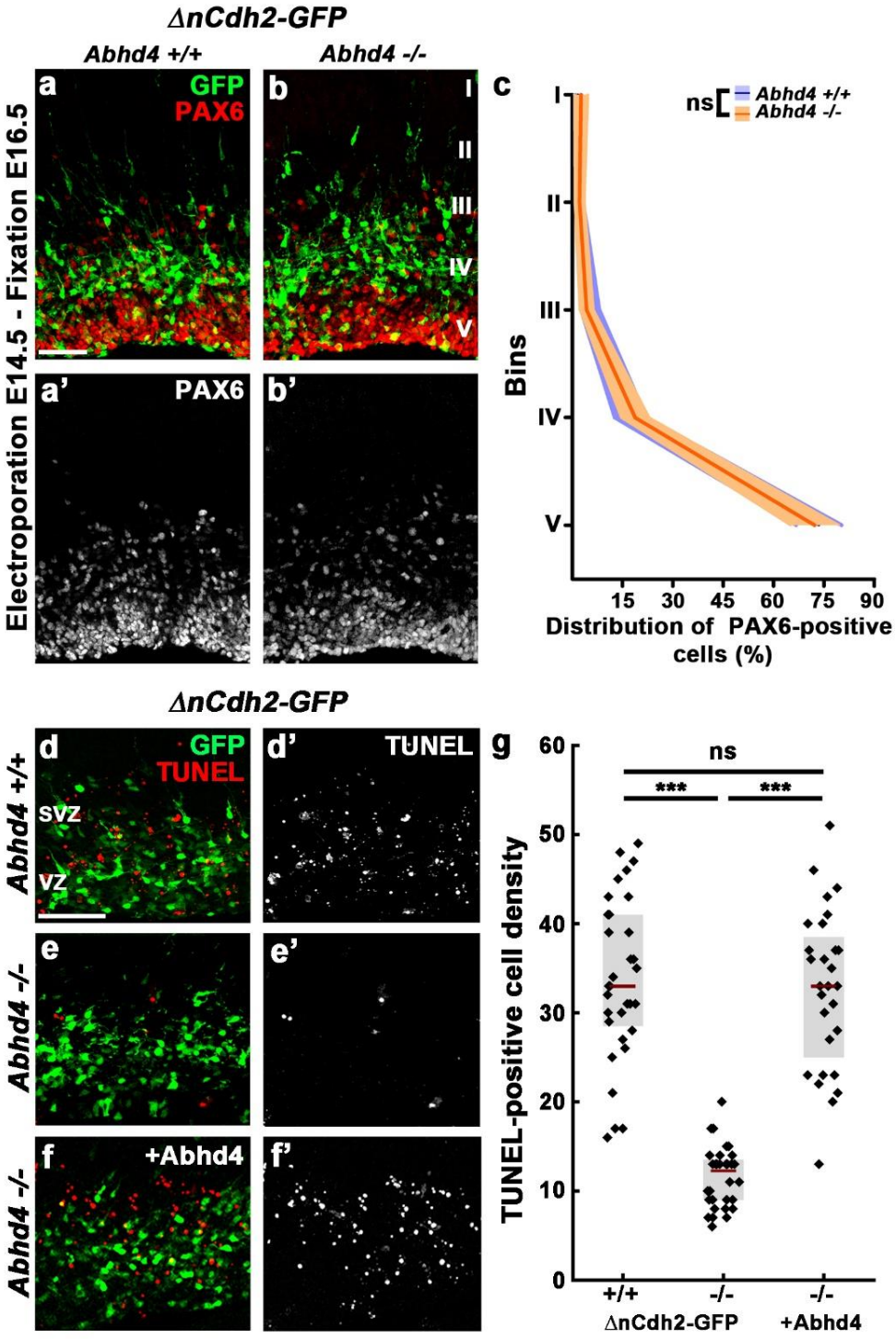

Figure 21. Abhd4 is necessary for cell death induced by loss of cadherin connection.

(a-b') *ΔnCdh2-GFP*-electroporation triggers abnormal dispersion of PAX6-positive radial glia progenitor cells in both *Abhd4* +/+ and -/- embryos. (c) Quantification of PAX6-positive cell distribution in five equally-sized bins (Roman numerals; two-sided Mann-Whitney U test for all bins; ns = not significant; Bin1: $P = 0.1985$, +/+: 1.773 ± 1.25, -/-: 2.706 ± 2.77, U: 81; Bin2: $P = 0.5897$, +/+: 1.835 ± 1.925, -/-: 2.618 ± 3.12, U:99; Bin3: $P = 0.2628$, +/+: 5.24 ± 3.81, -/-: 4.3 ± 2, U:85; Bin4: $P = 0.2134$, +/+: 15.64 ± 6.76, -/-: 17.9 ± 6.11, U:82; Bin5: $P = 0.6187$, +/+: 73.17 ± 9.85, -/-: 70.64 ± 14.21, U:100; n = 3 animals per genotypes). Data are shown as median (line) and interquartile range (transparent band in the same colour). (d-e') ΔnCdh2-GFP electroporation into Abhd4 +/+ and -/- animals provokes induced cell death in the +/+ but not in the -/-. (e-e'), ΔnCdh2-GFP and Abhd4-GFP co-electroporation can rescue the delamination-induced cell death. (g) Quantification shows TUNEL-positive cell density from each condition (Kruskal-Wallis test with post hoc Dunn's Multiple Comparison Test, ***$P < 0.0001$; ns = not significant, $P \approx 1$; Abhd4 +/+: 33 ± 12.75; Abhd4 -/-: 13 ± 4.75; Abhd4 -/- rescued: 33 ± 15.25; n = 4 from each treatment. Graph shows raw data and median ± interquartile range. n indicates the number of mice per group. VZ: ventricular zone; SVZ: subventricular zone. Scale bar indicates 25 μm (a-c').

Developmental cell death is an important regulator of the balance between the size of progenitor pools and final cortical cell number (Wong and Marín, 2019). Previously, we demonstrated that Abhd4 has a key role in delamination-induced cell death, so next we examined whether it has a similar function during developmental cell death. To this end, we examined the basal developmental cell death level in Abhd4 knockout animals. However, we could not detect any difference in basal, developmental cortical cell death levels of *Abhd4+/+* vs *Abhd4-/-* embryos at E16.5 (Figure 22a-c; n = 5 per genotype; two-sided Mann-Whitney U test, $P = 0.834$) or at P3 (Figure 22d-f; +/+: n = 6; -/-: n = 5; two-sided Mann-Whitney U test, $P = 0.792$) when the peak of programmed cell death of excitatory neurons occur (Wong et al., 2018). Furthermore, the loss of Abhd4 does not influence the cellular composition of the adult cortex. By using cell population markers such as *vGlut1* for excitatory neurons, *Gad67* for inhibitory neurons and *Glast1* for astrocytes we could not reveal any distribution differences between Abhd4 +/+ and -/- animals (Figure 23; n = 3 in both genotypes, two-sided Mann-Whitney U test , $P > 0.05$ in all bins of all experiments).

These data demonstrate that Abhd4 is a necessary molecular player of cadherin-loss induced cell death but not required for normal, developmental cell death processes.

DOI:10.14753/SE.2020.2378

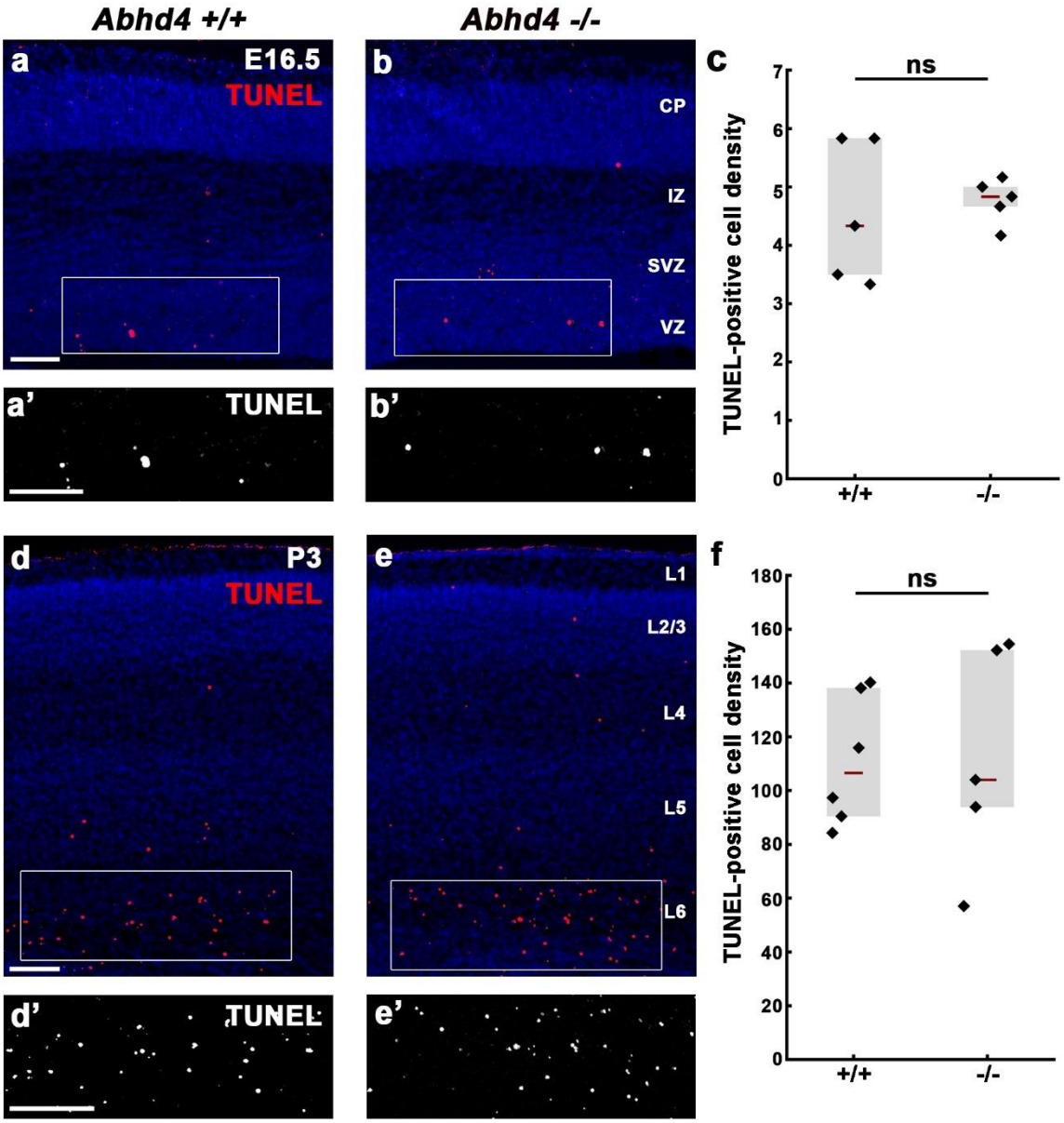

Figure 22. Loss of Abhd4 does not influence developmental cell death.
(a-b') Developmental cell death is not affected by loss of Abhd4 in the E16.5 embryonic cortex. (c) Quantification of TUNEL-positive cell density in +/+ and -/- embryonic cortices (two-sided Mann-Whitney U test, $P = 0.834$; +/+: 4.33 ± 2.41; -/-: 4.833 ± 0.66; n = 5 in both genotypes; U: 11). (d-e') Postnatal cell elimination is also not affected by the absence of Abhd4. (f) Statistical comparison of TUNEL-positive cell density in Abhd4 postnatal animals (two-sided Mann-Whitney U test, $P = 0.792$; +/+:106.6 ± 49.72, n = 6; -/-: 104 ± 77.91, n = 5; U: 13). Data are shown as median values per animals and median ± interquartile range. n indicates the number of mice per group. L1-6 mark the cortical layers. Scale bars show 50 µm (a-b'), 100 µm (d-e').

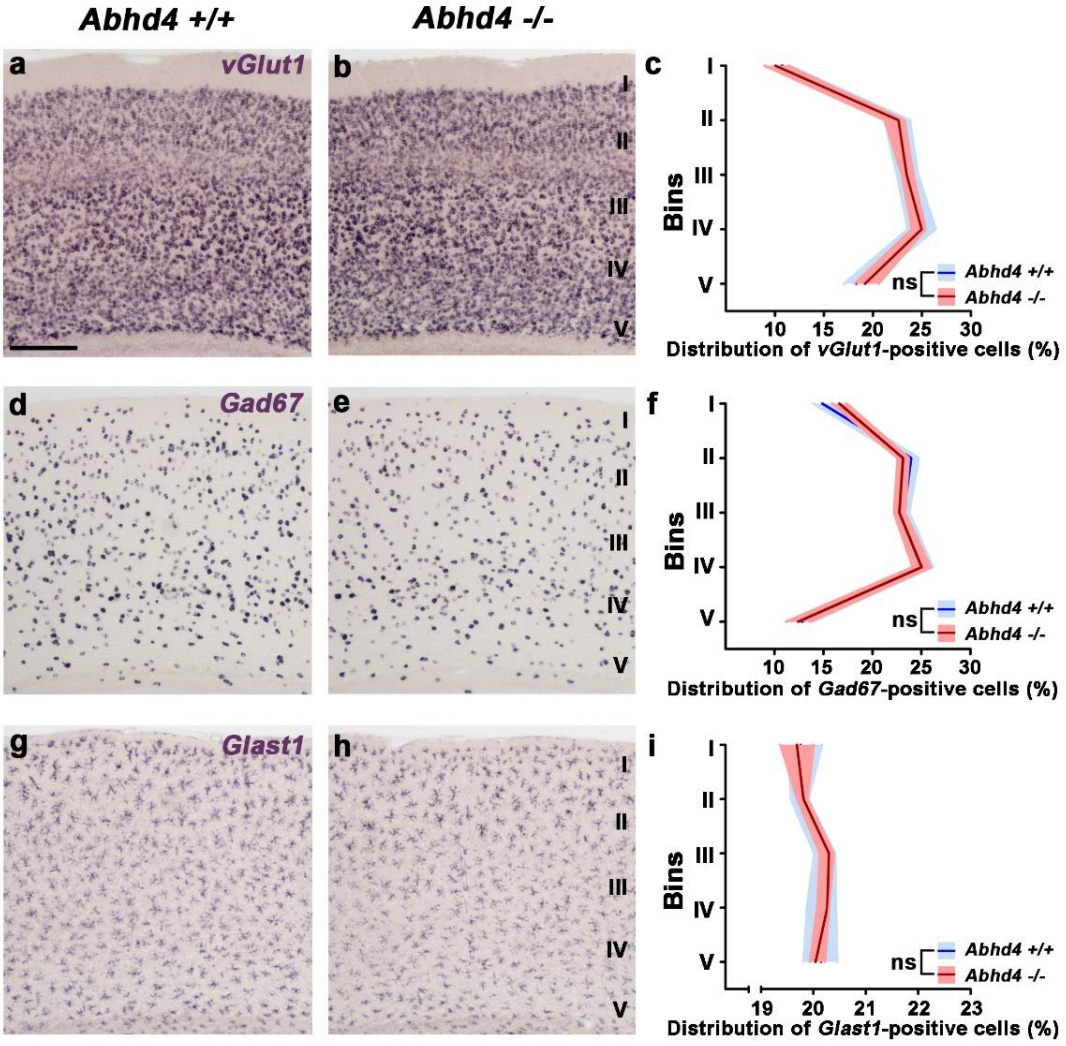

Figure 23. Genetic loss of Abhd4 does not affect the differentiation and distribution of distinct cell types in the adult cortex.

(a-b) *vGlut1* mRNA labels the excitatory neurons in the Abhd4 +/+ and -/- cortices. (c) Quantification of *vGlut1*-positive cell distribution between five identical sized cortical bins (Roman numerals; two-sided Mann-Whitney U test for all bins; ns = not significant; Bin1: *P* = 0.11446, +/+: 10.6 ± 1.86, -/-: 10 ± 2.4, U: 215; Bin2: *P* = 0.4753, +/+: 21.5 ± 2.3, -/-: 22.6 ± 2, U:251; Bin3: *P* = 0.6122, +/+: 23.3 ± 0.4, -/-: 23.4 ± 1.18, U:261; Bin4: *P* = 0.084, +/+: 25.2 ± 2.7, -/-: 25 ± 1.4, U:202; Bin5: *P* = 0.2773, +/+: 19 ± 3, -/-: 19 ± 2.4, U:233). (d-e) *Gad67* mRNA visualizes inhibitory cells. (f) Distribution of *Gad67*-positive cells (two-sided Mann-Whitney U test for all bins; ns = not significant; Bin1: *P* = 0.1245, +/+: 14.3 ± 9, -/-: 16.4 ± 6, U: 213; Bin2: *P* = 0.3588, +/+: 24 ± 7, -/-: 23.6 ± 5.6, U:243; Bin3: *P* = 0.279, +/+: 23.5 ± 5.5, -/-: 22.82 ± 5.2, U:235; Bin4: *P* = 0.9425, +/+: 26.1 ± 9.5, -/-: 26.2 ± 9.4, U:284; Bin5: *P* = 0.9261, +/+: 10.7 ± 11.2, -/-: 9.4 ± 12.6, U:283). (g-h) Astrocytes were labeled with *Glast1* in situ hybridization. (i) Quantification of *Glast1*-positive cell distribution in 5 bins (Roman numerals; two-sided Mann-Whitney U test for all bins; ns =

not significant; Bin1: P = 0.4154, +/+: 19.76 ± 0.6, -/-: 19.7 ± 0.6, U:248; Bin2: P = 0.27, +/+: 19.7 ± 0.3, -/-: 19.8 ± 0.2, U:234; Bin3: P = 0.2883, +/+: 20.1± 0.4, -/-: 20.3 ± 0.3, U:236; Bin4: P = 0.3481, +/+: 20.1 ± 0.6, -/-: 20.2 ± 0.2, U:242; Bin5: P = 0.1904, +/+: 20.1 ± 0.7, -/-: 20 ± 0.3, U:224). Abhd4 +/+ n=3, Abhd4 -/- n=3. Data are shown as median (line) and interquartile range (transparent band in the same color). Scale bar indicates 50 µm.

4.3.6. Fetal alcohol exposure induces Abhd4-dependent cell death in the embryonic cortex

Alcohol, the most commonly abused teratogen among pregnant women. Previously, it has been shown that alcohol exposure during pregnancy not only affects brain development, but also has negative long-term postnatal effects (Robertson et al., 2016). In the embryonic cortex, alcohol exposure can cause abnormal delamination (Ishii et al., 2017), cortical migration defect (Aronne et al., 2011; Delatour et al., 2019) and increased cell death (Farber et al., 2010; Ikonomidou et al., 2000; Wilhelm and Guizzetti, 2016). Therefore, we tested if Abhd4 is required for alcohol-induced changes in the embryonic cortex. Using a repeated drinking model over a span of three days, resulted in an elevation of cortical cell death levels in Abhd4+/+ embryonic cortices (Figure 24c-c'). However, lack of Abhd4 rescued the cell death (Figure 24a-e; vehicle +/+: n = 5; vehicle -/-: n = 4; EtOH +/+: n = 4; EtOH -/-: n = 3; Kruskal-Wallis test with post hoc Dunn's Multiple Comparison Test, Abhd4 +/+ vs -/- and vehicles ***P < 0.0001; Abhd4 -/- vs vehicles $P \approx 1$). Surprisingly, even a single dose of alcohol, simulating binge drinking, can elevate cell death levels in the ventricular zone of the developing cortex but again, lack of Abhd4 can prevent this (Figure 24f-j; n = 3 in each genotype and condition; Kruskal-Wallis test with post hoc Dunn's Multiple Comparison Test, Abhd4 +/+ vs -/- and vehicles ***P < 0.0001; Abhd4 -/- vs vehicles $P \approx 1$).

These results demonstrate that Abhd4 is also essential for mediating maternal alcohol exposure-induced cell death in the embryonic neocortex.

DOI:10.14753/SE.2020.2378

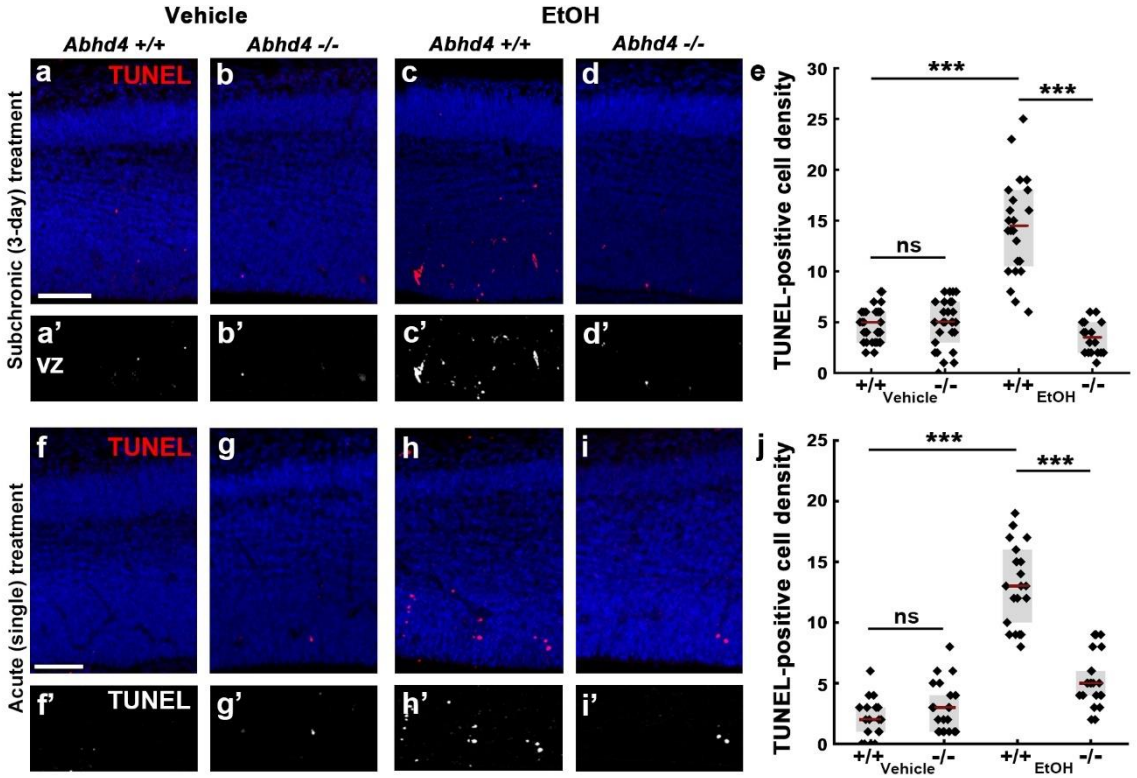

Figure 24. Maternal alcohol exposure evokes Abhd4-dependent cell death.
(a-d') Acute alcohol treatment evokes increased cell death in Abhd4 +/+ animals but not in -/- embryos when compared with vehicle controls. (e) Quantification of acute alcohol model (Kruskal-Wallis test with post hoc Dunn's Multiple Comparison Test, ***$P < 0.0001$; ns = not significant, $P \approx 1$, Vehicle Abhd4 +/+: 2 ± 2.25; Vehicle Abhd4 -/-: 3 ± 3.5; EtOH Abhd4 +/+: 13 ± 6.5; EtOH Abhd4 -/-: 5 ± 2; n = 3 in each condition). (f-i') Subchronic alcohol treatment of Abhd4 transgenic mice causes increased cell death in the +/+ but not in the -/- embryos. (j) Statistical summary of subchronic alcohol model (Kruskal-Wallis test with post hoc Dunn's Multiple Comparison Test, ***$P < 0.0001$; ns = not significant, $P \approx 1$; Vehicle Abhd4 +/+: 5 ± 3, n=5; Vehicle Abhd4 -/-: 5 ± 4, n=4; EtOH Abhd4 +/+: 14.5 ± 7.75, n=4; EtOH Abhd4 -/-: 3.5 ± 3, n=3). Graphs show raw data and median ± interquartile range. n indicates the number of mice per group. VZ: ventricular zone. Scale bars represent 100 µm (a-i').

DOI:10.14753/SE.2020.2378

5. Discussion

5.1. The role of N-cadherin during cortical development

5.1.1. *Cdh2* as a regulator of proliferation and differentiation

Cell adhesion is indispensable during brain development. It not only establishes cell-cell or cell-ECM connections but also regulates cell fate commitment, cell migration and circuit assembly (Chen et al., 2013; Hirano and Takeichi, 2012). N-cadherin is one of the main adhesion molecules which is responsible for cell-cell connections between progenitor cells in both the pallial and the subpallial germinative niches (Kadowaki et al., 2007; Luccardini et al., 2013).

Complete loss of N-cadherin disrupts cellular organization of the developing neuroepithelium both in lower vertebrates (Gänzler-Odenthal and Redies, 1998; Lele et al., 2002), and mammals (Radice et al., 1997). At later stages, neocortex/radial glia cell-specific elimination of *Cdh2* resulted in proliferation abnormalities, radial migration defects and misplaced progenitor cells in the pallium (Gil-Sanz et al., 2014; Kadowaki et al., 2007). Similarly, N-cadherin disruption in the ventricular zone of the subpallium also causes proliferation defects and abnormal tangential migration (Luccardini et al., 2013, 2015). In harmony with the above-mentioned data, our results demonstrate that disruption of N-cadherin-based adherens junction in aRGPCs triggers abnormal delamination and mis-positioning of PAX6-positive cells in the dorsal telencephalon. Active N-cadherin connections recruit several messenger molecules such as the pro-survival factor AKT (Zhang et al., 2010), which stabilizes the cytoplasmic level of β-catenin, therefore it can directly regulate the transcription of PAX6 (Gan et al., 2014). Due this signaling pathway, progenitor cells can inhibit their own differentiation and maintain proliferation through positive feedback regulation (Gan et al., 2014; Zhang et al., 2010, 2013).

5.1.2. The role of N-cadherin in the postmitotic phase of neuronal development

During postmitotic glutamatergic cell migration N-cadherin is expressed in the leading process and maintains the adhesion between the radial glia scaffold and the postmitotic cell (Kawauchi et al., 2010). Furthermore, N-cadherin engagement between CR cells and

migrating neurons promotes the final translocation of excitatory cells (Franco et al., 2011; Gil-Sanz et al., 2013). Accordingly, suppression of N-cadherin in pallial postmitotic cells disrupt their radial migration and final translocation (Franco et al., 2011; Kawauchi et al., 2010).

Similarly, we showed that selective elimination of *Cdh2* from postmitotic interneurons evokes a delay in their tangential migration at a very early (E14) stage. We also detected a decreased number of Gad65-GFP-positive cells in the adult somatosensory cortex but our experiments have excluded early mitotic problems or elevated apoptosis as potential causes. Additionally, migrating interneuron precursors in the knockout cortices have shown no sign of cell-fate changing or misdirected migration in the knockout animals, so we could only assume that the delayed cells could not enter the cortical plate and commence the radial phase of migration. Accordingly, it has been reported earlier that N-cadherin is an instructive signal for migrating INs, regulating cell polarity and leading process directionality in MGE-driven cells (Luccardini et al., 2013, 2015). It is important to note that according to our experiments, loss-of *Cdh2* postmitotically mainly affects cells of CGE origin (López-Bendito et al., 2004). Taken together, our observations and the previous data highlight the role and importance of N-cadherin signaling during tangential migration in both MGE- and CGE-driven cells.

Although the presence of N-cadherin during radial migration is controlled by both Rab GTPase-mediated endocytosis and reelin signaling (Franco et al., 2011; Gil-Sanz et al., 2013; Jossin and Cooper, 2011), such a regulatory mechanism during interneuron migration has not been reported yet. One possibility can be the Slit/Robo signaling, which determines the direction of the tangential migration due the actin-dependent collapse of the leading process (Andrews et al., 2007; Peyre et al., 2015). It is interesting to note in this regard that during axonal pathfinding, activation of Robo by Slit establishes a multimolecular complex including N-cadherin (Rhee et al., 2002) which results in a disassembly of cadherin-based adhesion (Rhee et al., 2007).

5.1.3. The long-term effects of N-cadherin elimination

The long-term effects of N-cadherin disruption were investigated in glutamatergic cell maturation (Wakimoto et al., 2015). Using *in utero* electroporation of dominant-negative N-

cadherin construct, disruption in barrel cortex formation and decreased axonal density of callosal trajectories were detected (Wakimoto et al., 2015). In interneuron development however, our experiments were the first to investigate the long-term effect of N-cadherin absence. We observed significantly less Gad65-GFP positive interneurons in the somatosensory cortex of adult knockout mice. More importantly loss of *Cdh2* had a cell-type-specific effect. Interestingly, after examination of the main interneuron subclasses, we observed less SST- and Calb2-positive interneurons in *Cdh2* knockout animals. Moreover, we provided evidence that the SST/Calb2 double positive population also decreased in the absence of *Cdh2*. Knowing the fact that cortical interneurons originate from distinct parts of the ganglionic eminences (Tremblay et al., 2016) this appears to be a bit of a contradiction since SST-positive interneurons are born in the MGE, while Calb2-positive interneurons are produced in the CGE (Lim et al., 2018). However, there is a common IN population which express both SST and Calb2 from the most-dorsal part of MGE (Fogarty et al., 2007; Sousa et al., 2009). Recent single-cell RNA-sequencing data analysis has revealed that this region contains a mixture of cells with MGE and CGE phenotypes, as it was reported that SST is also expressed in a unique CGE population (Mi et al., 2018). Additionally, another study also using high-throughput RNA-sequencing found another SST/Calb2 population in the adult cerebral cortex (Tasic et al., 2018).

Although we reported a reduction in the number of SST- and Calb2-positive interneurons, the loss of Calb2-positive cells was greater than the reduction in single SST-positive cell numbers. This suggests that another, only Calb2-positive cell population was also affected. These cells might be a part of the reelin-positive cell population which is also produced by CGE progenitors (Miyoshi et al., 2010). This is supported by the fact that we found a decrease in the number of reelin-positive INs which however did not reach significance probably because of the large number of Reln-positive cells. In contrast to our results, genetic ablation of *Cdh2* from excitatory neurons has not been reported to cause cell-type-specific effects (Gil-Sanz et al., 2014; Kadowaki et al., 2007). Although such an analysis would require possibly single-cell RNA-sequencing-based classifying of the cells in the adult cortex to see if its glutamatergic cell composition was changed (Tasic et al., 2016; Wang et

al., 2018). At this point however, it appears that N-cadherin has a more general function during glutamatergic than in interneuron development.

Regarding our presented data, the obvious question arises: "Why does the absence of N-cadherin affect only the SST and Calb2 subpopulations? First, it can be due to simple genetic redundancy, since several other structurally similar (ie. classic) cadherins are also present in the developing brain (Lefkovics et al., 2012). However, it is also possible that the regulation of N-cadherin therefore its availability during interneuron development is different between distinct subtypes. Several reports have claimed that interneuron fate-commitment is already established before the neuroblasts leave the subpallium (Gelman and Marín, 2010; Lim et al., 2018) and this early commitment is regulated by the precise temporal and sequential expression of transcription factors (Wonders and Anderson, 2006). Interestingly, there is a transcription factor Nkx6.2, which has a unique pattern in the dorsal part of the MGE (Stenman et al., 2003). Furthermore, researchers using genetically modified mouse models established that interneurons originating from this Nkx6.2-positive region are expressing both somatostatin and calretinin (Fogarty et al., 2007; Sousa et al., 2009). Finally, the SST/Calb2-positive interneuron population is missing in the Nkx6.2 knockout animals (Sousa et al., 2009) similarly to what we observed in *Cdh2* knockout mice. Therefore, it would be exciting to investigate whether Nkx6.2 directly or indirectly regulates *Cdh2* gene expression.

Another explanation for the subtype-specificity of N-cadherin could come due to the nature of interneuron production. It is well-known that different types of interneurons are born in a spatially and temporally controlled manner(Butt et al., 2007; Lim et al., 2018). Accordingly, MGE-driven interneurons are born and migrate first, followed by CGE-driven interneurons (Butt et al., 2007; Miyoshi et al., 2010). This raises the possibility that sequentially arriving interneurons occupy the appropriate cortical layers in distinct time windows. Interestingly, it has been reported that non fast spiking SST/Calb2-positive interneurons are produced at the same time as the CGE-driven Calb2-positive population, but only after the solely SST-positive interneurons from embryonic day 15 in rodents (Miyoshi et al., 2007). For this reason, it may be that calretinin-positive populations are uniquely

guided somehow to the dorsal cortex via N-cadherin mediated adhesion and/or signaling and if this signal is disrupted, they are unable to take part in the neocortical circuit assembly and removed via programmed cell death.

5.2. The role of N-cadherin in cellular survival

5.2.1. Mechanism of the anti-apoptotic effect of N-cadherin-based connections

In the course of this work we provided evidence that loss of N-cadherin induces an apoptotic cell death pathway *in vivo*. The main question is: What is the mechanism of this phenomenon? Previous *in vitro* studies might help answer this question. It has been described that, survival of primary hippocampal neurons on N-cadherin-containing substrate largely facilitates their survival when compared with poly-L-lysine (Lelièvre et al., 2012). Also, cadherin engagement protects GT1-7 neuronal cells against apoptosis even when other survival factors (eg. cell-ECM connections) are not present (Lelièvre et al., 2012). Mechanistically, active N-cadherin-based adherens junctions in PC3 cells have been described to mediate a large increase in the expression of the pro-survival protein Bcl-2 (Tran et al., 2002). Furthermore, N-cadherin engagement activated the Erk1/2 MAP kinase pathway in primary hippocampal cultures coupled with a significant decay of the pro-apoptotic protein Bim-EL (Lelièvre et al., 2012). This holds the cytoplasmic pool of β-catenin at an appropriate level meanwhile AKT can recruit anti-apoptotic proteins therefore promotes the cellular growth and survival (Lelièvre et al., 2012; Tran et al., 2002). In addition, *in vivo* results which examined loss-of N-cadherin function - but did not address the question of cell death - indicated that AKT/β-catenin signaling mediates the pro-stemness effect of N-cadherin-based connections (Zhang et al., 2013). Therefore, it appears most likely that loss of adherens junctions acts via the same pathway (ie. decrease in AKT and in turn β-catenin levels). This explains both the premature differentiation and, due to the pro-survival nature of AKT signaling, the pro-apoptotic effect as well.

5.2.2. The concept of developmental anoikis

Classic epithelial cells are tightly encored in a tissue environment via cell-cell and cell-extracellular matrix (ECM) molecules. In the latter, integrins establish the connection with

ECM proteins (laminins) which suppresses apoptosis by eliciting anti-apoptotic and pro-survival signals from the ECM (Radakovits et al., 2009). Cell-ECM connection-loss in epithelial tissues which can be observed during unwanted epithelial-mesenchymal transition (ie. the first step of metastatic process) induces a special form of apoptosis called anoikis (Frisch and Francis, 1994; Paoli et al., 2013).

Accordingly, disconnection of the laminin-integrin complex at the pial surface of the embryonic cortex also triggers apoptosis (Radakovits et al., 2009). Considering however, that radial glia cells and classic epithelial cells share common features (see introduction), we proposed to extend the concept of anoikis to the loss of cell to cell connections as well and suggested the term "developmental anoikis" for the phenomenon we discovered. This idea is supported by another study which claimed that adherens junction disruption provokes epithelial to mesenchymal transition-like changes in the developing cortex (Itoh et al., 2013). Another study demonstrated that loss of basal cell-ECM connections also disassembled the adherens junctions in the ventricular zone (Loulier et al., 2009) indicating a strong connection between the two processes. In contrast, our findings showed that perturbation of cadherin-based AJs did not dissociate the cell-ECM link at E15.5 when it was already inducing apoptosis. This highlights the possibility that the loss of cell-cell connections is in fact the ultimate signal for the induced apoptotic process at least in the developing cortex, but to prove this unambiguously would require several additional experiments.

5.2.3. Outlook: The functional impact of N-cadherin research in brain disease

Given that cell adhesion has a pivotal role during cortical development, its malfunction naturally can lead to several serious brain diseases. Surprisingly until recently, the N-cadherin gene itself has not been associated with any neural developmental defects. This has changed however, since a new study found that genetic mutations in the *Cdh2* gene were associated with different types of brain malformation (Accogli et al., 2019). In this work, 9 individuals were examined, 7 patients with missense mutations and two with frameshift mutations which mainly affected the extracellular binding domain of the protein (Accogli et al., 2019). The genetic variants of *Cdh2* described in the paper disrupt the adhesive function

of N-cadherin and elicit abnormalities in the brain and some other organs as well. Collectively, the genetic disorder linked to N-cadherin mutations is referred as ACOG syndrome (agenesis of corpus callosum, axon pathfinding, cardiac, ocular, and genital defects; Accogli et al., 2019). These symptoms correlate well with those described in mouse and even zebrafish loss-of-function mutations (Lele et al., 2002; Masai, 2003; Radice et al., 1997).

Before this publication however, there had been several lines of evidence linking N-cadherin, adherens junctions and the actin cytoskeleton to brain developmental defects. Impairments in neuronal migrations caused by genetic mutations or environmental insults lead to the disorganization of the normal cortical structure (Juric-Sekhar and Hevner, 2019). Mutation in filamin1 gene which encodes an actin-binding protein with important function in cytoskeletal dynamics during locomotion, evokes a dominant developmental disorder called periventricular heterotopia (Ferland et al., 2009; Fox et al., 1998). As a consequence, loss of filamin1 function disrupts the adhesion belt and promotes neuroblast accumulation into nodules along the ventricular wall therefore these patients have thicker cortex inducing various forms of mental disabilities in adulthood (Ferland et al., 2009; Fox et al., 1998). In contrast, genetic duplication or activating mutations in genes encoding the PI3K/AKT/mTOR protein triad cause focal cortical dysplasia and result in localized cortical overgrowth (Conti et al., 2015; Juric-Sekhar and Hevner, 2019).

Similarly, cortical dysplasia (and microcephaly) are the main symptoms of Warburg-Micro syndrome which is a rare autosomal recessive disease (Morris-Rosendahl et al., 2010). Genetic mapping identified mutations in the genes of Rab3 and Rab18 (Handley et al., 2013). These proteins are part of the endosomal recycling system and regulate radial migration via influencing the presence of N-cadherin in the membrane of neuroblasts (Wu et al., 2016). In addition, huntingtin, mutation of which causes Huntington's disease, was reported to regulate radial migration and cell polarization via Rab11-dependent N-cadherin trafficking (Barnat et al., 2017). Furthermore, huntingtin mutations recapitulating the human mutated form of the protein (PolyQ-HTT) results in morphological disruptions in the adult mouse brain (Barnat et al., 2017). Interestingly, interneuron loss and neurodegeneration were also observed in the

mouse model for Huntington' disease (Mehler et al., 2019). This coincides well with our data showing loss of interneurons in postmitotic *Cdh2* knockout mice. Moreover, striatal calretinin-positive interneurons are highly compromised in human diseases, such as the autism spectrum disorder (Adorjan et al., 2017), Parkinson's and Huntington's diseases (Petryszyn et al., 2018). Although the human striatum contains more and distinct types of calretinin-positive interneurons (Petryszyn et al., 2018), it would be interesting to investigate the Abhd4-dependency of these phenotypes in mouse models of the previously mentioned human diseases.

5. 3. Abhd4 function in normal and pathophysiological development of the cortex

5.3.1. Abhd4 as a pro-apoptotic protein

We have demonstrated that Abhd4, a serine hydrolase plays an essential role in adherens junction loss-induced anoikis. Abhd4 is a member of the alpha/beta hydrolase protein superfamily, which is named after the evolutionarily conserved, α-helices and β-sheets containing hydrolase domain. The so-called nucleophile elbow contains the consensus GXSXG motif with the catalytic serine residue located in the middle of the protein. Abhd4 was initially proposed to be an N-acyl-phosphatidyl-ethanolamine (NAPE) lipase involved in the synthesis of the endocannabinoid molecule, anandamide (Simon and Cravatt, 2006). However, a recent publication using Abhd4 knockout animals has revealed that the protein is also responsible for the synthesis of plasmalogen based lyso-NAPEs, glycerophospho-NAEs and N-acyl lysophosphatidylserines (Lee et al., 2015) which greatly expands the potential biolipid pool related to Abhd4 function and novel *in vivo* experiments (eg. lipid rescue after ΔnCdh2 EP in *Abhd4-/-* animals) will be required in the future to identify the exact target responsible for the developmental anoikis phenomenon.

Lipid molecules are known to be involved in all steps of the apoptotic process (Agmon and Stockwell, 2017). Consequently, Abhd4 as a PLA2-type enzyme could very well be carrying out alterations in lipid homeostasis which mediate cell death. The question is, what is the mechanism of this lipid-mediated cell death? There are 3 possibilities: 1. Abhd4 is

generating a pro-apoptotic lipid. 2. Abhd4 is removing a lipid that prevents cell death. 3. Abhd4 acts non-specifically as a lipase degrading various cellular membranes.

As for the first version, there are two obvious candidates. Beyond the role of anandamide in neuronal transmission, several studies proposed that anandamide has cell death regulating function as well (Katona and Freund, 2012; Maccarrone and Finazzi-Agró, 2003). Interestingly, these reports claimed that AEA activation induces ER-stress pathways which in turn via different apoptotic pathways leads to cell death (Carracedo et al., 2006; Gallelli et al., 2018). Moreover, another study using *in vitro* human neuroblastoma cells showed that AEA through p53-included signaling is able to trigger apoptosis in a dose-dependent manner (Pasquariello et al., 2009). AEA was also revealed to provoke concentration-dependent apoptosis via TRPV1 and CB1 receptors (Adinolfi et al., 2013). In contrast, another report showed a receptor-independent mechanism (Soliman and Van Dross, 2016). All these results suggest that Abhd4-dependent cell death might be mediated by AEA in the embryonic brain. Unfortunately, it was also shown that genetic elimination of Abhd4 is insufficient to influence AEA levels (Lee et al., 2015). It is important to note, that these experiments were conducted using total adult brain lysates, therefore the functional relationship between Abhd4 and AEA in the embryonic brain is in need of further investigation. Besides the fact that the main AEA synthesizing enzyme NAPE-PLD is reported to be enzymatically active only from the first postnatal week (Morishita et al., 2005) argues in favor of the possibility that AEA production is carried out via alternative synthetic pathways in the embryonic brain and two of these pathways are mediated via Abhd4.

On the other hand, N-acyl lysophosphatidylserine has also been proven to be a substrate of Abhd4 (Lee et al., 2015) and phosphatidylserine (PtdSer) has been well-documented to play a role in apoptosis (Segawa and Nagata, 2015). Normally, PtdSer localizes asymmetrically at the inner leaflet of the plasma membrane. Upon apoptotic stimuli, activated caspase cascade promotes the redistribution of PtdSer to the outer leaflet via the enzymatic activity of scramblase (Segawa et al., 2014). This result in the irreversible cell-surface presentation of PtdSer which is a primary signal for phagocytosis and final cell elimination (Segawa and Nagata, 2015). Conclusively, Abhd4 might be an intermediate pro-

apoptotic protein, which induces caspase cascade parallelly with the regulation of phosphatidylserine pool.

Finally, is conceivable that Abhd4 is involved in direct destruction of membranes upon reception of the cell-death signal. In this regard, it is important to mention the closest paralogue of the protein, Abhd5 which is a triglyceride-lipase involved in lipid homeostasis (Schweiger et al., 2009). Mutation in Abhd5 gene causes the human metabolic disease, neutral lipid storage disease or Chanarin-Dorfman syndrome, characterized by systematic triacylglycerol (TAG) accumulation in multiple tissues (Schweiger et al., 2009). Abhd5 is bound to lipid droplets which are responsible for the storage of excess lipids in the form of TAG, providing an energy reserve for the cell. Therefore, the mobilization of fatty acids from lipid droplets is crucial for normal lipid regulation (Olzmann and Carvalho, 2019). When there is no need for its function, Abhd5 is bound by Plin1, a lipid-droplet scaffold protein (Granneman et al., 2009). Upon activation, protein kinase A (PKA) phosphorylates perilipin 1 (PLIN1) which releases Abhd5. This is followed by a direct interaction between Abhd5 and the adipose triglyceride lipase (ATGL) inducing lipolysis (Granneman et al., 2009). Interestingly, Abhd4 has the same lipid-targeting motif as Abhd5, yet it cannot activate ATGL (Sanders et al., 2017). Nevertheless, it remains a distinct possibility that Abhd4 interacts and regulates a different protein in the developing brain. Interestingly, a study using biochemical methods has characterized Abhd4 as a mitochondrial protein (Paramanik and Thakur, 2012). This correlates well with our results indicating that ectopic expression of Abhd4 causes mitochondrial shrinkage and cytochrome c release. This leaves the distinct possibility of Abhd4 directly degrading the mitochondrial membrane and thereby causing cytochrome c release and apoptosis.

5.3.2. The potential mechanism and medical aspects of delamination-induced cell death

Abnormal delamination could be initiated by a wide variety of intracellular events as well as external signals some of which are known to be teratogenic. Previously, it was shown, that elimination of Sas4 (spindle assembly abnormal protein 4), an important factor in centriole biogenesis resulted in the misplacement of radial glia cells followed by p53-

dependent apoptosis (Insolera et al., 2014). In addition, Sas4 deletion led to selective increase in p53 expression in the ventricular zone cells. Interestingly, two different studies using *in vitro* and *in vivo* models identified Abhd4 gene as a direct target of p53 (Brady et al., 2011; Timofeev et al., 2019). Considering these data, it would be extremely interesting to examine if Abhd4 indeed mediates cell death induced by Sas4-loss. Furthermore, oxidative stress which is capable to activate p53 and related cell death pathways was also found by two different studies to cause a more than two-fold upregulation of Abhd4 levels opening up a wide range of internal and external stressors to be potentially evoking Abhd4-mediated cell death (Leszczynska et al., 2015; Ozer et al., 2015).

From all the external factors causing cortical development defects in the mechanism of which oxidative stress is implicated embryonic EtOH exposure is by far the most common (Brocardo et al., 2011; Heaton et al., 2002). Consumption of ethanol, the most widely misused drug during pregnancy in the world is known to cause cortical volume loss in affected children which is often associated with decreased plasticity and lower intelligence (Lebel et al., 2012). Moreover, in rodents, both cortical migration defects and apoptosis have been described in embryos exposed to ethanol *in utero* (Delatour et al., 2019; Gressens et al., 1992). Interestingly, this type of teratogenic insult also disrupts the adherens junction belt in the VZ and causes abnormal delamination and heterotopias in the embryonic cortex (Ishii et al., 2017). Our experiments not only revealed that already a single dose of EtOH exposure results in elevated cell death in the affected embryos, but also demonstrated the essential function of Abhd4 in mediating this cell death process. The question whether oxidative stress pathway is involved in this phenomenon is still open, but these results certainly nicely correlate with our data and implicate the potential importance of Abhd4 function in apoptosis regulation on a much wider scale.

Normally delaminating daughter cells and metastatic cancer cells display a very similar behavior. Both downregulate their adhesion proteins, rearrange their cytoskeleton and start to migrate without being eliminated via anoikis (Paoli et al., 2013; Tavano et al., 2018). In line with this, resistance to anoikis is a common feature of malignant cancers and this ability provides an opportunity to create metastasis through invasion into the cardiovascular system

and render efficient treatment far more challenging (Paoli et al., 2013). Identification of molecules which mediate anchorage-loss-induced cell death could therefore offer a potential solution. In accordance with our results, demonstrating that the absence of Abhd4 abolish the adherens junction disruption-triggered cell death, Simpson et. al. demonstrated that Abhd4 knockdown could inhibit anoikis in various types of prostate cancer cells thereby inducing their metastatic potential (Simpson et al., 2012). Since our results indicate a role for Abhd4 exclusively in the brain, when talking about Abhd4 and anoikis resistance, we have to take a look at tumors of the CNS. In this regard, glioblastoma multiforme (GBM) is by far the most devastating type of brain tumor. Surgical removal of the primary tumor combined with radiation and chemotherapy only projects average life expectancy to about one year (Persano et al., 2013). The aggressiveness of GBM can be explained with its molecular and cellular complexity established by the tumor microenvironment (Broekman et al., 2018). This hypoxic tumor are mostly initiated from the adult subventricular neurogenic niche of the telencephalon which consists of several type of stem cells responsible for adult neurogenesis (Kriegstein and Alvarez-buylla, 2011) but also contains dormant cancer stem cells (Capdevila et al., 2017; Lee et al., 2018). Considering the restricted expression of Abhd4 in adult neurogenic niches in the embryonic brain, it may well be that Abhd4 is not only important to control embryonic cell survival but could be a significant anti-metastatic weapon in adult tumors. In addition, Stock and his colleagues investigated a complex signaling hub where embryonic ventricular zone precursor cells (which express high levels of Abhd4 as we have showed) can migrate to and eliminate tumors formed from implanted GL261glioblastoma cells through the production of AEA and other NAEs which bind to the TRPV1 channels and causes ER stress and ATF3 (activating transcription factor-3) mediated cell death (Stock et al., 2012). This data not only reveals a possible endocannabinoid-mediated pathway through which Abhd4 could elicit its anti-metastatic function but even more importantly it also suggests that paracrine signaling is a distinct possibility although the details of this pathway are not very clear at the moment.

A recent publication substantiates this notion, where they found 4-fold higher level of Abhd4 in Alkbh5 knockout glioblastoma cells (Zhang et al., 2017). Alkbh5 (a-ketoglutarate-

dependent dioxygenase alkB homolog 5) is a demethylase and highly expressed in glioblastoma stem-like cells, mediating epigenetic changes and facilitating the preservation of proliferative capacity. Alkhb5 elimination from these cells led to impaired tumorigenesis (Zhang et al., 2017). These result highlight two interesting concepts related to Abhd4. First Alkbh5 could be a potential regulator of Abhd4 transcription, second Abhd4 may be silenced by Alkbh5 epigenetically to protect glioblastoma cells from anoikis. However, to unfold these concepts and to understand the role of Abhd4 in cancer metastasis, further investigations are needed.

During the past 5 years, Zika virus (ZIKV) has been the most prominent neonatal infection causing microcephaly and related mental retardation (Li et al., 2016). ZIKV is a member of the *Flaviviridae* family which includes different types of human pathogens. These viruses apply a wide variety of strategies to infect cells, but the two main affected signaling pathways are receptor - and lipid metabolism-mediated (Nowakowski et al., 2016; Olagnier et al., 2016). Previously, the closest paralogue of Abhd4, Abhd5 was reported to promote Hepatitis C virus (a close relative of the ZIKV virus) assembly and release (Vieyres et al., 2016). Hepatitis C virus uses the host's lipid metabolism to aid infection and it is released as lipo-viro-particles (Vieyres et al., 2016). During infection, Abhd5 mediated lipid droplet degradation supports viral production which depends on a conserved amino acid triplet, the so-called tribasic lipid droplet consumption motif (TBLC, Vieyres et al., 2016). Interestingly, Abhd4 also contains this TBLC motif (Sanders et al., 2017), which brings up the possibility of Abhd4 function in viral assembly. Regarding the abilities of Abhd4 in lipid homeostasis and its pro-apoptotic function it would be extremely exciting to investigate the role of Abhd4 in ZIKV-caused microcephaly. Several studies have demonstrated that ZIKV primarily affects neuronal progenitor cells and decrease their proliferation and increase cell death. Accordingly, it leads to a severely reduced neuron production and eventually a thinner cortex (Li et al., 2016; Zhang et al., 2019). More importantly, ZIKV can interact with and deplete adherens junction proteins causing neuronal progenitor cells to undergo abnormal delamination and dispersion in the embryonic cortex (Yoon et al., 2017) almost perfectly mimicking our experimental model.

DOI:10.14753/SE.2020.2378

6. Conclusions

This Ph.D. thesis provides insights into the importance of N-cadherin-based signaling during cortical development.

First, we generated a triple transgenic mouse line to investigate the function of *Cdh2* during interneuron development. Our data indicate that selective elimination of *Cdh2* from postmitotic interneurons causes a migration delay of interneuron precursors in the mouse embryonic brain. During postnatal development, these migrating neuroblasts are arrested in the subventricular zone of the cortex and consequently get eliminated. As a result of this, the interneuron composition of the somatosensory cortex in adult triple transgenic animals is changed in a cell-type specific manner. Our results show that the number of somatostatin (SST) – and calretinin (Calb2) – positive interneurons were decreased while other interneuron populations are unaffected. Finally, we found that there is an overlap between the affected SST- and Calb2-populations as the number of double-positive interneurons were also decreased.

To investigate the function of N-cadherin-releated signaling during abnormal delamination we used *in utero* electroporation to disrupt the adherens junction belt around apical RGPCs. Here, we provide evidence that selective elimination of cadherin-based connections causes a migration defect and caspase-dependent cell death in the ventricular and subventricular zones of the embryonic mouse cortex. Furthermore, we identified a key molecular player in this process, called Abhydrolase domain containing 4 (Abhd4). This enzyme has a specific expression pattern in the germinative niches of the lateral and third ventricles, overlapping strongly with *Glast1*. We find that ectopic expression of Abhd4 triggers a radial migration defect and cell death. We also establish that Abhd4 evokes cytochrome c release from the mitochondria and enhances the level of cleaved caspase – 3, *in vitro.* Furthermore, we show that absence of Abhd4 can prevent the cell death caused by abnormal delamination in the embryonic cortex. Finally, we examine the effect of acute and subchronic maternal alcohol exposure and find that alcohol causes elevated cell death in the ventricular zone of the embryonic cortex in an Abhd4-dependent manner.

DOI:10.14753/SE.2020.2378

7. Summary

The mammalian cerebral cortex has a well-organized, laminated structure which is generated by parallel but also sequential migration and differentiation events. Cadherins have a pivotal role during cortical development, however several important questions regarding the function of N-cadherin during both interneuron and excitatory neuron development are still unanswered. Here, we demonstrate that conditional removal of *Cdh2* from postmitotic interneurons causes migration delay of subpallial neuroblasts during tangential migration. As a result, we found a decreased number of Gad65-GFP positive interneurons in the somatosensory cortex of the knockout triple transgenic animals. By using distinct interneuron subtype markers, we established that the somatostatin (SST) – and calretinin (Calb2) – positive interneuron cell numbers were decreased in the adult somatosensory cortex. During early postnatal development, neuroblasts failed to invade the cortical layers and got arrested in the subventricular zone of the cortex which can be due to the observed migration delay. Using TUNEL assay we provide evidence, that these arrested neuroblasts are eliminated by cell death processes.

To investigate the outcome of abnormal delamination in the embryonic cortex, we used *in utero* electroporation to disrupt the adherens junction belt around aRGPCs. We observed that selective disruption of cadherin-based adherens junctions results in a migration defect and caspase-dependent cell death in the ventricular and subventricular zones of the embryonic cortex. We have identified a novel molecular player in this process, called Abhydrolase domain containing 4 (Abhd4) which was postulated before as an anandamide synthetizing enzyme. We found that perturbation of Abhd4 causes radial migration defects and triggers the conventional intrinsic apoptotic pathway. Furthermore, we showed that abnormal delamination-induced cell elimination is mediated by Abhd4, in addition, the absence of Abhd4 protects from cell death caused by prenatal alcohol exposure.

Our findings indicate that N-cadherin mediated signaling is crucial during interneuron development and the disruption adherens junction connections leads to Abhd4-mediated cell elimination in the embryonic cortex.

DOI:10.14753/SE.2020.2378

8. Összefoglalás

Az emlős agykéreg komplex szerkezetének kialakulása egymással párhuzamosan zajló sejtvándorlási és érési folyamatoknak köszönhető. A cadherin fehérje család tagjai kulcsszerepet játszanak a kortikális fejlődés folyamatában, azonban a neuronális cadherin (N-cadherin, *Cdh2*) által közvetített, a gátló és serkentő sejtek érése során fontos szabályozási folyamat részletei még feltérképezésre várnak. Kísérleteink során megmutattuk, hogy az N-cadherin szelektív eltávolítása a posztmitotikus interneuronokból azok migrációját korlátozza. Ennek eredményeképpen a felnőtt génkiütött egerek primer szomatoszenzoros agykérgében kevesebb Gad65-GFP-pozitív interneuron detektálható. Különböző, jól ismert interneuron altípus markerek alkalmazásával megállapítottuk, hogy specifikusan a szomatosztatin - és a kalretinin-pozitív interneuron sejtek száma csökkent a felnőttkori szomatoszenzoros kéregben. A korai posztnatális fejlődés során a neuroblasztok nem tudtak bevándorolni a kérgi rétegekbe és a cortex szubventrikularis zónájában ragadtak. Végül megmutattuk, hogy a megtorpant interneuronok sejthalál útján eliminálódtak az agykéregből.

A rendellenesen kialakuló delamináció vizsgálatához méhen belüli elektroporációt alkalmaztunk, mely során megszüntettük az apikális radiális glia sejtek közötti sejt-sejt kapcsolatokat. Megfigyeltük, hogy a N-cadherin alapú kötések szelektív megszakítása sejtvándorlási problémát és kaszpáz-függő sejthalált okoz az embrionális kéregben. Ebben a folyamatban egy új molekuláris szereplőt azonosítottunk, az Abhd4-et (Abhydrolase domain containing 4), amelyet korábban anandamid szintetizáló enzimként írtak le. Megállapítottuk, hogy az Abhd4 ektópikus expressziója radiális migrációs defektust és sejthalált okoz. Megmutattuk továbbá, hogy a rendellenes delamináció által kiváltott sejtek eliminációja Abhd4 közvetítette mechanizmuson keresztül zajlik le, emellett az Abhd4 hiánya megóvja a prenatális agykérget az alkohol okozta sejthaláltól.

Összeségében kísérleteink igazolják, hogy az N-cadherin által közvetített jelátvitel kritikus jelentőségű az interneuronok fejlődésében, valamint a palliális ventrikuláris zóna sejtjei közötti kapcsolatok rendellenes megszakítása Abhd4 által közvetített sejthalálhoz vezet az embrionális agykéregben.

9. References

Aaku-Saraste, E., Hellwig, A., and Huttner, W.B. (1996). Loss of Occludin and Functional Tight Junctions, but Not ZO-1, during Neural Tube Closure—Remodeling of the Neuroepithelium Prior to Neurogenesis. Dev. Biol. *180*, 664–679.

Accogli, A., Calabretta, S., St-Onge, J., Boudrahem-Addour, N., Dionne-Laporte, A., Joset, P., Azzarello-Burri, S., Rauch, A., Krier, J., Fieg, E., Pallais, J.C., McConkie-Rosell, A., McDonald, M., Freedman, S.F., Rivière, J.-B., Lafond-Lapalme, J., Simpson, B.N., Hopkin, R.J., Trimouille, A., Van-Gils, J., Begtrup, A., McWalter, K., Delphine, H., Keren, B., Genevieve, D., Argilli, E., Sherr, E.H., Severino, M., Rouleau, G.A., Yam, P.T., Charron, F., Srour, M., Acosta, M.T., Adams, D.R., Agrawal, P., Alejandro, M.E., Allard, P., Alvey, J., Andrews, A., Ashley, E.A., Azamian, M.S., Bacino, C.A., Bademci, G., Baker, E., Balasubramanyam, A., Baldridge, D., Bale, J., Barbouth, D., Batzli, G.F., Bayrak-Toydemir, P., Beggs, A.H., Bejerano, G., Bellen, H.J., Bernstein, J.A., Berry, G.T., Bican, A., Bick, D.P., Birch, C.L., Bivona, S., Bohnsack, J., Bonnenmann, C., Bonner, D., Boone, B.E., Bostwick, B.L., Botto, L., Briere, L.C., Brokamp, E., Brown, D.M., Brush, M., Burke, E.A., Burrage, L.C., Butte, M.J., Carey, J., Carrasquillo, O., Chang, T.C.P., Chao, H.-T., Clark, G.D., Coakley, T.R., Cobban, L.A., Cogan, J.D., Cole, F.S., Colley, H.A., Cooper, C.M., Cope, H., Craigen, W.J., D'Souza, P., Dasari, S., Davids, M., Dayal, J.G., Dell'Angelica, E.C., Dhar, S.U., Dorrani, N., Dorset, D.C., Douine, E.D., Draper, D.D., Duncan, L., Eckstein, D.J., Emrick, L.T., Eng, C.M., Esteves, C., Estwick, T., Fernandez, L., Ferreira, C., Fieg, E.L., Fisher, P.G., Fogel, B.L., Forghani, I., Fresard, L., Gahl, W.A., Godfrey, R.A., Goldman, A.M., Goldstein, D.B., Gourdine, J.-P.F., Grajewski, A., Groden, C.A., Gropman, A.L., Haendel, M., Hamid, R., Hanchard, N.A., Hayes, N., High, F., Holm, I.A., Hom, J., Huang, A., Huang, Y., Isasi, R., Jamal, F., Jiang, Y., Johnston, J.M., Jones, A.L., Karaviti, L., Kelley, E.G., Kiley, D., Koeller, D.M., Kohane, I.S., Kohler, J.N., Krakow, D., Krasnewich, D.M., Korrick, S., Koziura, M., Krier, J.B., Kyle, J.E., Lalani, S.R., Lam, B., Lanpher, B.C., Lanza, I.R., Lau, C.C., Lazar, J., LeBlanc, K., Lee, B.H., Lee, H., Levitt, R., Levy, S.E., Lewis, R.A., Lincoln, S.A., Liu, P., Liu, X.Z., Longo, N., Loo, S.K., Loscalzo, J., Maas, R.L., Macnamara, E.F., MacRae, C.A., Maduro, V. V., Majcherska, M.M., Malicdan, M.C. V., Mamounas, L.A., Manolio, T.A., Mao, R., Markello, T.C., Marom, R., Marth, G., Martin, B.A., Martin, M.G., Martínez-Agosto, J.A., Marwaha, S., May, T., McCauley, J., McConkie-Rosell, A., McCormack, C.E., McCray, A.T., Metz, T.O., Might, M., Morava-Kozicz, E., Moretti, P.M., Morimoto, M., Mulvihill, J.J., Murdock, D.R., Nath, A., Nelson, S.F., Newberry, J.S., Newman, J.H., Nicholas, S.K., Novacic, D., Oglesbee, D., Orengo, J.P., Pace, L., Pak, S., Pallais, J.C., Palmer, C.G.S., Papp, J.C., Parker, N.H., Phillips, J.A., Posey, J.E., Postlethwait, J.H., Potocki, L., Pusey, B.N., Quinlan, A., Raja, A.N., Renteria, G., Reuter, C.M., Rives, L., Robertson, A.K., Rodan, L.H., Rosenfeld, J.A., Rowley, R.K., Ruzhnikov, M., Sacco, R., Sampson, J.B., Samson, S.L., Saporta, M., Schaechter, J., Schedl, T., Schoch, K., Scott, D.A., Shakachite, L., Sharma, P., Shashi, V., Shields, K., Shin, J., Signer, R., Sillari, C.H., Silverman, E.K., Sinsheimer, J.S., Sisco, K., Smith, K.S., Solnica-Krezel, L., Spillmann, R.C., Stoler, J.M., Stong, N., Sullivan, J.A., Sutton, S., Sweetser, D.A., Tabor, H.K., Tamburro, C.P., Tan, Q.K.-G., Tekin, M., Telischi, F., Thorson, W., Tifft, C.J., Toro, C., Tran, A.A., Urv, T.K.,

Velinder, M., Viskochil, D., Vogel, T.P., Wahl, C.E., Walley, N.M., Walsh, C.A., Walker, M., Wambach, J., Wan, J., Wang, L., Wangler, M.F., Ward, P.A., Waters, K.M., Webb-Robertson, B.-J.M., Wegner, D., Westerfield, M., Wheeler, M.T., Wise, A.L., Wolfe, L.A., Woods, J.D., Worthey, E.A., Yamamoto, S., Yang, J., Yoon, A.J., Yu, G., Zastrow, D.B., Zhao, C., and Zuchner, S. (2019). De Novo Pathogenic Variants in N-cadherin Cause a Syndromic Neurodevelopmental Disorder with Corpus Collosum, Axon, Cardiac, Ocular, and Genital Defects. Am. J. Hum. Genet. *105*, 854–868.

Acebron, S.P., and Niehrs, C. (2016). β-Catenin-Independent Roles of Wnt/LRP6 Signaling. Trends Cell Biol. *26*, 956–967.

Adinolfi, B., Romanini, A., Vanni, A., Martinotti, E., Chicca, A., Fogli, S., and Nieri, P. (2013). Anticancer activity of anandamide in human cutaneous melanoma cells. Eur. J. Pharmacol. *718*, 154–159.

Adorjan, I., Ahmed, B., Feher, V., Torso, M., Krug, K., Esiri, M., Chance, S.A., and Szele, F.G. (2017). Calretinin interneuron density in the caudate nucleus is lower in autism spectrum disorder. Brain *140*, 2028–2040.

Agmon, E., and Stockwell, B.R. (2017). Lipid homeostasis and regulated cell death. Curr. Opin. Chem. Biol. *39*, 83–89.

De Anda, F.C., Meletis, K., Ge, X., Rei, D., and Tsai, L.H. (2010). Centrosome motility is essential for initial axon formation in the neocortex. J. Neurosci. *30*, 10391–10406.

Anderson, S.A., Eisenstat, D.D., Shi, L., and Rubenstein, J.L.R. (1997). Interneuron Migration from Basal Forebrain to Neocortex: Dependence on Dlx Genes. Science. *278*, 474–476.

Andersson, E.R., Sandberg, R., and Lendahl, U. (2011). Notch signaling: Simplicity in design, versatility in function. Development *138*, 3593–3612.

Andrews, W.D., Barber, M., and Parnavelas, J.G. (2007). Slit-Robo interactions during cortical development. J. Anat. *211*, 188–198.

Anthony, T.E., Klein, C., Fishell, G., and Heintz, N. (2004). Radial glia serve as neuronal progenitors in all regions of the central nervous system. Neuron *41*, 881–890.

Arai, Y., and Taverna, E. (2017). Neural progenitor cell polarity and cortical development. Front. Cell. Neurosci. *11*, 1–11.

Araya-Secchi, R., Neel, B.L., and Sotomayor, M. (2016). An elastic element in the protocadherin-15 tip link of the inner ear. Nat. Commun. *7*, 1–14.

Aronne, M.P., Guadagnoli, T., Fontanet, P., Evrard, S.G., and Brusco, A. (2011). Effects of prenatal ethanol exposure on rat brain radial glia and neuroblast migration. Exp. Neurol. *229*, 364–371.

Asami, M., Pilz, G.A., Ninkovic, J., Godinho, L., Schroeder, T., Huttner, W.B., and Götz, M. (2011). The role of Pax6 in regulating the orientation and mode of cell division of

progenitors in the mouse cerebral cortex. Development *138*, 5067–5078.

Ayala, R., Shu, T., and Tsai, L.-H. (2007). Trekking across the Brain: The Journey of Neuronal Migration. Cell *128*, 29–43.

Bandler, R.C., Mayer, C., and Fishell, G. (2017). Cortical interneuron specification: the juncture of genes, time and geometry. Curr. Opin. Neurobiol. *42*, 17–24.

Baranyi, M., Cervenak, J., Bender, B., and Kacskovics, I. (2013). Transgenic Rabbits That Overexpress the Neonatal Fc Receptor (FcRn) Generate Higher Quantities and Improved Qualities of Anti-Thymocyte Globulin (ATG). PLoS One *8*, e76839.

Barber, M., and Pierani, A. (2016). Tangential migration of glutamatergic neurons and cortical patterning during development: Lessons from Cajal-Retzius cells. Dev. Neurobiol. *76*, 847–881.

Barna, L., Dudok, B., Miczán, V., Horváth, A., László, Z.I., and Katona, I. (2016). Correlated confocal and super-resolution imaging by VividSTORM. Nat. Protoc. *11*, 163–183.

Barnat, M., Le Friec, J., Benstaali, C., and Humbert, S. (2017). Huntingtin-Mediated Multipolar-Bipolar Transition of Newborn Cortical Neurons Is Critical for Their Postnatal Neuronal Morphology. Neuron *93*, 99–114.

Bartolini, G., Sánchez-Alcañiz, J.A., Osório, C., Valiente, M., García-Frigola, C., and Marín, O. (2017). Neuregulin 3 Mediates Cortical Plate Invasion and Laminar Allocation of GABAergic Interneurons. Cell Rep. *18*, 1157–1170.

Bedogni, F., Hodge, R.D., Elsen, G.E., Nelson, B.R., Daza, R.A.M., Beyer, R.P., Bammler, T.K., Rubenstein, J.L.R., and Hevner, R.F. (2010). Tbr1 regulates regional and laminar identity of postmitotic neurons in developing neocortex. Proc. Natl. Acad. Sci. U. S. A. *107*, 13129–13134.

Ben-Ari, Y. (2002). Excitatory actions of GABA during development: The nature of the nurture. Nat. Rev. Neurosci. *3*, 728–739.

Berdnik, D., Török, T., González-Gaitán, M., and Knoblich, J.A. (2002). The endocytic protein α-adaptin is required for numb-mediated asymmetric cell division in Drosophila. Dev. Cell *3*, 221–231.

Berghuis, P., Dobszay, M.B., Wang, X., Spano, S., Ledda, F., Sousa, K.M., Schulte, G., Ernfors, P., Mackie, K., Paratcha, G., Hurd, Y.L., and Harkany, T. (2005). Endocannabinoids regulate interneuron migration and morphogenesis by transactivating the TrkB receptor. Proc. Natl. Acad. Sci. *102*, 19115–19120.

Berghuis, P., Rajnicek, A.M., Morozov, Y.M., Ross, R.A., Mulder, J., Urban, G.M., Monory, K., Marsicano, G., Matteoli, M., Canty, A., Irving, A.J., Katona, I., Yanagawa, Y., Rakic, P., Lutz, B., Mackie, K., and Harkany, T. (2007). Hardwiring the Brain: Endocannabinoids Shape Neuronal Connectivity. Science. *316*, 1212–1216.

Bielle, F., Griveau, A., Narboux-Nême, N., Vigneau, S., Sigrist, M., Arber, S., Wassef, M., and Pierani, A. (2005). Multiple origins of Cajal-Retzius cells at the borders of the developing pallium. Nat. Neurosci. *8*, 1002–1012.

Blanquie, O., Yang, J.W., Kilb, W., Sharopov, S., Sinning, A., and Luhmann, H.J. (2017). Electrical activity controls area-specific expression of neuronal apoptosis in the mouse developing cerebral cortex. Elife *6*, 1–21.

Bortone, D., and Polleux, F. (2009). KCC2 Expression Promotes the Termination of Cortical Interneuron Migration in a Voltage-Sensitive Calcium-Dependent Manner. Neuron *62*, 53–71.

Boyden, E.S., Zhang, F., Bamberg, E., Nagel, G., and Deisseroth, K. (2005). Millisecond-timescale, genetically targeted optical control of neural activity. Nat. Neurosci. *8*, 1263–1268.

Brady, C.A., Jiang, D., Mello, S.S., Johnson, T.M., Jarvis, L.A., Kozak, M.M., Broz, D.K., Basak, S., Park, E.J., McLaughlin, M.E., Karnezis, A.N., and Attardi, L.D. (2011). Distinct p53 Transcriptional Programs Dictate Acute DNA-Damage Responses and Tumor Suppression. Cell *145*, 571–583.

Brocardo, P.S., Gil-Mohapel, J., and Christie, B.R. (2011). The role of oxidative stress in fetal alcohol spectrum disorders. Brain Res. Rev. *67*, 209–225.

Broekman, M.L., Maas, S.L.N., Abels, E.R., Mempel, T.R., Krichevsky, A.M., and Breakefield, X.O. (2018). Multidimensional communication in the microenvirons of glioblastoma. Nat. Rev. Neurol. *14*, 1–14.

Brown, K.N., Chen, S., Han, Z., Lu, C.-H., Tan, X., Zhang, X.-J., Ding, L., Lopez-Cruz, A., Saur, D., Anderson, S.A., Huang, K., and Shi, S.-H. (2011). Clonal Production and Organization of Inhibitory Interneurons in the Neocortex. Science. *334*, 480–486.

Buchsbaum, I.Y., and Cappello, S. (2019). Neuronal migration in the CNS during development and disease: insights from in vivo and in vitro models. Development *146*, dev163766.

Bulfone, A., Smiga, S.M., Shimamura, K., Peterson, A., Puelles, L., and Rubenstein, J.L.R. (1995). T-Brain-1: A homolog of Brachyury whose expression defines molecularly distinct domains within the cerebral cortex. Neuron *15*, 63–78.

Bulfone, A., Martinez, S., Marigo, V., Campanella, M., Basile, A., Quaderi, N., Gattuso, C., Rubenstein, J.L.R., and Ballabio, A. (1999). Expression pattern of the Tbr2 (Eomesodermin) gene during mouse and chick brain development. Mech. Dev. *84*, 133–138.

Butt, S.J.B., Cobos, I., Golden, J., Kessaris, N., Pachnis, V., and Anderson, S. (2007). Transcriptional Regulation of Cortical Interneuron Development. J. Neurosci. *27*, 11847–11850.

Cadwell, C.M., Su, W., and Kowalczyk, A.P. (2016). Cadherin tales: Regulation of

cadherin function by endocytic membrane trafficking. Traffic *17*, 1262–1271.

Camp, J.G., Badsha, F., Florio, M., Kanton, S., Gerber, T., Wilsch-Bräuninger, M., Lewitus, E., Sykes, A., Hevers, W., Lancaster, M., Knoblich, J.A., Lachmann, R., Pääbo, S., Huttner, W.B., and Treutlein, B. (2015). Human cerebral organoids recapitulate gene expression programs of fetal neocortex development. Proc. Natl. Acad. Sci. *112*, 15672–15677.

Capdevila, C., Rodríguez Vázquez, L., and Martí, J. (2017). Glioblastoma Multiforme and Adult Neurogenesis in the Ventricular-Subventricular Zone: A Review. J. Cell. Physiol. *232*, 1596–1601.

Cappello, S., Gray, M.J., Badouel, C., Lange, S., Einsiedler, M., Srour, M., Chitayat, D., Hamdan, F.F., Jenkins, Z.A., Morgan, T., Preitner, N., Uster, T., Thomas, J., Shannon, P., Morrison, V., Di Donato, N., Van Maldergem, L., Neuhann, T., Newbury-Ecob, R., Swinkells, M., Terhal, P., Wilson, L.C., Zwijnenburg, P.J.G., Sutherland-Smith, A.J., Black, M.A., Markie, D., Michaud, J.L., Simpson, M.A., Mansour, S., McNeill, H., Götz, M., and Robertson, S.P. (2013). Mutations in genes encoding the cadherin receptor-ligand pair DCHS1 and FAT4 disrupt cerebral cortical development. Nat. Genet. *45*, 1300–1310.

Carney, R.S.E., Cocas, L.A., Hirata, T., Mansfield, K., and Corbin, J.G. (2009). Differential regulation of telencephalic pallial-subpallial boundary Patterning by Pax6 and Gsh2. Cereb. Cortex *19*, 745–759.

Carracedo, A., Lorente, M., Egia, A., Blázquez, C., García, S., Giroux, V., Malicet, C., Villuendas, R., Gironella, M., González-Feria, L., Piris, M.Á., Iovanna, J.L., Guzmán, M., and Velasco, G. (2006). The stress-regulated protein p8 mediates cannabinoid-induced apoptosis of tumor cells. Cancer Cell *9*, 301–312.

Caviness, V.S., and Sidman, R.L. (1973). Time of origin of corresponding cell classes in the cerebral cortex of normal and reeler mutant mice: An autoradiographic analysis. J. Comp. Neurol. *148*, 141–151.

Chai, X., Förster, E., Zhao, S., Bock, H.H., and Frotscher, M. (2009). Reelin stabilizes the actin cytoskeleton of neuronal processes by inducing n-cofilin phosphorylation at serine. J. Neurosci. *29*, 288–299.

Chen, S., Lewallen, M., and Xie, T. (2013). Adhesion in the stem cell niche: biological roles and regulation. Development *140*, 255–265.

Chenn, A., and Walsh, C.A. (2003). Increased neuronal production, enlarged forebrains and cytoarchitectural distortions in β-catenin overexpressing transgenic mice. Cereb. Cortex *13*, 599–606.

Chouchane, M., and Costa, M.R. (2019). Instructing neuronal identity during CNS development and astroglial-lineage reprogramming: Roles of NEUROG2 and ASCL1. Brain Res. *1705*, 66–74.

Chowdhury, T.G., Jimenez, J.C., Bomar, J.M., Cruz-Martin, A., Cantle, J.P., and Portera-

Cailliau, C. (2010). Fate of Cajal-Retzius neurons in the postnatal mouse neocortex. Front. Neuroanat. *4*, 1–8.

Clarke, P.H. (1990). Developmental cell death: morphological diversity and multiple mechanisms. Anat. Embryol. (Berl). *181*, 195–213.

Conti, V., Pantaleo, M., Barba, C., Baroni, G., Mei, D., Buccoliero, A.M., Giglio, S., Giordano, F., Baek, S.T., Gleeson, J.G., and Guerrini, R. (2015). Focal dysplasia of the cerebral cortex and infantile spasms associated with somatic 1q21.1-q44 duplication including the AKT3 gene. Clin. Genet. *88*, 241–247.

Corbin, J.G., Gaiano, N., Machold, R.P., Langston, A., and Fishell, G. (2000). The Gsh2 homeodomain gene controls multiple aspects of telencephalic development. Development *127*, 5007–5020.

D'Arcangelo, G., G. Miao, G., Chen, S.-C., Scares, H.D., Morgan, J.I., and Curran, T. (1995). A protein related to extracellular matrix proteins deleted in the mouse mutant reeler. Nature *374*, 719–723.

Dantas, T.J., Carabalona, A., Hu, D.J.K., and Vallee, R.B. (2016). Emerging roles for motor proteins in progenitor cell behavior and neuronal migration during brain development. Cytoskeleton *73*, 566–576.

Das, R.M., and Storey, K.G. (2014). Apical abscission alters cell polarity and dismantles the primary cilium during neurogenesis. Science. *343*, 200–204.

Delatour, L.C., Yeh, P.W., and Yeh, H.H. (2019). Ethanol Exposure In Utero Disrupts Radial Migration and Pyramidal Cell Development in the Somatosensory Cortex. Cereb. Cortex *29*, 2125–2139.

Derkinderen, P., Valjent, E., Toutant, M., Corvol, J.-C., Enslen, H., Ledent, C., Trzaskos, J., Caboche, J., and Girault, J.-A. (2003). Regulation of extracellular signal-regulated kinase by cannabinoids in hippocampus. J. Neurosci. *23*, 2371–2382.

Díaz-Alonso, J., Guzman, M., Galve-Roperh, I., Díaz-Alonso, J., Guzmán, M., and Galve-Roperh, I. (2012). Endocannabinoids via CB1 receptors act as neurogenic niche cues during cortical development. Philos. Trans. R. Soc. B *367*, 3229–3241.

Díaz-Alonso, J., de Salas-Quiroga, A., Paraíso-Luna, J., García-Rincón, D., Garcez, P.P., Parsons, M., Andradas, C., Sánchez, C., Guillemot, F., Guzmán, M., and Galve-Roperh, I. (2017). Loss of Cannabinoid CB1 Receptors Induces Cortical Migration Malformations and Increases Seizure Susceptibility. Cereb. Cortex *27*, 5303–5317.

Dimidschstein, J., Passante, L., Dufour, A., vandenAmeele, J., Tiberi, L., Hrechdakian, T., Adams, R., Klein, R., Lie, D.C., Jossin, Y., and Vanderhaeghen, P. (2013). Ephrin-B1 controls the columnar distribution of cortical pyramidal neurons by restricting their tangential migration. Neuron *79*, 1123–1135.

Dogterom, M., and Koenderink, G.H. (2019). Actin–microtubule crosstalk in cell biology. Nat. Rev. Mol. Cell Biol. *20*, 38–54.

Dudok, B., Barna, L., Ledri, M., Szabó, S.I., Szabadits, E., Pintér, B., Woodhams, S.G., Henstridge, C.M., Balla, G.Y., Nyilas, R., Varga, C., Lee, S.-H., Matolcsi, M., Cervenak, J., Kacskovics, I., Watanabe, M., Sagheddu, C., Melis, M., Pistis, M., Soltesz, I., and Katona, I. (2015). Cell-specific STORM super-resolution imaging reveals nanoscale organization of cannabinoid signaling. Nat. Neurosci. *18*, 75–86.

Eisenstat, D.D., Liu, J.K., Mione, M., Zhong, W., Yu, G., Anderson, S.A., Ghattas, I., Puelles, L., and Rubenstein, J.L.R. (1999). DLX-1, DLX-2, and DLX-5 expression define distinct stages of basal forebrain differentiation. J. Comp. Neurol. *414*, 217–237.

Elias, L.A.B., Wang, D.D., and Kriegstein, A.R. (2007). Gap junction adhesion is necessary for radial migration in the neocortex. Nature *448*, 901–907.

Elias, L.A.B., Turmaine, M., Parnavelas, J.G., and Kriegstein, A.R. (2010). Connexin 43 mediates the tangential to radial migratory switch in ventrally derived cortical interneurons. J. Neurosci. *30*, 7072–7077.

Elsen, G.E., Bedogni, F., Hodge, R.D., Bammler, T.K., MacDonald, J.W., Lindtner, S., Rubenstein, J.L.R., and Hevner, R.F. (2018). The Epigenetic Factor Landscape of Developing Neocortex Is Regulated by Transcription Factors Pax6→ Tbr2→ Tbr1. Front. Neurosci. *12*, 571.

Englund, C., Fink, A., Lau, C., Pham, D., Daza, R.A.M., Bulfone, A., Kowalczyk, T., and F., H.R. (2005). Pax6, Tbr2, and Tbr1 Are Expressed Sequentially by Radial Glia, Intermediate Progenitor Cells, and Postmitotic Neurons in Developing Neocortex. J. Neurosci. *25*, 247–251.

Erlander, M.G., Tillakaratne, N.J.K., Feldblum, S., Patel, N., and Tobin, A.J. (1991). Two genes encode distinct glutamate decarboxylases. Neuron *7*, 91–100.

Van Essen, D.C., Donahue, C.J., and Glasser, M.F. (2018). Development and Evolution of Cerebral and Cerebellar Cortex. Brain. Behav. Evol. *91*, 158–169.

Farber, N.B., Creeley, C.E., and Olney, J.W. (2010). Alcohol-induced neuroapoptosis in the fetal macaque brain. Neurobiol. Dis. *40*, 200–206.

Ferland, R.J., Batiz, L.F., Neal, J., Lian, G., Bundock, E., Lu, J., Hsiao, Y.C., Diamond, R., Mei, D., Banham, A.H., Brown, P.J., Vanderburg, C.R., Joseph, J., Hecht, J.L., Folkerth, R., Guerrini, R., Walsh, C.A., Rodriguez, E.M., and Sheen, V.L. (2009). Disruption of neural progenitors along the ventricular and subventricular zones in periventricular heterotopia. Hum. Mol. Genet. *18*, 497–516.

Flames, N., Long, J.E., Garratt, A.N., Fischer, T.M., Gassmann, M., Birchmeier, C., Lai, C., Rubenstein, J.L.R., and Marín, O. (2004). Short- and long-range attraction of cortical GABAergic interneurons by neuregulin-1. Neuron *44*, 251–261.

Flames, N., Pla, R., Gelman, D.M., Rubenstein, J.L.R., Puelles, L., and Marin, O. (2007). Delineation of Multiple Subpallial Progenitor Domains by the Combinatorial Expression of Transcriptional Codes. J. Neurosci. *27*, 9682–9695.

Fogarty, M., Grist, M., Gelman, D., Marin, O., Pachnis, V., and Kessaris, N. (2007). Spatial Genetic Patterning of the Embryonic Neuroepithelium Generates GABAergic Interneuron Diversity in the Adult Cortex. J. Neurosci. *27*, 10935–10946.

Fox, J.W., Lamperti, E.D., Ekşioğlu, Y.Z., Hong, S.E., Feng, Y., Graham, D.A., Scheffer, I.E., Dobyns, W.B., Hirsch, B.A., Radtke, R.A., Berkovic, S.F., Huttenlocher, P.R., and Walsh, C.A. (1998). Mutations in filamin 1 prevent migration of cerebral cortical neurons in human Periventricular heterotopia. Neuron *21*, 1315–1325.

Franco, S.J., Martinez-Garay, I., Gil-Sanz, C., Harkins-Perry, S.R., and Müller, U. (2011). Reelin Regulates Cadherin Function via Dab1/Rap1 to Control Neuronal Migration and Lamination in the Neocortex. Neuron *69*, 482–497.

Frau, R., Miczán, V., Traccis, F., Aroni, S., Pongor, C.I., Saba, P., Serra, V., Sagheddu, C., Fanni, S., Congiu, M., Devoto, P., Cheer, J.F., Katona, I., and Melis, M. (2019). Prenatal THC exposure produces a hyperdopaminergic phenotype rescued by pregnenolone. Nat. Neurosci. *22*, 1975–1985.

Frazer, S., Prados, J., Niquille, M., Cadilhac, C., Markopoulos, F., Gomez, L., Tomasello, U., Telley, L., Holtmaat, A., Jabaudon, D., and Dayer, A. (2017). Transcriptomic and anatomic parcellation of 5-HT3A R expressing cortical interneuron subtypes revealed by single-cell RNA sequencing. Nat. Commun. *8*, 1–12.

Freund, T.F., and Katona, I. (2007). Perisomatic Inhibition. Neuron *56*, 33–42.

Frisch, S., and Francis, H. (1994). Disruption of epithelial cell matrix interactions induces apoptosis. J. Cell Biol. *124*, 619–626.

Fujimori, T., and Takeichi, M. (1993). Disruption of epithelial cell-cell adhesion by exogenous expression of a mutated nonfunctional N-cadherin. Mol. Biol. Cell *4*, 37–47.

Furutachi, S., Miya, H., Watanabe, T., Kawai, H., Yamasaki, N., Harada, Y., Imayoshi, I., Nelson, M., Nakayama, K.I., Hirabayashi, Y., and Gotoh, Y. (2015). Slowly dividing neural progenitors are an embryonic origin of adult neural stem cells. Nat Neurosci *18*, 657–665.

Gal, J.S., Morozov, Y.M., Ayoub, A.E., Chatterjee, M., Rakic, P., and Haydar, T.F. (2006). Molecular and morphological heterogeneity of neural precursors in the mouse neocortical proliferative zones. J. Neurosci. *26*, 1045–1056.

Gallelli, C., Calcagnini, S., Romano, A., Koczwara, J., de Ceglia, M., Dante, D., Villani, R., Giudetti, A., Cassano, T., and Gaetani, S. (2018). Modulation of the Oxidative Stress and Lipid Peroxidation by Endocannabinoids and Their Lipid Analogues. Antioxidants *7*, 93.

Galluzzi, L., Vitale, I., Aaronson, S.A., Abrams, J.M., Adam, D., Agostinis, P., Alnemri, E.S., Altucci, L., Amelio, I., Andrews, D.W., Annicchiarico-Petruzzelli, M., Antonov, A. V., Arama, E., Baehrecke, E.H., Barlev, N.A., Bazan, N.G., Bernassola, F., Bertrand, M.J.M., Bianchi, K., Blagosklonny, M. V., Blomgren, K., Borner, C., Boya, P., Brenner,

C., Campanella, M., Candi, E., Carmona-Gutierrez, D., Cecconi, F., Chan, F.K.M., Chandel, N.S., Cheng, E.H., Chipuk, J.E., Cidlowski, J.A., Ciechanover, A., Cohen, G.M., Conrad, M., Cubillos-Ruiz, J.R., Czabotar, P.E., D'Angiolella, V., Dawson, T.M., Dawson, V.L., De Laurenzi, V., De Maria, R., Debatin, K.M., Deberardinis, R.J., Deshmukh, M., Di Daniele, N., Di Virgilio, F., Dixit, V.M., Dixon, S.J., Duckett, C.S., Dynlacht, B.D., El-Deiry, W.S., Elrod, J.W., Fimia, G.M., Fulda, S., García-Sáez, A.J., Garg, A.D., Garrido, C., Gavathiotis, E., Golstein, P., Gottlieb, E., Green, D.R., Greene, L.A., Gronemeyer, H., Gross, A., Hajnoczky, G., Hardwick, J.M., Harris, I.S., Hengartner, M.O., Hetz, C., Ichijo, H., Jäättelä, M., Joseph, B., Jost, P.J., Juin, P.P., Kaiser, W.J., Karin, M., Kaufmann, T., Kepp, O., Kimchi, A., Kitsis, R.N., Klionsky, D.J., Knight, R.A., Kumar, S., Lee, S.W., Lemasters, J.J., Levine, B., Linkermann, A., Lipton, S.A., Lockshin, R.A., López-Otín, C., Lowe, S.W., Luedde, T., Lugli, E., MacFarlane, M., Madeo, F., Malewicz, M., Malorni, W., Manic, G., Marine, J.C., Martin, S.J., Martinou, J.C., Medema, J.P., Mehlen, P., Meier, P., Melino, S., Miao, E.A., Molkentin, J.D., Moll, U.M., Muñoz-Pinedo, C., Nagata, S., Nuñez, G., Oberst, A., Oren, M., Overholtzer, M., Pagano, M., Panaretakis, T., Pasparakis, M., Penninger, J.M., Pereira, D.M., Pervaiz, S., Peter, M.E., Piacentini, M., Pinton, P., Prehn, J.H.M., Puthalakath, H., Rabinovich, G.A., Rehm, M., Rizzuto, R., Rodrigues, C.M.P., Rubinsztein, D.C., Rudel, T., Ryan, K.M., Sayan, E., Scorrano, L., Shao, F., Shi, Y., Silke, J., Simon, H.U., Sistigu, A., Stockwell, B.R., Strasser, A., Szabadkai, G., Tait, S.W.G., Tang, D., Tavernarakis, N., Thorburn, A., Tsujimoto, Y., Turk, B., Vanden Berghe, T., Vandenabeele, P., Vander Heiden, M.G., Villunger, A., Virgin, H.W., Vousden, K.H., Vucic, D., Wagner, E.F., Walczak, H., Wallach, D., Wang, Y., Wells, J.A., Wood, W., Yuan, J., Zakeri, Z., Zhivotovsky, B., Zitvogel, L., Melino, G., and Kroemer, G. (2018). Molecular mechanisms of cell death: Recommendations of the Nomenclature Committee on Cell Death 2018. Cell Death Differ. *25*, 486–541.

Galve-Roperh, I., Chiurchiù, V., Díaz-Alonso, J., Bari, M., Guzmán, M., and Maccarrone, M. (2013). Cannabinoid receptor signaling in progenitor/stem cell proliferation and differentiation. Prog. Lipid Res. *52*, 633–650.

Gan, Q., Lee, A., Suzuki, R., Yamagami, T., Stokes, A., Nguyen, B.C., Pleasure, D., Wang, J., Chen, H.-W., and Zhou, C.J. (2014). Pax6 Mediates ß-Catenin Signaling for Self-Renewal and Neurogenesis by Neocortical Radial Glial Stem Cells. Stem Cells *32*, 45–58.

Gänzler-Odenthal, S.I.I., and Redies, C. (1998). Blocking N-Cadherin Function Disrupts the Epithelial Structure of Differentiating Neural Tissue in the Embryonic Chicken Brain. J. Neurosci. *18*, 5415–5425.

Gao, C., Xiao, G., and Hu, J. (2014). Regulation of Wnt/β-catenin signaling by posttranslational modifications. Cell Biosci. *4*, 13.

Gärtner, A., Fornasiero, E.F., Munck, S., Vennekens, K., Seuntjens, E., Huttner, W.B., Valtorta, F., and Dotti, C.G. (2012). N-cadherin specifies first asymmetry in developing neurons. EMBO J. *31*, 1893–1903.

Gärtner, A., Fornasiero, E.F., and Dotti, C.G. (2015). Cadherins as regulators of neuronal polarity. Cell Adh. Migr. *9*, 175–182.

Gelman, D.M., and Marín, O. (2010). Generation of interneuron diversity in the mouse cerebral cortex. Eur. J. Neurosci. *31*, 2136–2141.

Gelman, D., Griveau, A., Dehorter, N., Teissier, A., Varela, C., Pla, R., Pierani, A., and Marín, O. (2011). A wide diversity of cortical GABAergic interneurons derives from the embryonic preoptic area. J. Neurosci. *31*, 16570–16580.

Gelman, D.M., Martini, F.J., Nobrega-Pereira, S., Pierani, A., Kessaris, N., and Marin, O. (2009). The Embryonic Preoptic Area Is a Novel Source of Cortical GABAergic Interneurons. J. Neurosci. *29*, 9380–9389.

Ghanem, N. (2003). Regulatory Roles of Conserved Intergenic Domains in Vertebrate Dlx Bigene Clusters. Genome Res. *13*, 533–543.

Ghanem, N., Yu, M., Long, J., Hatch, G., Rubenstein, J.L.R., and Ekker, M. (2007). Distinct cis-Regulatory Elements from the Dlx1/Dlx2 Locus Mark Different Progenitor Cell Populations in the Ganglionic Eminences and Different Subtypes of Adult Cortical Interneurons. J. Neurosci. *27*, 5012–5022.

Gil-Sanz, C., Franco, S.J., Martinez-Garay, I., Espinosa, A., Harkins-Perry, S., and Müller, U. (2013). Cajal-Retzius Cells Instruct Neuronal Migration by Coincidence Signaling between Secreted and Contact-Dependent Guidance Cues. Neuron *79*, 461–477.

Gil-Sanz, C., Landeira, B., Ramos, C., Costa, M.R., and Muller, U. (2014). Proliferative Defects and Formation of a Double Cortex in Mice Lacking Mltt4 and Cdh2 in the Dorsal Telencephalon. J. Neurosci. *34*, 10475–10487.

Götz, M., and Barde, Y.-A. (2005). Radial Glial Cells. Neuron *46*, 369–372.

Götz, M., and Huttner, W.B. (2005). The cell biology of neurogenesis. Nat. Rev. Mol. Cell Biol. *6*, 777–788.

Götz, M., Stoykova, A., and Gruss, P. (1998). Pax6 Controls Radial Glia Differentiation in the Cerebral Cortex. Neuron *21*, 1031–1044.

Granneman, J.G., Moore, H.P.H., Krishnamoorthy, R., and Rathod, M. (2009). Perilipin controls lipolysis by regulating the interactions of AB-hydrolase containing 5 (Abhd5) and adipose triglyceride lipase (Atgl). J. Biol. Chem. *284*, 34538–34544.

Gressens, P., Lammens, M., Picard, J.J., and Evrard, P. (1992). Ethanol-induced disturbances of gliogenesis and neuronogenesis in the developing murine brain: an in vitro and in vivo immunohistochemical and ultrastructural study. Alcohol Alcohol *27*, 219–226.

Griveau, A., Borello, U., Causeret, F., Tissir, F., Boggetto, N., Karaz, S., and Pierani, A. (2010). A Novel Role for Dbx1-Derived Cajal-Retzius Cells in Early Regionalization of the Cerebral Cortical Neuroepithelium. PLoS Biol. *8*, e1000440.

Guillemot, F. (2005). Cellular and molecular control of neurogenesis in the mammalian telencephalon. Curr. Opin. Cell Biol. *17*, 639–647.

Gul, I.S., Hulpiau, P., Saeys, Y., and van Roy, F. (2017). Evolution and diversity of cadherins and catenins. Exp. Cell Res. *358*, 3–9.

Gupta, A., Tsai, L.-H., and Wynshaw-Boris, A. (2002). Life Is a Journey: a Genetic Look At Neocortical Development. Nat. Rev. Genet. *3*, 342–355.

Handley, M.T., Morris-Rosendahl, D.J., Brown, S., Macdonald, F., Hardy, C., Bem, D., Carpanini, S.M., Borck, G., Martorell, L., Izzi, C., Faravelli, F., Accorsi, P., Pinelli, L., Basel-Vanagaite, L., Peretz, G., Abdel-Salam, G.M.H., Zaki, M.S., Jansen, A., Mowat, D., Glass, I., Stewart, H., Mancini, G., Lederer, D., Roscioli, T., Giuliano, F., Plomp, A.S., Rolfs, A., Graham, J.M., Seemanova, E., Poo, P., García-Cazorla, À., Edery, P., Jackson, I.J., Maher, E.R., and Aligianis, I.A. (2013). Mutation Spectrum in RAB3GAP1, RAB3GAP2, and RAB18 and Genotype-Phenotype Correlations in Warburg Micro Syndrome and Martsolf Syndrome. Hum. Mutat. *34*, 686–696.

Hansen, A.H., Duellberg, C., Mieck, C., Loose, M., and Hippenmeyer, S. (2017). Cell Polarity in Cerebral Cortex Development—Cellular Architecture Shaped by Biochemical Networks. Front. Cell. Neurosci. *11*, 1–16.

Hansen, D. V., Lui, J.H., Parker, P.R.L., and Kriegstein, A.R. (2010). Neurogenic radial glia in the outer subventricular zone of human neocortex. Nature *464*, 554–561.

Harwell, C.C., Fuentealba, L.C., Gonzalez-Cerrillo, A., Parker, P.R.L., Gertz, C.C., Mazzola, E., Garcia, M.T., Alvarez-Buylla, A., Cepko, C.L., and Kriegstein, A.R. (2015). Wide Dispersion and Diversity of Clonally Related Inhibitory Interneurons. Neuron *87*, 999–1007.

Hatakeyama, J., Wakamatsu, Y., Nagafuchi, A., Kageyama, R., Shigemoto, R., and Shimamura, K. (2014). Cadherin-based adhesions in the apical endfoot are required for active Notch signaling to control neurogenesis in vertebrates. Development *141*, 1671–1682.

Hatanaka, Y., Hisanaga, S.I., Heizmann, C.W., and Murakami, F. (2004). Distinct migratory behavior of early- and late-born neurons derived from the cortical ventricular zone. J. Comp. Neurol. *479*, 1–14.

Hatanaka, Y., Zhu, Y., Torigoe, M., Kita, Y., and Murakami, F. (2016). From migration to settlement: the pathways, migration modes and dynamics of neurons in the developing brain. Proc. Japan Acad. Ser. B *92*, 1–19.

Haubensak, W., Attardo, A., Denk, W., and Huttner, W.B. (2004). Neurons arise in the basal neuroepithelium of the early mammalian telencephalon: A major site of neurogenesis. Proc. Natl. Acad. Sci. U. S. A. *101*, 3196–3201.

Heaton, M.B., Paiva, M., Mayer, J., and Miller, R. (2002). Ethanol-mediated generation of reactive oxygen species in developing rat cerebellum. Neurosci. Lett. *334*, 83–86.

Heng, J.I.T., Nguyen, L., Castro, D.S., Zimmer, C., Wildner, H., Armant, O., Skowronska-Krawczyk, D., Bedogni, F., Matter, J.M., Hevner, R., and Guillemot, F. (2008). Neurogenin

2 controls cortical neuron migration through regulation of Rnd2. Nature *455*, 114–118.

Hernández-Miranda, L.R., Cariboni, A., Faux, C., Ruhrberg, C., Cho, J.H., Cloutier, J.F., Eickholt, B.J., Parnavelas, J.G., and Andrews, W.D. (2011). Robo1 regulates semaphorin signaling to guide the migration of cortical interneurons through the ventral forebrain. J. Neurosci. *31*, 6174–6187.

Hevner, R.F. (2019). Intermediate progenitors and Tbr2 in cortical development. J. Anat. *235*, 616–625.

Hirano, S., and Takeichi, M. (2012). Cadherins in Brain Morphogenesis and Wiring. Physiol. Rev. *92*, 597–634.

Hirota, Y., and Nakajima, K. (2017). Control of Neuronal Migration and Aggregation by Reelin Signaling in the Developing Cerebral Cortex. Front. Cell Dev. Biol. *5*, 1–8.

Hirotsune, S., Takahara, T., Sasaki, N., Hirose, K., Yoshiki, A., Ohashi, T., Kusakabe, M., Murakami, Y., Muramatsu, M., Watanabe, S., Nakao, K., Katsuki, M., and Hayashizaki, Y. (1995). The reeler gene encodes a protein with an EGF–like motif expressed by pioneer neurons. Nat. Genet. *10*, 77–83.

Hodge, R.G., and Ridley, A.J. (2016). Regulating Rho GTPases and their regulators. Nat. Rev. Mol. Cell Biol. *17*, 496–510.

Hoerder-Suabedissen, A., and Molnár, Z. (2015). Development, evolution and pathology of neocortical subplate neurons. Nat. Rev. Neurosci. *16*, 133–146.

Hollville, E., Romero, S.E., and Deshmukh, M. (2019). Apoptotic cell death regulation in neurons. FEBS J. *286*, 3276–3298.

Hor, C.H.H., and Goh, E.L.K. (2018). Rab23 regulates radial migration of projection neurons via N-cadherin. Cereb. Cortex *28*, 1516–1531.

Huang, Z. (2009). Molecular regulation of neuronal migration during neocortical development. Mol. Cell. Neurosci. *42*, 11–22.

Hussain, Z., Uyama, T., Tsuboi, K., and Ueda, N. (2017). Mammalian enzymes responsible for the biosynthesis of N -acylethanolamines. Biochim. Biophys. Acta - Mol. Cell Biol. Lipids *1862*, 1546–1561.

Huttner, W.B., and Kosodo, Y. (2005). Symmetric versus asymmetric cell division during neurogenesis in the developing vertebrate central nervous system. Curr. Opin. Cell Biol. *17*, 648–657.

Ikonomidou, C., Bittigau, P., Ishimaru, M.J., Wozniak, D.F., Koch, C., Genz, K., Price, M.T., Stefovska, V., Hörster, F., Tenkova, T., Dikranian, K., and Olney, J.W. (2000). Ethanol-induced apoptotic neurodegeneration and fetal alcohol syndrome. Science. *287*, 1056–1060.

Insolera, R., Bazzi, H., Shao, W., Anderson, K. V., and Shi, S.-H. (2014). Cortical

neurogenesis in the absence of centrioles. Nat. Neurosci. *17*, 1528–1535.

Ishii, S., Torii, M., Son, A.I., Rajendraprasad, M., Morozov, Y.M., Kawasawa, Y.I., Salzberg, A.C., Fujimoto, M., Brennand, K., Nakai, A., Mezger, V., Gage, F.H., Rakic, P., and Hashimoto-Torii, K. (2017). Variations in brain defects result from cellular mosaicism in the activation of heat shock signalling. Nat. Commun. *8*, 1–15.

Itoh, Y., Moriyama, Y., Hasegawa, T., Endo, T.A., Toyoda, T., and Gotoh, Y. (2013). Scratch regulates neuronal migration onset via an epithelial-mesenchymal transition-like mechanism. Nat. Neurosci. *16*, 416–425.

Iwashita, M., Kataoka, N., Toida, K., and Kosodo, Y. (2014). Systematic profiling of spatiotemporal tissue and cellular stiffness in the developing brain. Development *141*, 3793–3798.

Jiang, J., Zhang, Z. hong, Yuan, X. bin, and Poo, M. ming (2015). Spatiotemporal dynamics of traction forces show three contraction centers in migratory neurons. J. Cell Biol. *209*, 759–774.

Johansson, P.A., Cappello, S., and Götz, M. (2010). Stem cells niches during development--lessons from the cerebral cortex. Curr. Opin. Neurobiol. *20*, 400–407.

Jossin, Y., and Cooper, J.A. (2011). Reelin, Rap1 and N-cadherin orient the migration of multipolar neurons in the developing neocortex. Nat. Neurosci. *14*, 697–703.

Junghans, D., Hack, I., Frotscher, M., Taylor, V., and Kemler, R. (2005). β-catenin-mediated cell-adhesion is vital for embryonic forebrain development. Dev. Dyn. *233*, 528–539.

Juric-Sekhar, G., and Hevner, R.F. (2019). Malformations of Cerebral Cortex Development: Molecules and Mechanisms. Annu. Rev. Pathol. Mech. Dis. *14*, 293–318.

Kadowaki, M., Nakamura, S., Machon, O., Krauss, S., Radice, G.L., and Takeichi, M. (2007). N-cadherin mediates cortical organization in the mouse brain. Dev. Biol. *304*, 22–33.

Kageyama, R., Ohtsuka, T., Shimojo, H., and Imayoshi, I. (2008). Dynamic Notch signaling in neural progenitor cells and a revised view of lateral inhibition. Nat. Neurosci. *11*, 1247–1251.

Katona, I., and Freund, T.F. (2008). Endocannabinoid signaling as a synaptic circuit breaker in neurological disease. Nat. Med. *14*, 923–930.

Katona, I., and Freund, T.F. (2012). Multiple Functions of Endocannabinoid Signaling in the Brain. Annu. Rev. Neurosci. *35*, 529–558.

Katsamba, P., Carroll, K., Ahlsen, G., Bahna, F., Vendome, J., Posy, S., Rajebhosale, M., Price, S., Jessell, T.M., Ben-Shaul, A., Shapiro, L., and Honig, B.H. (2009). Linking molecular affinity and cellular specificity in cadherin-mediated adhesion. Proc. Natl. Acad. Sci. U. S. A. *106*, 11594–11599.

Kawauchi, T., Chihama, K., Nabeshima, Y.I., and Hoshino, M. (2003). The in vivo roles of STEF/Tiam1, Rac1 and JNK in cortical neuronal migration. EMBO J. *22*, 4190–4201.

Kawauchi, T., Sekine, K., Shikanai, M., Chihama, K., Tomita, K., Kubo, K.I., Nakajima, K., Nabeshima, Y.I., and Hoshino, M. (2010). Rab GTPases-dependent endocytic pathways regulate neuronal migration and maturation through N-cadherin trafficking. Neuron *67*, 588–602.

Keimpema, E., Barabas, K., Morozov, Y.M., Tortoriello, G., Torii, M., Cameron, G., Yanagawa, Y., Watanabe, M., Mackie, K., and Harkany, T. (2010). Differential Subcellular Recruitment of Monoacylglycerol Lipase Generates Spatial Specificity of 2-Arachidonoyl Glycerol Signaling during Axonal Pathfinding. J. Neurosci. *30*, 13992–14007.

Keimpema, E., MacKie, K., and Harkany, T. (2011). Molecular model of cannabis sensitivity in developing neuronal circuits. Trends Pharmacol. Sci. *32*, 551–561.

Keimpema, E., Tortoriello, G., Alpar, A., Capsoni, S., Arisi, I., Calvigioni, D., Hu, S.S.-J., Cattaneo, A., Doherty, P., Mackie, K., and Harkany, T. (2013). Nerve growth factor scales endocannabinoid signaling by regulating monoacylglycerol lipase turnover in developing cholinergic neurons. Proc. Natl. Acad. Sci. *110*, 1935–1940.

Kintner, C. (1992). Regulation of embryonic cell adhesion by the cadherin cytoplasmic domain. Cell *69*, 225–236.

Klausberger, T., and Somogyi, P. (2008). Neuronal Diversity and Temporal Dynamics: The Unity of Hippocampal Circuit Operations. Science. *321*, 53–57.

Kon, E., Cossard, A., and Jossin, Y. (2017). Neuronal Polarity in the Embryonic Mammalian Cerebral Cortex. Front. Cell. Neurosci. *11*, 1–15.

Kondratskyi, A., Kondratska, K., Skryma, R., and Prevarskaya, N. (2015). Ion channels in the regulation of apoptosis. Biochim. Biophys. Acta - Biomembr. *1848*, 2532–2546.

Konno, D., Yoshimura, S., Hori, K., Maruoka, H., and Sobue, K. (2005). Involvement of the phosphatidylinositol 3-kinase/Rac1 and Cdc42 pathways in radial migration of cortical neurons. J. Biol. Chem. *280*, 5082–5088.

Kosodo, Y., Röper, K., Haubensak, W., Marzesco, A.M., Corbeil, D., and Huttner, W.B. (2004). Asymmetric distribution of the apical plasma membrane during neurogenic divisions of mamalian neuroepithelial cells. EMBO J. *23*, 2314–2324.

Kovach, C., Dixit, R., Li, S., Mattar, P., Wilkinson, G., Elsen, G.E., Kurrasch, D.M., Hevner, R.F., and Schuurmans, C. (2013). Neurog2 simultaneously activates and represses alternative gene expression programs in the developing neocortex. Cereb. Cortex *23*, 1884–1900.

Kowalczyk, T., Pontious, A., Englund, C., Daza, R.A.M., Bedogni, F., Hodge, R., Attardo, A., Bell, C., Huttner, W.B., and Hevner, R.F. (2009). Intermediate neuronal progenitors (basal progenitors) produce pyramidal-projection neurons for all layers of cerebral cortex. Cereb. Cortex *19*, 2439–2450.

Kriegstein, A., and Alvarez-buylla, A. (2011). The Glial Nature of Embryonic and Adult Neural Stem Cells. Annu. Rev. Neurosci. 149–184.

Kriegstein, A.R., and Noctor, S.C. (2004). Patterns of neuronal migration in the embryonic cortex. Trends Neurosci. *27*, 392–399.

Kubo, K.I., Honda, T., Tomita, K., Sekine, K., Ishii, K., Uto, A., Kobayashi, K., Tabata, H., and Nakajima, K. (2010). Ectopic reelin induces neuronal aggregation with a normal birthdate-dependent "inside-out" alignment in the developing neocortex. J. Neurosci. *30*, 10953–10966.

Kumar, S., Stecher, G., and Tamura, K. (2016). MEGA7: Molecular Evolutionary Genetics Analysis Version 7.0 for Bigger Datasets. Mol. Biol. Evol. *33*, 1870–1874.

László, Z.I., Bercsényi, K., Mayer, M., Lefkovics, K., Szabó, G., Katona, I., and Lele, Z. (2019). N-cadherin (Cdh2) Maintains Migration and Postmitotic Survival of Cortical Interneuron Precursors in a Cell-Type-Specific Manner. Cereb. Cortex 1–12.

Lavdas, A.A., Grigoriou, M., Pachnis, V., and Parnavelas, J.G. (1999). The medial ganglionic eminence gives rise to a population of early neurons in the developing cerebral cortex. J. Neurosci. *19*, 7881–7888.

Le, T.N., Zhou, Q.P., Cobos, I., Zhang, S., Zagozewski, J., Japoni, S., Vriend, J., Parkinson, T., Du, G., Rubenstein, J.L., and Eisenstat, D.D. (2017). GABAergic interneuron differentiation in the basal forebrain is mediated through direct regulation of glutamic acid decarboxylase isoforms by Dlx homeobox transcription factors. J. Neurosci. *37*, 8816–8829.

Lebel, C., Mattson, S.N., Riley, E.P., Jones, K.L., Adnams, C.M., May, P.A., Bookheimer, S.Y., O'Connor, M.J., Narr, K.L., Kan, E., Abaryan, Z., and Sowell, E.R. (2012). A Longitudinal Study of the Long-Term Consequences of Drinking during Pregnancy: Heavy In Utero Alcohol Exposure Disrupts the Normal Processes of Brain Development. J. Neurosci. *32*, 15243–15251.

Lee, H.C., Simon, G.M., and Cravatt, B.F. (2015). ABHD4 Regulates Multiple Classes of N -Acyl Phospholipids in the Mammalian Central Nervous System. Biochemistry *54*, 2539–2549.

Lee, J.H., Lee, J.E., Kahng, J.Y., Kim, S.H., Park, J.S., Yoon, S.J., Um, J.Y., Kim, W.K., Lee, J.K., Park, J., Kim, E.H., Lee, J.H., Lee, J.H., Chung, W.S., Ju, Y.S., Park, S.H., Chang, J.H., Kang, S.G., and Lee, J.H. (2018). Human glioblastoma arises from subventricular zone cells with low-level driver mutations. Nature *560*, 243–247.

Lefkovics, K., Mayer, M., Bercsényi, K., Szabó, G., and Lele, Z. (2012). Comparative analysis of type II classic cadherin mRNA distribution patterns in the developing and adult mouse somatosensory cortex and hippocampus suggests significant functional redundancy. J. Comp. Neurol. *520*, 1387–1405.

Lele, Z., Folchert, A., Concha, M., Rauch, G.-J., Geisler, R., Rosa, F., Wilson, S.W.,

Hammerschmidt, M., and Bally-Cuif, L. (2002). Parachute/N-Cadherin Is Required for Morphogenesis and Maintained Integrity of the Zebrafish Neural Tube. Development *129*, 3281–3294.

Lelièvre, E.C., Plestant, C., Boscher, C., Wolff, E., Mège, R.-M., and Birbes, H. (2012). N-Cadherin Mediates Neuronal Cell Survival through Bim Down-Regulation. PLoS One *7*, e33206.

Leszczynska, K.B., Foskolou, I.P., Abraham, A.G., Anbalagan, S., Tellier, C., Haider, S., Span, P.N., O'Neill, E.E., Buffa, F.M., and Hammond, E.M. (2015). Hypoxia-induced p53 modulates both apoptosis and radiosensitivity via AKT. J. Clin. Invest. *125*, 2385–2398.

Li, C., Xu, D., Ye, Q., Hong, S., Jiang, Y., Liu, X., Zhang, N., Shi, L., Qin, C.-F., and Xu, Z. (2016). Zika Virus Disrupts Neural Progenitor Development and Leads to Microcephaly in Mice. Cell Stem Cell *19*, 120–126.

Li, G., Adesnik, H., Li, J., Long, J., Nicoll, R.A., Rubenstein, J.L.R., and Pleasure, S.J. (2008). Regional distribution of cortical interneurons and development of inhibitory tone are regulated by Cxcl12/Cxcr4 signaling. J. Neurosci. *28*, 1085–1098.

Lim, L., Mi, D., Llorca, A., and Marín, O. (2018). Development and Functional Diversification of Cortical Interneurons. Neuron *100*, 294–313.

Lin, Y.-C., Boone, M., Meuris, L., Lemmens, I., Van Roy, N., Soete, A., Reumers, J., Moisse, M., Plaisance, S., Drmanac, R., Chen, J., Speleman, F., Lambrechts, D., Van de Peer, Y., Tavernier, J., and Callewaert, N. (2014). Genome dynamics of the human embryonic kidney 293 lineage in response to cell biology manipulations. Nat. Commun. *5*, 4767.

Lindtner, S., Catta-Preta, R., Tian, H., Su-Feher, L., Price, J.D., Dickel, D.E., Greiner, V., Silberberg, S.N., McKinsey, G.L., McManus, M.T., Pennacchio, L.A., Visel, A., Nord, A., and Rubenstein, J.L.R. (2019). Genomic Resolution of DLX-Orchestrated Transcriptional Circuits Driving Development of Forebrain GABAergic Neurons. Cell Rep. *28*, 2048-2063.e8.

Linford, A., Yoshimura, S., Bastos, R.N., Langemeyer, L., Gerondopoulos, A., Rigden, D.J., and Barr, F.A. (2012). Rab14 and Its Exchange Factor FAM116 Link Endocytic Recycling and Adherens Junction Stability in Migrating Cells. Dev. Cell *22*, 952–966.

Liu, X., Sun, L., Torii, M., and Rakic, P. (2012). Connexin 43 controls the multipolar phase of neuronal migration to the cerebral cortex. Proc. Natl. Acad. Sci. U. S. A. *109*, 8280–8285.

Lodato, S., Rouaux, C., Quast, K.B., Jantrachotechatchawan, C., Studer, M., Hensch, T.K., and Arlotta, P. (2011). Excitatory Projection Neuron Subtypes Control the Distribution of Local Inhibitory Interneurons in the Cerebral Cortex. Neuron *69*, 763–779.

Loh, Chai, Tang, Wong, Sethi, Shanmugam, Chong, and Looi (2019). The E-Cadherin and N-Cadherin Switch in Epithelial-to-Mesenchymal Transition: Signaling, Therapeutic

Implications, and Challenges. Cells *8*, 1118.

Long, J.E., Cobos, I., Potter, G.B., and Rubenstein, J.L.R. (2009). Dlx1&2 and Mash1 Transcription Factors Control MGE and CGE Patterning and Differentiation through Parallel and Overlapping Pathways. Cereb. Cortex *19*, 96–106.

López-Bendito, G., Sturgess, K., Erdélyi, F., Szabó, G., Molnár, Z., and Paulsen, O. (2004). Preferential origin and layer destination of GAD65-GFP cortical interneurons. Cereb. Cortex *14*, 1122–1133.

López-Bendito, G., Sanchez-Alcaniz, J.A., Pla, R., Borrell, V., Pico, E., Valdeolmillos, M., and Marin, O. (2008). Chemokine Signaling Controls Intracortical Migration and Final Distribution of GABAergic Interneurons. J. Neurosci. *28*, 1613–1624.

Loulier, K., Lathia, J.D., Marthiens, V., Relucio, J., Mughal, M.R., Tang, S.-C., Coksaygan, T., Hall, P.E., Chigurupati, S., Patton, B., Colognato, H., Rao, M.S., Mattson, M.P., Haydar, T.F., and Ffrench-Constant, C. (2009). β1 Integrin Maintains Integrity of the Embryonic Neocortical Stem Cell Niche. PLoS Biol. *7*, e1000176.

Luccardini, C., Hennekinne, L., Viou, L., Yanagida, M., Murakami, F., Kessaris, N., Ma, X., Adelstein, R.S., Mege, R.-M., and Metin, C. (2013). N-Cadherin Sustains Motility and Polarity of Future Cortical Interneurons during Tangential Migration. J. Neurosci. *33*, 18149–18160.

Luccardini, C., Leclech, C., Viou, L., Rio, J.-P., and Métin, C. (2015). Cortical interneurons migrating on a pure substrate of N-cadherin exhibit fast synchronous centrosomal and nuclear movements and reduced ciliogenesis. Front. Cell. Neurosci. *9*, 1–15.

Maccarrone, M., and Finazzi-Agró, A. (2003). The endocannabinoid system, anandamide and the regulation of mammalian cell apoptosis. Cell Death Differ. *10*, 946–955.

Maccarrone, M., Guzmán, M., Mackie, K., Doherty, P., and Harkany, T. (2014). Programming of neural cells by (endo)cannabinoids: from physiological rules to emerging therapies. Nat. Rev. Neurosci. *15*, 786–801.

Magdaleno, S., Keshvara, L., and Curran, T. (2002). Rescue of ataxia and preplate splitting by ectopic expression of Reelin in reeler mice. Neuron *33*, 573–586.

Malatesta, P., Hack, M.A., Hartfuss, E., Kettenmann, H., Klinkert, W., Kirchhoff, F., and Götz, M. (2003). Neuronal or glial progeny: Regional differences in radial glia fate. Neuron *37*, 751–764.

Marín, O. (2013). Cellular and molecular mechanisms controlling the migration of neocortical interneurons. Eur. J. Neurosci. *38*, 2019–2029.

Marín, O., and Rubenstein, J.L.R. (2003). Cell migration in the forebrain. Annu. Rev. Neurosci. *26*, 441–483.

Marín, O., Anderson, S.A., and Rubenstein, J.L.R. (2000). Origin and molecular specification of striatal interneurons. J. Neurosci. *20*, 6063–6076.

Marín, O., Yaron, A., Bagri, A., Tessier-Lavigne, M., and Rubenstein, J.L.R. (2001). Sorting of striatal and cortical interneurons regulated by semaphorin-neuropilin interactions. Science. *293*, 872–875.

Marsicano, G., and Lutz, B. (1999). Expression of the cannabinoid receptor CB1 in distinct neuronal subpopulations in the adult mouse forebrain. Eur. J. Neurosci. *11*, 4213–4225.

Martynoga, B., Drechsel, D., and Guillemot, F. (2012). Molecular Control of Neurogenesis: A View from the Mammalian Cerebral Cortex. Cold Spring Harb. Perspect. Biol. *4*, a008359.

Di Marzo, V. (2018). New approaches and challenges to targeting the endocannabinoid system. Nat. Rev. Drug Discov. *17*, 623–639.

Masai, I. (2003). N-cadherin mediates retinal lamination, maintenance of forebrain compartments and patterning of retinal neurites. Development *130*, 2479–2494.

Matsuda, T., and Cepko, C.L. (2004). Electroporation and RNA interference in the rodent retina in vivo and in vitro. Proc. Natl. Acad. Sci. *101*, 16–22.

Matsunaga, Y., Noda, M., Murakawa, H., Hayashi, K., Nagasaka, A., Inoue, S., Miyata, T., Miura, T., Kubo, K.I., and Nakajima, K. (2017). Reelin transiently promotes N-cadherin-dependent neuronal adhesion during mouse cortical development. Proc. Natl. Acad. Sci. U. S. A. *114*, 2048–2053.

Mayer, C., Hafemeister, C., Bandler, R.C., Machold, R., Batista Brito, R., Jaglin, X., Allaway, K., Butler, A., Fishell, G., and Satija, R. (2018). Developmental diversification of cortical inhibitory interneurons. Nature *555*, 457–462.

Mayer, M., Bercsényi, K., Géczi, K., Szabó, G., and Lele, Z. (2010). Expression of two type II cadherins, Cdh12 and Cdh22 in the developing and adult mouse brain. Gene Expr. Patterns *10*, 351–360.

Mehler, M.F., Petronglo, J.R., Arteaga-Bracho, E.E., Gulinello, M.E., Winchester, M.L., Pichamoorthy, N., Young, S.K., Dejesus, C.D., Ishtiaq, H., Gokhan, S., and Molero, A.E. (2019). Loss-of-huntingtin in medial and lateral ganglionic lineages differentially disrupts regional interneuron and projection neuron subtypes and promotes huntington's disease-associated behavioral, cellular, and pathological hallmarks. J. Neurosci. *39*, 1892–1909.

Mi, D., Li, Z., Lim, L., Li, M., Moissidis, M., Yang, Y., Gao, T., Hu, T.X., Pratt, T., Price, D.J., Sestan, N., and Marín, O. (2018). Early emergence of cortical interneuron diversity in the mouse embryo. Science. *360*, 81–85.

Mihalas, A.B., Elsen, G.E., Bedogni, F., Daza, R.A.M., Ramos-Laguna, K.A., Arnold, S.J., and Hevner, R.F. (2016). Intermediate Progenitor Cohorts Differentially Generate Cortical Layers and Require Tbr2 for Timely Acquisition of Neuronal Subtype Identity. Cell Rep. *16*, 92–105.

Miller, D.J., Bhaduri, A., Sestan, N., and Kriegstein, A. (2019). Shared and derived features of cellular diversity in the human cerebral cortex. Curr. Opin. Neurobiol. *56*, 117–124.

Miyata, T., Kawaguchi, A., Okano, H., and Ogawa, M. (2001). Asymmetric inheritance of radial glial fibers by cortical neurons. Neuron *31*, 727–741.

Miyoshi, G. (2019). Elucidating the developmental trajectories of GABAergic cortical interneuron subtypes. Neurosci. Res. *138*, 26–32.

Miyoshi, G., and Fishell, G. (2011). GABAergic interneuron lineages selectively sort into specific cortical layers during early postnatal development. Cereb. Cortex *21*, 845–852.

Miyoshi, G., Butt, S.J.B., Takebayashi, H., and Fishell, G. (2007). Physiologically Distinct Temporal Cohorts of Cortical Interneurons Arise from Telencephalic Olig2-Expressing Precursors. J. Neurosci. *27*, 7786–7798.

Miyoshi, G., Hjerling-Leffler, J., Karayannis, T., Sousa, V.H., Butt, S.J.B., Battiste, J., Johnson, J.E., Machold, R.P., and Fishell, G. (2010). Genetic Fate Mapping Reveals That the Caudal Ganglionic Eminence Produces a Large and Diverse Population of Superficial Cortical Interneurons. J. Neurosci. *30*, 1582–1594.

Monory, K., Nave, K.-A., Kelsch, W., Dodt, H.-U., During, M., Lutz, B., Wölfel, B., Long, J., Klugmann, M., Blaudzun, H., Rubenstein, J.L., Eder, M., Massa, F., Marsicano, G., Elphick, M.R., Westenbroek, R., Ekker, M., Wotjak, C.T., Jacob, W., Egertová, M., Mackie, K., Goebbels, S., Marsch, R., and Zieglgänsberger, W. (2006). The Endocannabinoid System Controls Key Epileptogenic Circuits in the Hippocampus. Neuron *51*, 455–466.

Morishita, J., Okamoto, Y., Tsuboi, K., Ueno, M., Sakamoto, H., Maekawa, N., and Ueda, N. (2005). Regional distribution and age-dependent expression of N-acylphosphatidylethanolamine-hydrolyzing phospholipase D in rat brain. J. Neurochem. *94*, 753–762.

Morozov, Y.M., Torii, M., and Rakic, P. (2009). Origin, Early Commitment, Migratory Routes, and Destination of Cannabinoid Type 1 Receptor-Containing Interneurons. Cereb. Cortex *19*, i78–i89.

Morris-Rosendahl, D.J., Segel, R., Born, A.P., Conrad, C., Loeys, B., Brooks, S.S., Müller, L., Zeschnigk, C., Botti, C., Rabinowitz, R., Uyanik, G., Crocq, M.A., Kraus, U., Degen, I., and Faes, F. (2010). New RAB3GAP1 mutations in patients with Warburg Micro Syndrome from different ethnic backgrounds and a possible founder effect in the Danish. Eur. J. Hum. Genet. *18*, 1100–1106.

Mountoufaris, G., Canzio, D., Nwakeze, C.L., Chen, W. V., and Maniatis, T. (2018). Writing, Reading, and Translating the Clustered Protocadherin Cell Surface Recognition Code for Neural Circuit Assembly. Annu. Rev. Cell Dev. Biol. *34*, 471–493.

Mulder, J., Aguado, T., Keimpema, E., Barabás, K., Ballester Rosado, C.J., Nguyen, L., Monory, K., Marsicano, G., Di Marzo, V., Hurd, Y.L., Guillemot, F., Mackie, K., Lutz, B., Guzmán, M., Lu, H.-C., Galve-Roperh, I., and Harkany, T. (2008). Endocannabinoid signaling controls pyramidal cell specification and long-range axon patterning. Proc. Natl. Acad. Sci. U. S. A. *105*, 8760–8765.

Murao, N., Noguchi, H., and Nakashima, K. (2016). Epigenetic regulation of neural stem cell property from embryo to adult. Neuroepigenetics *5*, 1–10.

Nadarajah, B., Brunstrom, J.E., Grutzendler, J., Wong, R.O.L., and Pearlman, A.L. (2001). Two modes of radial migration in early development of the cerebral cortex. Nat. Neurosci. *4*, 143–150.

Nadarajah, B., Alifragis, P., Wong, R.O.L., and Parnavelas, J.G. (2002). Ventricle-directed migration in the developing cerebral cortex. Nat. Neurosci. *5*, 218–224.

Namba, T., Kibe, Y., Funahashi, Y., Nakamuta, S., Takano, T., Ueno, T., Shimada, A., Kozawa, S., Okamoto, M., Shimoda, Y., Oda, K., Wada, Y., Masuda, T., Sakakibara, A., Igarashi, M., Miyata, T., Faivre-Sarrailh, C., Takeuchi, K., and Kaibuchi, K. (2014). Pioneering axons regulate neuronal polarization in the developing cerebral cortex. Neuron *81*, 814–829.

Nieman, M.T., Kim, J.B., Johnson, K.R., and Wheelock, M.J. (1999). Mechanism of extracellular domain-deleted dominant negative cadherins. J. Cell Sci. *112*, 1621–1632.

Noctor, S.C., Flint, A.C., Weissman, T.A., Dammerman, R.S., and Kriegstein, A.R. (2001). Neurons derived from radial glial cells establish radial units in neocortex. Nature *409*, 714–720.

Noctor, S.C., Martinez-Cerdeño, V., Ivic, L., and Kriegstein, A.R. (2004). Cortical neurons arise in symmetric and asymmetric division zones and migrate through specific phases. Nat. Neurosci. *7*, 136–144.

Nowakowski, T.J., Pollen, A.A., Di Lullo, E., Sandoval-Espinosa, C., Bershteyn, M., and Kriegstein, A.R. (2016). Expression Analysis Highlights AXL as a Candidate Zika Virus Entry Receptor in Neural Stem Cells. Cell Stem Cell *18*, 591–596.

Nowakowski, T.J., Bhaduri, A., Pollen, A.A., Alvarado, B., Mostajo-Radji, M.A., Di Lullo, E., Haeussler, M., Sandoval-Espinosa, C., Liu, S.J., Velmeshev, D., Ounadjela, J.R., Shuga, J., Wang, X., Lim, D.A., West, J.A., Leyrat, A.A., Kent, W.J., and Kriegstein, A.R. (2017). Spatiotemporal gene expression trajectories reveal developmental hierarchies of the human cortex. Science. *358*, 1318–1323.

O'Rourke, N.A., Dailey, M.E., Smith, S.J., and McConnell, S.K. (1992). Diverse migratory pathways in the developing cerebral cortex. Science. *258*, 299–302.

Ohtaka-Maruyama, C., and Okado, H. (2015). Molecular pathways underlying projection neuron production and migration during cerebral cortical development. Front. Neurosci. *9*, 1–24.

Olagnier, D., Muscolini, M., Coyne, C.B., Diamond, M.S., and Hiscott, J. (2016). Mechanisms of Zika Virus Infection and Neuropathogenesis. DNA Cell Biol. *35*, 367–372.

Olzmann, J.A., and Carvalho, P. (2019). Dynamics and functions of lipid droplets. Nat. Rev. Mol. Cell Biol. *20*, 137–155.

Ostrem, B., Di Lullo, E., and Kriegstein, A. (2017). oRGs and mitotic somal translocation — a role in development and disease. Curr. Opin. Neurobiol. *42*, 61–67.

Ozer, U., Barbour, K.W., Clinton, S.A., and Berger, F.G. (2015). Oxidative stress and response to thymidylate synthase-targeted antimetabolites. Mol. Pharmacol. *88*, 970–981.

Paoli, P., Giannoni, E., and Chiarugi, P. (2013). Anoikis molecular pathways and its role in cancer progression. Biochim. Biophys. Acta - Mol. Cell Res. *1833*, 3481–3498.

Paramanik, V., and Thakur, M.K. (2012). Estrogen Receptor and Its Domains Interact with Casein Kinase 2, Phosphokinase C, and N-Myristoylation Sites of Mitochondrial and Nuclear Proteins in Mouse Brain. J. Biol. Chem. *287*, 22305–22316.

Pasquariello, N., Catanzaro, G., Marzano, V., Amadio, D., Barcaroli, D., Oddi, S., Federici, G., Urbani, A., Agrò, A.F., and Maccarrone, M. (2009). Characterization of the endocannabinoid system in human neuronal cells and proteomic analysis of anandamide-induced apoptosis. J. Biol. Chem. *284*, 29413–29426.

Persano, L., Rampazzo, E., Basso, G., and Viola, G. (2013). Glioblastoma cancer stem cells: Role of the microenvironment and therapeutic targeting. Biochem. Pharmacol. *85*, 612–622.

Petros, T.J., Bultje, R.S., Ross, M.E., Fishell, G., and Anderson, S.A. (2015). Apical versus Basal Neurogenesis Directs Cortical Interneuron Subclass Fate. Cell Rep. *13*, 1090–1095.

Petryszyn, S., Parent, A., and Parent, M. (2018). The calretinin interneurons of the striatum: comparisons between rodents and primates under normal and pathological conditions. J. Neural Transm. *125*, 279–290.

Peyre, E., Silva, C.G., and Nguyen, L. (2015). Crosstalk between intracellular and extracellular signals regulating interneuron production, migration and integration into the cortex. Front. Cell. Neurosci. *9*, 1–18.

Pilz, G.A., Shitamukai, A., Reillo, I., Pacary, E., Schwausch, J., Stahl, R., Ninkovic, J., Snippert, H.J., Clevers, H., Godinho, L., Guillemot, F., Borrell, V., Matsuzaki, F., and Götz, M. (2013). Amplification of progenitors in the mammalian telencephalon includes a new radial glial cell type. Nat. Commun. *4*, 1–11.

Piomelli, D. (2003). The molecular logic of endocannabinoid signalling. Nat. Rev. Neurosci. *4*, 873–884.

Pla, R., Borrell, V., Flames, N., and Marín, O. (2006). Layer acquisition by cortical GABAergic interneurons is independent of reelin signaling. J. Neurosci. *26*, 6924–6934.

Polleux, F., Whitford, K.L., Dijkhuizen, P.A., Vitalis, T., and Ghosh, A. (2002). Control of cortical interneuron migration by neurotrophins and PI3-kinase signaling. Development *129*, 3147–3160.

Priya, R., Paredes, M.F., Karayannis, T., Yusuf, N., Liu, X., Jaglin, X., Graef, I., Alvarez-Buylla, A., and Fishell, G. (2018). Activity Regulates Cell Death within Cortical

Interneurons through a Calcineurin-Dependent Mechanism. Cell Rep. *22*, 1695–1709.

Quinn, J.C., Molinek, M., Martynoga, B.S., Zaki, P.A., Faedo, A., Bulfone, A., Hevner, R.F., West, J.D., and Price, D.J. (2007). Pax6 controls cerebral cortical cell number by regulating exit from the cell cycle and specifies cortical cell identity by a cell autonomous mechanism. Dev. Biol. *302*, 50–65.

Radakovits, R., Barros, C.S., Belvindrah, R., Patton, B., and Muller, U. (2009). Regulation of Radial Glial Survival by Signals from the Meninges. J. Neurosci. *29*, 7694–7705.

Radice, G.L., Rayburn, H., Matsunami, H., Knudsen, K.A., Takeichi, M., and Hynes, R.O. (1997). Developmental defects in mouse embryos lacking N-cadherin. Dev. Biol. *181*, 64–78.

Rakic, P. (1972). Mode of cell migration to the superficial layers of fetal monkey neocortex. J. Comp. Neurol. *145*, 61–83.

Rakic, P. (1988). Specification of Cerebral Cortical Areas. Science. *241*, 170–176.

de Ramon Francàs, G., Alther, T., and Stoeckli, E.T. (2017). Calsyntenins Are Expressed in a Dynamic and Partially Overlapping Manner during Neural Development. Front. Neuroanat. *11*, 1–13.

Rasin, M.-R., Gazula, V.-R., Breunig, J.J., Kwan, K.Y., Johnson, M.B., Liu-Chen, S., Li, H.-S., Jan, L.Y., Jan, Y.-N., Rakic, P., and Sestan, N. (2007). Numb and Numbl are required for maintenance of cadherin-based adhesion and polarity of neural progenitors. Nat. Neurosci. *10*, 819–827.

Reiss, K., Maretzky, T., Ludwig, A., Tousseyn, T., De Strooper, B., Hartmann, D., and Saftig, P. (2005). ADAM10 cleavage of N-cadherin and regulation of cell-cell adhesion and β-catenin nuclear signalling. EMBO J. *24*, 742–752.

Rhee, J., Mahfooz, N.S., Arregui, C., Lilien, J., Balsamo, J., and VanBerkum, M.F.A. (2002). Activation of the repulsive receptor roundabout inhibits N-cadherin-mediated cell adhesion. Nat. Cell Biol. *4*, 798–805.

Rhee, J., Buchan, T., Zukerberg, L., Lilien, J., and Balsamo, J. (2007). Cables links Robo-bound Abl kinase to N-cadherin-bound β-catenin to mediate Slit-induced modulation of adhesion and transcription. Nat. Cell Biol. *9*, 883–892.

Ridley, A.J. (2015). Rho GTPase signalling in cell migration. Curr. Opin. Cell Biol. *36*, 103–112.

Robertson, F.C., Narr, K.L., Molteno, C.D., Jacobson, J.L., Jacobson, S.W., and Meintjes, E.M. (2016). Prenatal Alcohol Exposure is Associated with Regionally Thinner Cortex During the Preadolescent Period. Cereb. Cortex *26*, 3083–3095.

Rogers, C.D., Sorrells, L.K., and Bronner, M.E. (2018). A catenin-dependent balance between N-cadherin and E-cadherin controls neuroectodermal cell fate choices. Mech. Dev. *152*, 44–56.

Ross, M.E. (2011). Cell cycle regulation and interneuron production. Dev. Neurobiol. *71*, 2–9.

Rousso, D.L., Pearson, C.A., Gaber, Z.B., Miquelajauregui, A., Li, S., Portera-Cailliau, C., Morrisey, E.E., and Novitch, B.G. (2012). Foxp-Mediated Suppression of N-Cadherin Regulates Neuroepithelial Character and Progenitor Maintenance in the CNS. Neuron *74*, 314–330.

Rowley, N.M., Madsen, K.K., Schousboe, A., and Steve White, H. (2012). Glutamate and GABA synthesis, release, transport and metabolism as targets for seizure control. Neurochem. Int. *61*, 546–558.

Rubinstein, R., Goodman, K.M., Maniatis, T., Shapiro, L., and Honig, B. (2017). Structural origins of clustered protocadherin-mediated neuronal barcoding. Semin. Cell Dev. Biol. *69*, 140–150.

Rudolph, J., Gerstmann, K., Zimmer, G., Steinecke, A., Döding, A., and Bolz, J. (2014). A dual role of EphB1/ephrin-B3 reverse signaling on migrating striatal and cortical neurons originating in the preoptic area: Should I stay or go away? Front. Cell. Neurosci. *8*, 1–20.

Rueda, D., Navarro, B., Martínez-Serrano, A., Guzmán, M., and Galve-Roperh, I. (2002). The Endocannabinoid Anandamide Inhibits Neuronal Progenitor Cell Differentiation through Attenuation of the Rap1/B-Raf/ERK Pathway. J. Biol. Chem. *277*, 46645–46650.

Saez, T.M.M., Aronne, M.P., Caltana, L., and Brusco, A.H. (2014). Prenatal exposure to the CB1 and CB2 cannabinoid receptor agonist WIN 55,212-2 alters migration of early-born glutamatergic neurons and GABAergic interneurons in the rat cerebral cortex. J. Neurochem. *129*, 637–648.

de Salas-Quiroga, A., Díaz-Alonso, J., García-Rincón, D., Remmers, F., Vega, D., Gómez-Cañas, M., Lutz, B., Guzmán, M., and Galve-Roperh, I. (2015). Prenatal exposure to cannabinoids evokes long-lasting functional alterations by targeting CB $_1$ receptors on developing cortical neurons. Proc. Natl. Acad. Sci. *112*, 13693–13698.

Sanders, M.A., Zhang, H., Mladenovic, L., Tseng, Y.Y., and Granneman, J.G. (2017). Molecular Basis of ABHD5 Lipolysis Activation. Sci. Rep. *7*, 42589.

Sansom, S.N., Griffiths, D.S., Faedo, A., Kleinjan, D.J., Ruan, Y., Smith, J., Van Heyningen, V., Rubenstein, J.L., and Livesey, F.J. (2009). The level of the transcription factor Pax6 is essential for controlling the balance between neural stem cell self-renewal and neurogenesis. PLoS Genet. *5*, 20–23.

Schmidt, A., and Jäger, S. (2005). Plakophilins - Hard work in the desmosome, recreation in the nucleus? Eur. J. Cell Biol. *84*, 189–204.

Schweiger, M., Lass, A., Zimmermann, R., Eichmann, T.O., and Zechner, R. (2009). Neutral lipid storage disease: genetic disorders caused by mutations in adipose triglyceride lipase/ PNPLA2 or CGI-58 / ABHD5. Am. J. Physiol. Metab. *297*, E289–E296.

Segawa, K., and Nagata, S. (2015). An Apoptotic "Eat Me" Signal: Phosphatidylserine

Exposure. Trends Cell Biol. *25*, 639–650.

Segawa, K., Kurata, S., Yanagihashi, Y., Brummelkamp, T.R., Matsuda, F., and Nagata, S. (2014). Caspase-mediated cleavage of phospholipid flippase for apoptotic phosphatidylserine exposure. Science. *344*, 1164–1168.

Sekine, K., Honda, T., Kawauchi, T., Kubo, K. ichiro, and Nakajima, K. (2011). The outermost region of the developing cortical plate is crucial for both the switch of the radial migration mode and the dab1-dependent "inside-out" lamination in the neocortex. J. Neurosci. *31*, 9426–9439.

Sekine, K., Kawauchi, T., Kubo, K.I., Honda, T., Herz, J., Hattori, M., Kinashi, T., and Nakajima, K. (2012). Reelin Controls Neuronal Positioning by Promoting Cell-Matrix Adhesion via Inside-Out Activation of Integrin α5β1. Neuron *76*, 353–369.

Sessa, A., Mao, C.A., Colasante, G., Nini, A., Klein, W.H., and Broccoli, V. (2010). Tbr2-positive intermediate (basal) neuronal progenitors safeguard cerebral cortex expansion by controlling amplification of pallial glutamatergic neurons and attraction of subpallial GABAergic interneurons. Genes Dev. *24*, 1816–1826.

Shapiro, L., and Weis, W.I. (2009). Structure and biochemistry of cadherins and catenins. Cold Spring Harb. Perspect. Biol. *1*, 1–21.

Shimojo, H., Ohtsuka, T., and Kageyama, R. (2008). Oscillations in Notch Signaling Regulate Maintenance of Neural Progenitors. Neuron *58*, 52–64.

Shoukimas, G.M., and Hinds, J.W. (1978). The development of the cerebral cortex in the embryonic mouse: An electron microscopic serial section analysis. J. Comp. Neurol. *179*, 795–830.

Simon, G.M., and Cravatt, B.F. (2006). Endocannabinoid Biosynthesis Proceeding through Glycerophospho- N -acyl Ethanolamine and a Role for α/β-Hydrolase 4 in This Pathway. J. Biol. Chem. *281*, 26465–26472.

Simpson, C.D., Hurren, R., Kasimer, D., MacLean, N., Eberhard, Y., Ketela, T., Moffat, J., and Schimmer, A.D. (2012). A genome wide shRNA screen identifies α/β hydrolase domain containing 4 (ABHD4) as a novel regulator of anoikis resistance. Apoptosis *17*, 666–678.

Soliman, E., and Van Dross, R. (2016). Anandamide-induced endoplasmic reticulum stress and apoptosis are mediated by oxidative stress in non-melanoma skin cancer: Receptor-independent endocannabinoid signaling. Mol. Carcinog. *55*, 1807–1821.

Sousa, V.H., Miyoshi, G., Hjerling-Leffler, J., Karayannis, T., and Fishell, G. (2009). Characterization of Nkx6-2-Derived Neocortical Interneuron Lineages. Cereb. Cortex *19*, i1–i10.

Southwell, D.G., Paredes, M.F., Galvao, R.P., Jones, D.L., Froemke, R.C., Sebe, J.Y., Alfaro-Cervello, C., Tang, Y., Garcia-Verdugo, J.M., Rubenstein, J.L., Baraban, S.C., and Alvarez-Buylla, A. (2012). Intrinsically determined cell death of developing cortical

interneurons. Nature *491*, 109–113.

Steinecke, A., Gampe, C., Zimmer, G., Rudolph, J., and Bolz, J. (2014). EphA/ephrin A reverse signaling promotes the migration of cortical interneurons from the medial ganglionic eminence. Development *141*, 460–471.

Stenman, J.M., Wang, B., and Campbell, K. (2003). Tlx Controls Proliferation and Patterning of Lateral Telencephalic Progenitor Domains. J. Neurosci. *23*, 10568–10576.

Stock, K., Kumar, J., Synowitz, M., Petrosino, S., Imperatore, R., Smith, E.S.J., Wend, P., Purfürst, B., Nuber, U.A., Gurok, U., Matyash, V., Wälzlein, J.H., Chirasani, S.R., Dittmar, G., Cravatt, B.F., Momma, S., Lewin, G.R., Ligresti, A., De Petrocellis, L., Cristino, L., Di Marzo, V., Kettenmann, H., and Glass, R. (2012). Neural precursor cells induce cell death of high-grade astrocytomas through stimulation of TRPV1. Nat. Med. *18*, 1232–1238.

Stocker, A.M., and Chenn, A. (2015). The role of adherens junctions in the developing neocortex. Cell Adh. Migr. *9*, 167–174.

Szutorisz, H., and Hurd, Y.L. (2018). High times for cannabis: Epigenetic imprint and its legacy on brain and behavior. Neurosci. Biobehav. Rev. *85*, 93–101.

Tabata, H., and Nakajima, K. (2003). Multipolar Migration: The Third Mode of Radial Neuronal Migration in the Developing Cerebral Cortex. J. Neurosci. *23*, 9996–10001.

Tabata, H., Kanatani, S., and Nakajima, K. (2009). Differences of migratory behavior between direct progeny of apical progenitors and basal progenitors in the developing cerebral cortex. Cereb. Cortex *19*, 2092–2105.

Tamamaki, N., Nakamura, K., Okamoto, K., and Kaneko, T. (2001). Radial glia is a progenitor of neocortical neurons in the developing cerebral cortex. Neurosci. Res. *41*, 51–60.

Tamamaki, N., Yanagawa, Y., Tomioka, R., Miyazaki, J.I., Obata, K., and Kaneko, T. (2003). Green Fluorescent Protein Expression and Colocalization with Calretinin, Parvalbumin, and Somatostatin in the GAD67-GFP Knock-In Mouse. J. Comp. Neurol. *467*, 60–79.

Tan, X., Liu, W.A., Zhang, X.J., Shi, W., Ren, S.Q., Li, Z., Brown, K.N., and Shi, S.H. (2016). Vascular Influence on Ventral Telencephalic Progenitors and Neocortical Interneuron Production. Dev. Cell *36*, 624–638.

Taniguchi, H., Lu, J., and Huang, Z.J. (2013). The Spatial and Temporal Origin of Chandelier Cells in Mouse Neocortex. Science. *339*, 70–74.

Tasic, B., Menon, V., Nguyen, T.N., Kim, T.K., Jarsky, T., Yao, Z., Levi, B., Gray, L.T., Sorensen, S.A., Dolbeare, T., Bertagnolli, D., Goldy, J., Shapovalova, N., Parry, S., Lee, C., Smith, K., Bernard, A., Madisen, L., Sunkin, S.M., Hawrylycz, M., Koch, C., and Zeng, H. (2016). Adult mouse cortical cell taxonomy revealed by single cell transcriptomics. Nat. Neurosci. *19*, 335–346.

Tasic, B., Yao, Z., Graybuck, L.T., Smith, K.A., Nguyen, T.N., Bertagnolli, D., Goldy, J., Garren, E., Economo, M.N., Viswanathan, S., Penn, O., Bakken, T., Menon, V., Miller, J., Fong, O., Hirokawa, K.E., Lathia, K., Rimorin, C., Tieu, M., Larsen, R., Casper, T., Barkan, E., Kroll, M., Parry, S., Shapovalova, N. V., Hirschstein, D., Pendergraft, J., Sullivan, H.A., Kim, T.K., Szafer, A., Dee, N., Groblewski, P., Wickersham, I., Cetin, A., Harris, J.A., Levi, B.P., Sunkin, S.M., Madisen, L., Daigle, T.L., Looger, L., Bernard, A., Phillips, J., Lein, E., Hawrylycz, M., Svoboda, K., Jones, A.R., Koch, C., and Zeng, H. (2018). Shared and distinct transcriptomic cell types across neocortical areas. Nature *563*, 72–78.

Tavano, S., Taverna, E., Kalebic, N., Haffner, C., Namba, T., Dahl, A., Wilsch-Bräuninger, M., Paridaen, J.T.M.L., and Huttner, W.B. (2018). Insm1 Induces Neural Progenitor Delamination in Developing Neocortex via Downregulation of the Adherens Junction Belt-Specific Protein Plekha7. Neuron *97*, 1299–1314.

Telley, L., Govindan, S., Prados, J., Stevant, I., Nef, S., Dermitzakis, E., Dayer, A., and Jabaudon, D. (2016). Sequential transcriptional waves direct the differentiation of newborn neurons in the mouse neocortex. Science. *351*, 1443–1446.

Timofeev, O., Klimovich, B., Schneikert, J., Wanzel, M., Pavlakis, E., Noll, J., Mutlu, S., Elmshäuser, S., Nist, A., Mernberger, M., Lamp, B., Wenig, U., Brobeil, A., Gattenlöhner, S., Köhler, K., and Stiewe, T. (2019). Residual apoptotic activity of a tumorigenic p53 mutant improves cancer therapy responses. EMBO J. *38*, 1–23.

Toresson, H., Potter, S.S., and Campbell, K. (2000). Genetic control of dorsal-ventral identity in the telencephalon: Opposing roles for Pax6 and Gsh2. Development *127*, 4361–4371.

Torii, M., Hashimoto-Torii, K., Levitt, P., and Rakic, P. (2009). Integration of neuronal clones in the radial cortical columns by EphA and ephrin-A signalling. Nature *461*, 524–528.

Tran, N.L., Adams, D.G., Vaillancourt, R.R., and Heimark, R.L. (2002). Signal transduction from N-cadherin increases Bcl-2. Regulation of the phosphatidylinositol 3-kinase/Akt pathway by homophilic adhesion and actin cytoskeletal organization. J. Biol. Chem. *277*, 32905–32914.

Trazzi, S., Steger, M., Mitrugno, V.M., Bartesaghi, R., and Ciani, E. (2010). CB1 cannabinoid receptors increase neuronal precursor proliferation through AKT/glycogen synthase kinase-3β/β-catenin signaling. J. Biol. Chem. *285*, 10098–10109.

Tremblay, R., Lee, S., and Rudy, B. (2016). GABAergic Interneurons in the Neocortex: From Cellular Properties to Circuits. Neuron *91*, 260–292.

Tsai, J.W., Bremner, K.H., and Vallee, R.B. (2007). Dual subcellular roles for LIS1 and dynein in radial neuronal migration in live brain tissue. Nat. Neurosci. *10*, 970–979.

Tsuboi, K., Uyama, T., Okamoto, Y., and Ueda, N. (2018). Endocannabinoids and related N-acylethanolamines: biological activities and metabolism. Inflamm. Regen. *38*, 28.

Turrero García, M., and Harwell, C.C. (2017). Radial glia in the ventral telencephalon. FEBS Lett. *591*, 3942–3959.

Valiente, M., and Marín, O. (2010). Neuronal migration mechanisms in development and disease. Curr. Opin. Neurobiol. *20*, 68–78.

Vasistha, N.A., García-Moreno, F., Arora, S., Cheung, A.F.P., Arnold, S.J., Robertson, E.J., and Molnár, Z. (2015). Cortical and clonal contribution of Tbr2 expressing progenitors in the developing mouse brain. Cereb. Cortex *25*, 3290–3302.

Vieyres, G., Welsch, K., Gerold, G., Gentzsch, J., Kahl, S., Vondran, F.W.R., Kaderali, L., and Pietschmann, T. (2016). ABHD5/CGI-58, the Chanarin-Dorfman Syndrome Protein, Mobilises Lipid Stores for Hepatitis C Virus Production. PLOS Pathog. *12*, e1005568.

Wakimoto, M., Sehara, K., Ebisu, H., Hoshiba, Y., Tsunoda, S., Ichikawa, Y., and Kawasaki, H. (2015). Classic cadherins mediate selective intracortical circuit formation in the mouse neocortex. Cereb. Cortex *25*, 3535–3546.

Wang, D.D., and Kriegstein, A.R. (2009). Defining the role of GABA in cortical development. J. Physiol. *587*, 1873–1879.

Wang, J., and Ueda, N. (2009). Biology of endocannabinoid synthesis system. Prostaglandins Other Lipid Mediat. *89*, 112–119.

Wang, X., Tsai, J.W., Imai, J.H., Lian, W.N., Vallee, R.B., and Shi, S.H. (2009). Asymmetric centrosome inheritance maintains neural progenitors in the neocortex. Nature *461*, 947–955.

Wang, Y., Dye, C.A., Sohal, V., Long, J.E., Estrada, R.C., Roztocil, T., Lufkin, T., Deisseroth, K., Baraban, S.C., and Rubenstein, J.L.R. (2010). Dlx5 and Dlx6 regulate the development of parvalbumin-expressing cortical interneurons. J. Neurosci. *30*, 5334–5345.

Wang, Y., Li, G., Stanco, A., Long, J.E., Crawford, D., Potter, G.B., Pleasure, S.J., Behrens, T., and Rubenstein, J.L.R. (2011). CXCR4 and CXCR7 Have Distinct Functions in Regulating Interneuron Migration. Neuron *69*, 61–76.

Wang, Y., Ye, M., Kuang, X., Li, Y., and Hu, S. (2018). A simplified morphological classification scheme for pyramidal cells in six layers of primary somatosensory cortex of juvenile rats. IBRO Reports *5*, 74–90.

Wilhelm, C.J., and Guizzetti, M. (2016). Fetal Alcohol Spectrum Disorders: An Overview from the Glia Perspective. Front. Integr. Neurosci. *9*, 65.

Williams, E.J., Walsh, F.S., and Doherty, P. (2003). The FGF receptor uses the endocannabinoid signaling system to couple to an axonal growth response. J. Cell Biol. *160*, 481–486.

Wonders, C.P., and Anderson, S.A. (2006). The origin and specification of cortical interneurons. Nat. Rev. Neurosci. *7*, 687–696.

Wong, F.K., and Marín, O. (2019). Developmental Cell Death in the Cerebral Cortex. Annu. Rev. Cell Dev. Biol. *35*, 523–542.

Wong, F.K., Bercsenyi, K., Sreenivasan, V., Portalés, A., Fernández-Otero, M., and Marín, O. (2018). Pyramidal cell regulation of interneuron survival sculpts cortical networks. Nature *557*, 668–673.

Wu, Q., Sun, X., Yue, W., Lu, T., Ruan, Y., Chen, T., and Zhang, D. (2016). RAB18, a protein associated with Warburg Micro syndrome, controls neuronal migration in the developing cerebral cortex. Mol. Brain *9*, 1–12.

Xie, Z., Sanada, K., Samuels, B.A., Shih, H., and Tsai, L.H. (2003). Serine 732 phosphorylation of FAK by Cdk5 is important for microtubule organization, nuclear movement, and neuronal migration. Cell *114*, 469–482.

Xu, Z., Chen, Y., and Chen, Y. (2019). Spatiotemporal Regulation of Rho GTPases in Neuronal Migration. Cells *8*, 568.

Yamaguchi, Y., and Miura, M. (2013). How to form and close the brain: Insight into the mechanism of cranial neural tube closure in mammals. Cell. Mol. Life Sci. *70*, 3171–3186.

Yang, T., Sun, Y., Zhang, F., Zhu, Y., Shi, L., Li, H., and Xu, Z. (2012). POSH Localizes Activated Rac1 to Control the Formation of Cytoplasmic Dilation of the Leading Process and Neuronal Migration. Cell Rep. *2*, 640–651.

Yoon, K.J., Koo, B.K., Im, S.K., Jeong, H.W., Ghim, J., Kwon, M. chul, Moon, J.S., Miyata, T., and Kong, Y.Y. (2008). Mind Bomb 1-Expressing Intermediate Progenitors Generate Notch Signaling to Maintain Radial Glial Cells. Neuron *58*, 519–531.

Yoon, K.J., Song, G., Qian, X., Pan, J., Xu, D., Rho, H.-S., Kim, N.-S., Habela, C., Zheng, L., Jacob, F., Zhang, F., Lee, E.M., Huang, W.-K., Ringeling, F.R., Vissers, C., Li, C., Yuan, L., Kang, K., Kim, S., Yeo, J., Cheng, Y., Liu, S., Wen, Z., Qin, C.-F., Wu, Q., Christian, K.M., Tang, H., Jin, P., Xu, Z., Qian, J., Zhu, H., Song, H., and Ming, G. (2017). Zika-Virus-Encoded NS2A Disrupts Mammalian Cortical Neurogenesis by Degrading Adherens Junction Proteins. Cell Stem Cell *21*, 349–358.

Yoshida, M., Assimacopoulos, S., Jones, K.R., and Grove, E.A. (2006). Massive loss of Cajal-Retzius cells does not disrupt neocortical layer order. Development *133*, 537–545.

Yozu, M., Tabata, H., and Nakajima, K. (2004). Birth-date dependent alignment of GABAergic neurons occurs in a different pattern from that of non-GABAergic neurons in the developing mouse visual cortex. Neurosci. Res. *49*, 395–403.

Yun, K., Potter, S., and Rubenstein, J.L.R. (2001). Gsh2 and Pax6 play complementary roles in dorsoventral patterning of the mammalian telencephalon. Development *128*, 193–205.

Yun, K., Fischman, S., Johnson, J., Hrabe de Angelis, M., Weinsmaster, G., and Rubenstein, J.L.R. (2002). Modulation of the notch signalling by Mash1 and Dlx1/2 regulates sequential specification and differentiation of progenitor cell types in the

subcortical telencephalon. Development *129*, 5029–5040.

Zeisel, A., Munoz-Manchado, A.B., Codeluppi, S., Lonnerberg, P., La Manno, G., Jureus, A., Marques, S., Munguba, H., He, L., Betsholtz, C., Rolny, C., Castelo-Branco, G., Hjerling-Leffler, J., and Linnarsson, S. (2015). Cell types in the mouse cortex and hippocampus revealed by single-cell RNA-seq. Science. *347*, 1138–1142.

Zhang, J., Woodhead, G.J., Swaminathan, S.K., Noles, S.R., McQuinn, E.R., Pisarek, A.J., Stocker, A.M., Mutch, C.A., Funatsu, N., and Chenn, A. (2010). Cortical Neural Precursors Inhibit Their Own Differentiation via N-Cadherin Maintenance of β-Catenin Signaling. Dev. Cell *18*, 472–479.

Zhang, J., Shemezis, J.R., McQuinn, E.R., Wang, J., Sverdlov, M., and Chenn, A. (2013). AKT activation by N-cadherin regulates beta-catenin signaling and neuronal differentiation during cortical development. Neural Dev. *8*, 7.

Zhang, S., Zhao, B.S., Zhou, A., Lin, K., Zheng, S., Lu, Z., Chen, Y., Sulman, E.P., Xie, K., Bögler, O., Majumder, S., He, C., and Huang, S. (2017). m 6 A Demethylase ALKBH5 Maintains Tumorigenicity of Glioblastoma Stem-like Cells by Sustaining FOXM1 Expression and Cell Proliferation Program. Cancer Cell *31*, 591–606.

Zhang, W., Tan, Y.W., Yam, W.K., Tu, H., Qiu, L., Tan, E.K., Chu, J.J.H., and Zeng, L. (2019). In utero infection of Zika virus leads to abnormal central nervous system development in mice. Sci. Rep. *9*, 7298.

Zhou, Q.P., Le, T.N., Qiu, X., Spencer, V., de Melo, J., Du, G., Plews, M., Fonseca, M., Sun, J.M., Davie, J.R., and Eisenstat, D.D. (2004). Identification of a direct Dlx homeodomain target in the developing mouse forebrain and retina by optimization of chromatin immunoprecipitation. Nucleic Acids Res. *32*, 884–892.

Zhou, R., Han, B., Xia, C., and Zhuang, X. (2019). Membrane-associated periodic skeleton is a signaling platform for RTK transactivation in neurons. Science. *365*, 929–934.

Zimmer, G., Garcez, P., Rudolph, J., Niehage, R., Weth, F., Lent, R., and Bolz, J. (2008). Ephrin-A5 acts as a repulsive cue for migrating cortical interneurons. Eur. J. Neurosci. *28*, 62–73.

Zou, S., and Kumar, U. (2018). Cannabinoid Receptors and the Endocannabinoid System: Signaling and Function in the Central Nervous System. Int. J. Mol. Sci. *19*, 833.

DOI:10.14753/SE.2020.2378

10. List of publications

Publications related to this thesis:

László ZI[1], Bercsényi K[1], Mayer M, Lefkovics K, Szabó G, Katona I, and Lele Z. (2020) N-cadherin (Cdh2) *Maintains Migration and Postmitotic Survival of Cortical Interneuron Precursors in a Cell-Type-Specific Manner*. **Cerebral Cortex** 30, 1318-1329.

Barna L[1], Dudok B[1], Miczán V, Horváth A, László ZI, and Katona I. (2016) *Correlated confocal and super-resolution imaging by VividSTORM*. **Nature Protocols** 11, 163–183.

[1] equal contribution

DOI:10.14753/SE.2020.2378

11. Acknowledgements

I would like to express my special gratitude to my supervisor Zsolt Lele, who is not just a teacher but my scientific father. It has been nearly 10 years since we have been working together and during this time, he taught me how to smile even after a hard day full of unsuccessful experiments or negative results. His enthusiasm as a developmental scientist has motivated me every day. I also thank him for all the experimental knowledge that I have and for teaching me that nothing is impossible you just need to try. I wish him endless free and wild riding and don't forget, never ride faster than your guardian angel can fly!

I am also really grateful to István Katona, the group leader of the Laboratory of Molecular Neurobiology, who gave me the opportunity to mature in this lab and helped me to always think ahead and manage my projects. I also thank him in expanding my perspective by sharing his deep knowledge in the field. I wish him many many birds in the future!

I am also thankful all the past and present members of the lab, for always being helpful and supportive, especially my young colleges who contributed to the presented research: Fruzsina Mógor, Vivien Miczán and Miklós Zöldi. I also thank Erika Tischler who kindly provided everyday assistance for my experiments. I would like to express my great appreciation to the members of the Nikon Microscopy Center and the everyday help for the members of Medical Genetics Unit of IEM.

I would like to also express my greatest gratitude to Nóra Hádinger, who kindly allowed to review my dissertation for the institutional defense, and her critics and advices help me a lot to improve the quality of this thesis.

I would like to thank to my lovely friends from the institute, especially Anett Szilvásy-Szabó and Lilla Otrokocsi, and outside of science Kata Balogh, Zsófia Ruszkai, Andrea Szabó and Fruzsina Rabi, who always make me smile and help me to get through the difficult periods.

I feel the greatest gratitude to my parents and my sisters who created a wonderful family environment and always encouraged me to finish my PhD.

DOI:10.14753/SE.2020.2378

Most importantly, I am the most thankful to my beloved husband, beyond his own scientific carrier and PhD he is always supportive as nobody in my entire life. Without him I would have never finished my PhD.